# Functional Analysis of the Potassium Channel Beta Subunit KCNE3

Dissertation

zur Erlangung des akademischen Grades
*doctor rerum naturalium* (Dr. rer. nat.)

im Fach Biologie

eingereicht an der
Mathematisch-Naturwissenschaftlichen Fakultät I
der Humboldt-Universität zu Berlin

von
Diplom-Biologin Patricia Preston Ferrer

Präsident der Humboldt-Universität zu Berlin
Prof. Dr. Dr. h.c. C. Markschies
Dekan der Mathematisch-Naturwissenschaftlichen Fakultät I
Prof. Dr. A. Herrmann

Gutachter: 1. Prof. Dr. T.J Jentsch
2. Prof. Dr. W. Lockau
3. PD Dr. D. Günzel

Tag der mündlichen Prüfung: 22.October 2010

# Table of Contents

# 1 ZUSAMMENFASSUNG

KCNE-Hilfsuntereinheiten assoziieren mit Spannungs-abhängigen $K^+$-Kanälen und verändern dadurch deren subzelluläre Lokalisation, Regulation sowie deren biophysikalische Eigenschaften. Bei heterologer Expression interagiert KCNE3 mit mehreren Poren-bildenden $K^+$-Kanal-Hauptuntereinheiten, deren Ströme dadurch stark modifiziert werden. Aufgrund dieser *in vitro*-Experimente wurden verschiedenste Funktionen von KCNE3 in den verschiedenen Geweben, wie Gehirn, Herz, Muskel, Kolon und Niere, vermutet. Außerdem wurden Variationen im *kcne3*-Gen mit menschlichen Skelettmuskelpathologien in Verbindung gesetzt (Abbott *et al.* 2001). In der gegenwärtigen Literatur wird die physiologische Funktion von KCNE3 eher als komplex und heterogen dargestellt. Auch die direkte Beteiligung von KCNE3 an Krankheiten ist immer noch spekulativ.

Zur Untersuchung der physiologischen Funktion von KCNE3 *in vivo* sowie der potentiellen Rolle bei Krankheiten generierten wir ein *kcne3*$^{-/-}$ Mausmodell. Die vorliegende Arbeit unterstützt die kritische Rolle der KCNQ1/KCNE3-Kanäle beim Salz- und Flüssigkeitstransport über intestinale und respiratorische Epithelien. Insbesondere fanden wir für die KCNQ1/KCNE3-Heteromere eine basolaterale Lokalisation in Darm- und Trachea-Epithelzellen, wo sie die transepitheliale $Cl^-$-Sekretion über basolaterales Recycling von $K^+$-Ionen sowie über Erhöhung der elektrochemischen Triebkraft für apikalen $Cl^-$-Austritt fördern. Da weder Veränderungen in der KCNQ1-Expressionsmenge noch in dessen subzellulärer Lokalisation festgestellt wurden, ist die durch KCNE3 verursachte Modifikation der KCNQ1-Kanaleigenschaften essenziell für die hier beschriebene physiologische Rolle im Intestinal- und Trachealtransport.

Ferner wird von unserer Arbeit die postulierte Funktion von KCNE3-Heteromeren im Skelettmuskel, Herz und zentralen Nervensystem nicht unterstützt und erweckt somit erhebliche Zweifel über den Beitrag von KCNE3 zu menschlichen Krankheiten, die mit diesen Organen in Verbindung stehen.

# 2 INTRODUCTION

## 2.1 Ion Channels

An ion channel is a pore-forming protein inserted into the membrane that allows the flow of ions through its pore. Ion channels' functions are basic for several cellular processes. Depending on the cell type, the currents generated by the ion flow produce a broad spectrum of effects. For instance, cell cycle, muscle contraction, neuronal action potential, epithelial ion secretion and reabsorption, nutrient absorption, programmed cell death and mucous secretion are processes influenced by ion channel activity.

Ion channel dysfunctions can lead to dramatic changes in cell physiology causing severe pathologies, known as channelopathies (e.g. LQTs, seizures, cystic fibrosis, myotonia congenita, Bartter syndrome). According to their ionic permeability, different ion channel structures have been described: channels selective for monovalent cations, like sodium ($Na^+$) or potassium ($K^+$), divalent cations like calcium ($Ca^{++}$), or monovalent anions like chloride ($Cl^-$).

Given the essential role of ion channels in many different physiological functions, their activity is highly regulated *in vivo*. Voltage changes, chemical (ATP/GTP increases, neurotransmitters, phosphorylations, etc) or mechanical signals (like increases in osmotic pressure) regulate channel gating and inactivation.

### 2.1.1 Resting Membrane Potential and NERNST Equilibrium Potential

All living cells have a plasma membrane, a lipid bilayer that encloses its contents, which represents an almost impermeable seal. The internal compartment differs from the extracellular space in ionic concentrations, which are generated thanks to energy consuming pumps, ion cotransporters and antiporters (table 2.1). Different $Na^+$, $K^+$ and $Cl^-$ concentrations across the membrane produce an electric potential difference, which is known as the "resting potential". In all living cells, several different ion types, each with its own gradient, contribute to this charge separation. Each ion has a determined concentration inside and outside the cell producing its Nernst equilibrium potential,

which is calculated according to the following equation:

$$E = (RT/zF) \ln ([\text{ion outside cell}]/[\text{ion inside cell}])$$

Where:

$R$ is the universal gas constant: $R = 8.314\ JK^{-1}mol^{-1}$

$T$ is the absolute temperature

$F$ is the Faraday constant, the number of coulombs per mole of electrons: $F = 9.648 \times 10^4\ C\ mol^{-1}$

$z$ is the charge of the ion.

At the Nernst equilibrium potential, there are no net charge fluxes through a channel because an electric and chemical equilibrium has been reached.

Ion channel activity generates rapid ion fluxes driven by chemical concentration and electrical charge gradients across the plasma membrane, which modify the cell resting membrane potential. Each ion is naturally moved towards its equilibrium potential. In the case of $K^+$, which is usually more concentrated intracellularly (140 mM) than in the extracellular space (5 mM), its equilibrium potential is more negative (-84 mV) than the membrane potential at rest. The opposite is true for $Na^+$, which is more concentrated in the extracellular space (140 mM outside and 12 mM inside the cell) and its corresponding equilibrium potential is positive (+40 mV). $Na^+/K^+$ pumps keep a high $K^+$ concentration inside the cell, since they extrude $Na^+$ towards the extracellular space and import $K^+$ ions.

**Table 2.1 Ionic concentrations inside and outside a mammalian cell. Physiological ionic concentrations of the most relevant ions in the mammalian cell (Alberts 2003).**

| Ion | Intracellular (mM) | Extracellular (mM) |
|---|---|---|
| Sodium | 5-15 | 145 |
| Potassium | 140 | 5 |
| Magnesium | 0.5 | 1-2 |
| Calcium | $10^{-4}$ | 1-2 |
| Chloride | 5-30 | 110 |

These pumps work against chemical concentrations, and therefore consume energy. The opening of $K^+$ channels promotes an outward flux that brings the membrane potential to negative values, following its Nernst equilibrium potential. Therefore, with few rare

exceptions (e.g. KCNQ1/KCNE1 channels in stria vascularis), all $K^+$ channels are hyperpolarizing, and they are considered responsible for repolarizing the cell membrane after depolarizations. On the other hand, $Na^+$ channels are known to be depolarizing, since they allow the entry of $Na^+$ into the cell, bringing the membrane potential towards positive values.

## 2.2 Potassium Channels

$K^+$ channels are critical for physiological processes that involve rapid responses like propagation of electrical signals throughout the nervous system, cardiac, skeletal and smooth muscle contraction, transepithelial transport of electrolytes and nutrients, maintenance of salt-water absorption in gastrointestinal epithelia. They are as well involved in insulin secretion, cell cycle regulation, immune system response, cell volume and pH regulation, body balance and hearing.

Despite the diverse kinetic properties and tissue distribution, $K^+$ channels share a common basic architecture. $K^+$ channels are tetrameric structures spanning the plasma membrane (MacKinnon 1991), consisting of 4 pore forming subunits, called alpha subunits. The subunits are probably assembled as dimer of dimers and symmetrically arranged around the pore (Tu and Deutsch 1999). A huge number of $K^+$ channels have been described so far (Gutman et al. 2003) and according to their structure and biophysical properties, they have been classified into the following subdivisions (Figure 1.1): six transmembrane domains and one pore loop (6TM/1P), two transmembrane domains and one pore loop (2TM/1P), four transmembrane domains and 2 pore loops (4TM/2P).

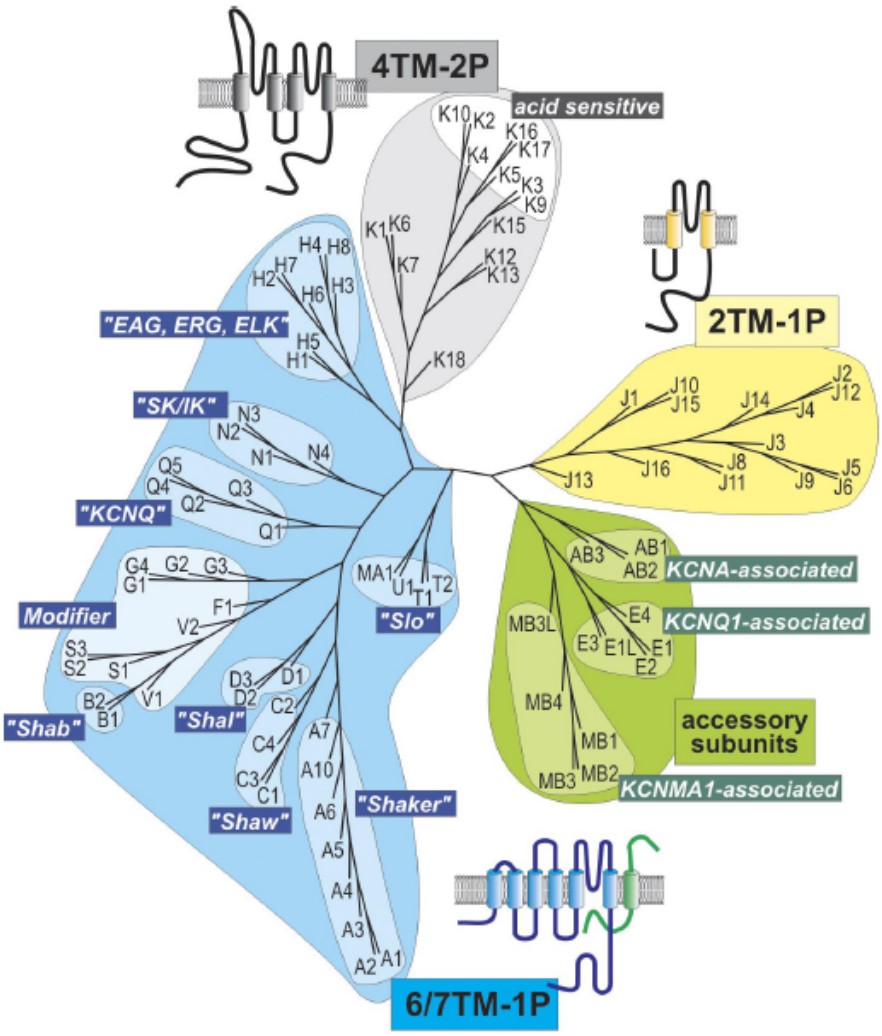


**Figure 2.1 "KCN" potassium channel families.** Phylogenetical relations among human $K^+$ channels. The KCN- letter code has been omitted (for instance "E3" stands for KCNE3 and "Q1" for KCNQ1). In some cases, also the most common used family aliases are highlighted (Adapted from Heitzmann et al 2008).

## 2.3 Voltage Gated Potassium Channels

The voltage gated $K^+$ channels (Kv) group includes 40 of the 90 genes of $K^+$ channels described so far. According to phylogenetic homology, they are divided into 12 families (Kv1 to Kv12) and classified into two main groups. The first group encloses Kv1 to Kv9, the second Kv10 to Kv12.

All Kv channels subunits share the similar 6TM/1P structure and they get activated upon membrane voltage changes. Kv channels subunits contain two essential domains: the pore domain and the voltage-sensing domain (VSD). Each alpha subunit contains one pore domain (p-loop), thus the channel pore contains 4 copies of the p-loop. The

pore domain contains a highly conserved amino acid sequence consisting of TVGYG (Threonine, Valine, Glycine, Tyrosine, Glycine) that works as a selectivity filter. The S4 transmembrane domain is known as VSD because is able to move physically in response to changes in membrane potential, due to its positively charged amino acids. The VSD transduce electrical potential differences in conformational changes in the conduction pore, which open or occlude the ion conduction pathway.

## 2.4 KCNQ Family

KCNQ channels are a family of voltage gated $K^+$ channels, also named Kv7 family. They have been described and intensely studied in central nervous system (KCNQ2, 3 and 5), skeletal muscle (KCNQ5), intestine, cochlea, heart (KCNQ1), inner ear (KCNQ4), dorsal root ganglia, and recently reported in portal vein (KCNQ4 and 5), gastric smooth muscle, and pulmonary artery (KCNQ4 and 5).

Five members of the family have been described (KCNQ1 to 5). They are all located in different chromosomes and share 30% to 65% of homology, mostly in transmembrane domains and in the C-terminus. In fact, all KCNQs have a highly conserved KCNQ-specific domain, the "A-domain" or "subunit interaction (*si*) domain" in the distal C-terminal region. This domain contains two double coiled-coil domains TCC1 and TCC2 (tetramerizing coiled coil 1 and 2), also called A-domain head and tail, that are important for subunit recognition, channel assembly and surface expression (Schwake et al. 2003). Some of the members of the KCNQ family are able to assemble in functional heterotetramers, like KCNQ2 and 3 (Wang et al. 1998), KCNQ3 and 5 (Lerche et al. 2000; Schroeder et al. 2000), KCNQ3 and 4 (Kubisch et al. 1999).

KCNQ channel activation promotes outward $K^+$ current that slowly activate under depolarizing voltages, being already active close to resting membrane potentials. KCNQs are considered hyperpolarizing channels because of their action in repolarizing the cell membrane after a strong depolarization. KCNQ channels show very little or no inactivation at all.

The neuronal KCNQ family members show M-current properties (Wang et al. 1998; Jentsch 2000), defined by its kinetics and modulation, e.g. they are inhibited by acetylcholine-mediated activation of muscarinic receptors.

Concerning their pharmacological properties, KCNQs are inhibited by $Ba^{++}$, are insensitive to charibodotoxin ($Ca^{++}$ activated $K^+$ channel blocker) and to 4-

aminopiridine (a general $K^+$ channel blocker). KCNQs are blocked by linopirdine and its more potent analog 10,10-bis(4-pyridinyl-methyl)-9(10H)-anthracenone (XE991). Besides, the neuronal forms of KCNQs are also efficiently activated by retigabine. Interestingly, KCNQ channels display a diverse sensitivity to tetraethylammonion (TEA) according to the following decreasing scale of sensitivity: KCNQ2>KCNQ4=KCNQ1>KCNQ5> KCNQ3. This effect indicate differences in relevant residues downstream the selectivity filter sequence.

## 2.5 KCNQ1

KCNQ1 contains 676 amino acids, and its C-terminal domain is longer than of other Kv7, conferring a scaffolding structure for many intracellular signaling proteins. Secondary structure studies suggest that the KCNQ1 C-terminal domain possesses four conserved alpha helical regions (Yus-Najera et al. 2002). The first two contain protein-binding domains for channel modulation and the other two form a so called “coiled coil” domain, which is important for subunit recognition and channel assembly. It is believed that this region is responsible for alpha subunit homo-oligomerization. Unlike other KCNQ family members, KCNQ1 channel forms only homotetramers (Howard et al. 2007; Wiener et al. 2008).

The fact that KCNQ1 displays slower activation kinetics compared to the other KCNQs, is most probably due to the less charged residues in its S4 voltage sensor domain (Panaghie and Abbott 2007).

KCNQ1 is expressed in epithelia and cardiac tissue (Barhanin et al. 1996; Sanguinetti et al. 1996; Lee et al. 2000). More recent reports also claim its expression in skeletal muscle (Yang et al. 1997) and brain (Goldman et al. 2009).

Five KCNQ1 splice variants have been described, with only two of them giving rise to functional proteins. In heart, the first isoform was identified by Barhanin and Sanguinetti, the second one was described by Wang in 1996 (Wang et al. 1996). Expression of a third KCNQ1 isoform has been also reported in heart. When compared to the other two functional isoforms, this isoform lacks 127 amino acids in its N-terminal sequence, and gives rise to a non-functional protein. Interestingly, this third isoform seems to inhibit the KCNQ1 wild type currents when heterologously co-expressed with functional KCNQ1 isoforms. Moreover, this isoform is insensitive to KCNE-mediated kinetic modulations. The physiological role of this non-functional

KCNQ1 isoform is still not clear, although the fact that it is expressed in specific areas of the heart and at different levels might implicate a role in fine-tuning the expression of functional KCNQ1 channels. This fine modulation could possibly account for the vast heterogeneity of $K^+$ conductances observed in cardiac tissue (Jiang et al. 1997).

### 2.5.1 Electrophysiological Properties of KCNQ1

KCNQ1 activation kinetics are slow compared to KCNQ2/KCNQ3 heterotetramers or Shaker-type $K^+$ channels, probably due to the less positively charged S4 VSD.

When KCNQ1 channels are heterologously expressed in *Xenopus* oocytes or mammalian cells, the currents recorded do not resemble any physiologically observed current, most probably because KCNQ1 is always part of a heteromeric complex with KCNE subunits *in vivo*.

*In vitro* studies of KCNQ1 channels show half maximal activation ($V_{1/2}$) at voltages that range from -12 mV to 36 mV depending on the expression system used (oocytes or mammalian cells). The channels activate following an exponential curve within 100 and 200 milliseconds. In *Xenopus* oocytes, maximal activation is reached after two seconds depolarization pulse and very slow deactivation is usually observed (Barhanin et al. 1996; Tristani-Firouzi and Sanguinetti 1998) (Figure 2.2).

KCNQ1 channels display a delayed inactivation process that differs from the classic C-type inactivation. Tail currents recorded in high $K^+$ concentrations revealed that KCNQ1 channels do inactivate (Figure 2.2), being inactivation the third state for the channel together with open and closed states (closed < >open < > inactive). Although inactivation is difficult to observe in KCNQ1 channels, the transition among inactive and closed state is readily seen as a “hook” present in the tail current. This is due to the fact that KCNQ1 channels pass from inactive to open state ten times faster than passing from open to close state (Pusch et al. 1998). KCNQ1 inactivation does not play a relevant physiological role since *in vivo* it is removed or completely masked by the interaction with KCNE beta subunits.

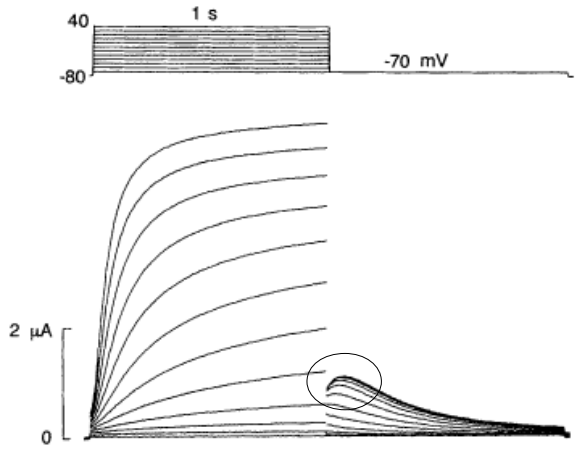


**Figure 2.2 Recordings from KCNQ1 expressing *Xenopus* oocytes.** Slow activating KCNQ1 currents were recorded under depolarizing voltages steps. Pulses were applied in 10 mV increments from -70 mv to +40 mV. The current tail indicates inactivation (shown by the circle) (adapted Sanguinetti et al 1996).

## 2.5.2 Pharmacology

XE991 inhibits KCNQ1 with an $IC_{50}$ (concentration necessary to block half of the current) of 0.8 µM. However, XE991 $IC_{50}$ for KCNQ1/KCNE1 is about 11 µM. XE991 action is however rather unspecific, since it also inhibits other members of the KCNQ family in a similar concentration range. The most specific drug which ensures quite selective inhibition of KCNQ1 is chromanol 293B (293B, *trans*-6-cyano-4-(*N*-ethylsulfonyl-*N*-methylamino)-3-hydroxy-2,2-dimethyl-chroman) with a $IC_{50}$= 27 µM. It is important to note that the sensitivity of KCNQ1 to chromanol 293B is increased by coassembly with KCNE1 ($IC_{50}$= 7 µM), and even more with KCNE3 ($IC_{50}$= 3 µM). At much higher concentrations however, chromanol 293B also inhibits CFTR $Cl^-$ channel ($IC_{50}$= 19 µM).

## 2.5.3 Intracellular Modulation of KCNQ1

KCNQ1 channels probably do not exist *in vivo* in the homooligomeric form, but they are always coexpressed together with KCNE subunits. In this section, we will describe the biochemical mechanisms responsible for the functional regulation of KCNQ1/KCNE complexes, which are always part of a major macromolecular signaling complex (Marx et al. 2002).

### 2.5.3.1 cAMP

High levels of intracellular cAMP activate KCNQ1, KCNQ1/KCNE1 (Yang et al. 1997), and KCNQ1/KCNE3 (Schroeder et al. 2000).

Under beta adrenergic signaling in cardiac myocytes, Yotiao, an A-kinase anchoring protein (AKAP) binds first to the leucine zipper motif present in the long KCNQ1 C-

terminus, then recruits cAMP-activated protein kinase A (PKA) which phosphorylates KCNQ1 on serine 27 (Marx et al. 2002), and activates the channel. Beta-adrenergic stimulation therefore, by promoting KCNQ1 phosphorylation, leads to increase in cardiac slowly activating delayed rectifier $K^+$ current ($I_{ks}$).

Interestingly, a mutation in the leucine zipper motif (hKCNQ1-G589D), which abolishes cAMP-mediated regulation of the KCNQ1 by preventing Yotiao recruiting, has been linked to Long QT syndrome (Marx et al. 2002). This cAMP regulation is also impaired when KCNE1 C-terminus is mutated (D76N and W87R), mutations which are also associated with some forms of long QT syndrome (Kurokawa et al. 2003).

#### 2.5.3.2 Calcium

Studies addressing the involvement of $Ca^{++}$ signaling in the regulation KCNQ1-containing channels yielded to contradictory results (Gamper et al. 2005). It is however accepted that calmodulin (a $Ca^{++}$ binding protein) interacts with KCNQ channels. Calmodulin binds to the IQ motif present in the KCNQ1 C-terminal domain, even in the absence of $Ca^{++}$. This interaction is thought to be responsible for "solubilizing" the large C-terminal domain, a necessary requirement for the channel to traffick to the plasma membrane (Ghosh et al. 2006; Shamgar et al. 2006). Interestingly, a KCNQ1 mutation, which abolishes its interaction with calmodulin, resulted in diminished $K^+$ current amplitudes in myocytes and had been linked to LQT disease in humans (Schmitt et al. 2007).

#### 2.5.3.3 $PIP_2$

Phosphatidylinositol 4,5-bisphosphate ($PIP_2$) is able to interact directly with the C-terminal domain of KCNQ1. $PIP_2$ stimulates KCNQ1/KCNE1 complex by increasing current amplitude and left shifting its voltage dependence of activation (Loussouarn et al. 2003; Kwon et al. 2007).

#### 2.5.3.4 pH

Extracellular pH has different effects on KCNQ1 homo- and heterocomplexes. Low values of extracellular pH strongly decrease the current amplitude of KCNQ1 homomeric complexes, activate KCNQ1/KCNE2 heteromeric channels (of relevance during gastric acid secretion) and induce variable effects on KCNE1/KCNQ1 kinetics

and current amplitude. This latter effect could represent an adaptative mechanism during the acidosis associated with cardiac ischemia (Heitzmann et al. 2007).

#### 2.5.3.5 Cell Volume

Changes in cell volume are also known to regulate KCNQ1 activity. Increases in KCNQ1-mediated currents have been reported in rat hepatocytes, myocytes, upper airways cells, and MCF-7 epithelial cells, upon swelling (Kubota et al. 2002; Lan et al. 2005; vanTol et al. 2007). It is believed that the KCNQ1 N-terminus senses the changes in cell volume via direct interaction with the cytoskeletal network (Grunnet et al. 2003).

## 2.6 KCNE Accessory Subunits

Beta subunits are regulatory or auxiliary proteins that interact with ion channels in order to target them to the plasma membrane, to modify the ion channel activity, kinetics and sensitivity to certain compounds.

Several regulatory beta subunits have been described to interact with $K^+$ channels, which may be cytosolic, or may span the lipid bilayer with one or several transmembrane domains. The KCNE beta subunits contain one transmembrane domain, a long extracytoplasmatic N-terminus and an intracellular C-terminus (Takumi et al. 1988; Abbott and Goldstein 2001). The KCNE family seems to be quite promiscuous and *in vitro,* it is able to interact with multiple members of the voltage gated $K^+$ channel family: KCNQ1, KCNQ4, KCNH1, KCNH2 (hERG), KCNC1 (here referred as Kv3.1), KCNC4 (here referred as Kv3.4), the KCND3 and KCNB1 (Zhang et al. 2001; Grunnet et al. 2003).

### 2.6.1 KCNE Family Members

The KCNE family consists of five members (KCNE1-5) which share a high homology in their transmembrane and C-terminal domains. They are small (106-177 amino acids) single transmembrane-spanning proteins, and their molecular weight ranges from 12 to 19 kDa, depending on the sugar chains attached at their N-terminal sequences. The long and glycosylated N-terminal is extracellular, whilst the intracellular C-terminal length is variable and it contains a predicted consensus PKC phosphorylation site (Abbott et al. 2006). Sequence similarity predict that KCNE1, KCNE2, KCNE3 and KCNE5 posses a

structural motif in the C-terminal domain (e.g. proline 77 in KCNE1) that would bend the intracellular structure. This structural scaffold would be important for channel modulation (Rocheleau et al. 2006).

KCNE1 has been the first member of the KCNE family to be cloned (Takumi et al. 1988), and it had been originally named IsK and later MinK (Minimal $K^+$ channel) because of its small size. In fact, KCNE1 was first described as a channel promoting $K^+$ currents upon overexpression in *Xenopus* oocytes, though later it was shown to co-assemble with endogenous KCNQ1. KCNE2, 3 and 4 were cloned by homology and named after MinK as Related Peptides (MiRP) 1, 2 and 3 respectively. Besides, KCNE5, which is also known as KCNE1L (KCNE1 like protein), was first discovered as a deleted gene in the contiguous gene AMME syndrome (Alport syndrome, Mental retardation, Midface hypoplasia and Elliptocytosis) and was named after its high homology to KCNE1. Loss of of KCNE5 could be involved in the cardiac and neurological abnormalities seen in AMME syndrome (Piccini et al. 1999).

Several *in vitro* studies demonstrated that KCNE proteins interact with a subgroup of $K^+$ channels, the KCNQ channels, and particularly with KCNQ1 (Schroeder et al. 2000). Interactions with other $K^+$ channels (kv3.4, kv2.1, kv3.1 and kv4.3) have been reported too. However, in many cases, it is unclear whether these promiscuous interactions are indeed occurring *in vivo* and are physiologically relevant, or they are just artifacts in overexpression *in vitro* systems employed to describe the interaction (Abbott et al. 2001; McCrossan et al. 2003; Lundby and Olesen 2006).

Furthermore, some reports have claimed the co-assembly of KCNQ1 with several different KCNE subunits in one KCNQ1/KCNE heteromeric complex. These mixed complexes would give rise to a greater variety of $K^+$ currents (Morin and Kobertz 2007; Manderfield and George 2008). Along these lines, it is important to mention that all KCNE transcripts have been indeed found in human cardiac tissue to be co-expressed with KCNQ1 (Bendahhou et al. 2005; Lundquist et al. 2005).

#### 2.6.1.1 KCNE1

KCNE1 mRNA undergoes alternative splicing, which results in two different isoforms: KCNE1a, which is ubiquitously expressed, and KCNE1b, which is typically found in cardiac tissue (Lundquist et al. 2006). KCNE1 is strongly expressed and plays a functional role in heart, kidney and inner ear. Consistently, *kcne1*$^{-/-}$ mice suffer from the

classical shaker/waltzer behavior (characterized by bidirectional circling, hyperactivity, head bobbing, and inability to swim) (Vetter et al. 1996), as well as cardiac arrhythmias and increased renal excretion of $Na^+$ and glucose (Arrighi et al. 2001; Vallon et al. 2001).

KCNE1 interacts with KCNQ1 in heart and inner ear, where they form an extremely slowly activating and deactivating, delayed rectifying complex (Barhanin et al. 1996; Sanguinetti et al. 1996) (Figure 2.3). In addition, some reports showed that KCNE1 is able to alter Kv4.3 currents *in vitro* (Radicke et al. 2006), and modify Kv3.1 and Kv3.2 currents (Lewis et al. 2004).

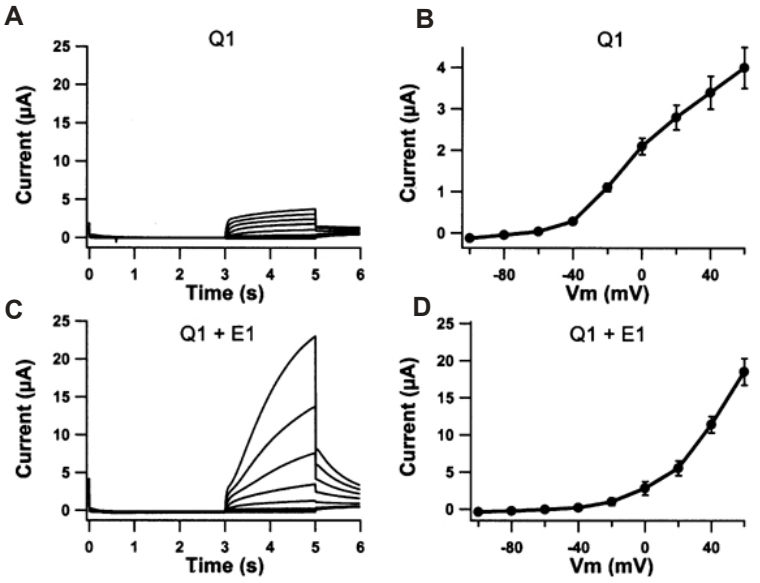


**Figure 2.3 Modification of KCNQ1 currents by KCNE1.** KCNQ1 (A and B) or KCNQ1/KCNE1 (C and D) currents recorded from Xenopus oocytes. Voltage was clamped from -100 to +60 mV in 20 mV increments. The corresponding averaged *I–V* curves are shown in B and D. KCNQ1/KCNE1 channel complex elicited extremely slow activating and deactivating currents under depolarizing potentials (adapted from Grunnet et al. 2002).

### 2.6.1.2 KCNE2

Compared to KCNQ1 homomers, co-assembly of KCNE2 with KCNQ1 changes the current kinetics, renders the complex voltage independent and strongly reduces its currents (Tinel et al. 2000) (Figure 2.4).

The KCNQ1/KCNE2 complex has been found in stomach, namely in parietal cells, being involved in acid gastric secretion (Roepke et al. 2006). Recently the complex has been localized to the thyroid and described as essential for normal thyroid hormone

biosynthesis (Roepke et al. 2009). Loss of KCNE2 function in mice resulted in a broad spectrum of endocrine pathologies like mental retardation, dwarfism and cardiac arrhythmia. In addition, *kcne2*$^{-/-}$ mice show achlorhydria (reduced acid secretion) and gastric hyperplasia due to the lack of KCNE2 in parietal cells of the stomach (Roepke et al. 2006). Mutant mice also display hypothyroidism, dwarfism, alopecia, goiter, impaired maternal milk ejection and cardiac abnormalities. All of this endocrine dysfunction are most probably due to the novel role of KCNQ1/KCNE2 as thyrocyte $K^+$ channel regulating production of thyroid hormones (Roepke et al. 2009).

Moreover, *in vitro* data showed that KCNE2 is able to modulate cardiac Kv4.2 (modulating Transient Outward $K^+$ currents, $I_{to}$) (Zhang et al. 2001), as well as the neuronal Kv4.3 together with KChIP2 (Radicke et al. 2006). KCNE2 has also been reported to interact with Hyperpolarization-activated, Cyclic Nucleotide-modulated (HCN) channels in heart (Decher et al. 2003) and to modulate *in vitro* kinetic properties of Kv3.1 and Kv3.2 (Lewis et al. 2004). KCNE2 has been also shown to co-assemble in cardiac tissue with Kv 11 (HERG) channels, thereby producing slowly activating and fast inactivating delayed rectifier currents ($I_{Kr}$) (Abbott et al. 1999).

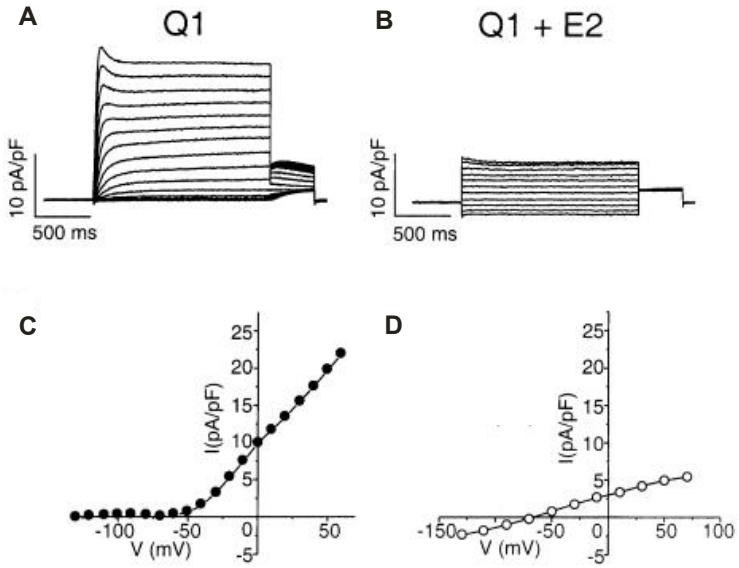


**Figure 2.4 Modification of KCNQ1 currents by KCNE2.** Compared KCNQ1 (A and C) or KCNQ1/KCNE2 (B and D) currents recorded from transfected COS-7 cells after 2 s voltage steps from a holding potential of –80 mV over the range of –130 to +60 mV in 10 mV increments (A) or to +70 mV in 20 mV increments (B). The corresponding averaged *I–V* curves are shown in C and D. KCNQ1/KCNE2 channel complex elicited small amplitude voltage independent currents (adapted from Tinel et al 2000).

### 2.6.1.3 KCNE3

Co-expression of KCNQ1 with KCNE3 in heterologous systems gives rise to linear, voltage independent $K^+$ currents (Schroeder et al. 2000) (Figure 2.5).

In addition, *in vitro* KCNE3 is able to interact with many other Kv family members. These putative interactions have led to many speculative hypothesis for the function of the KCNE3 protein.

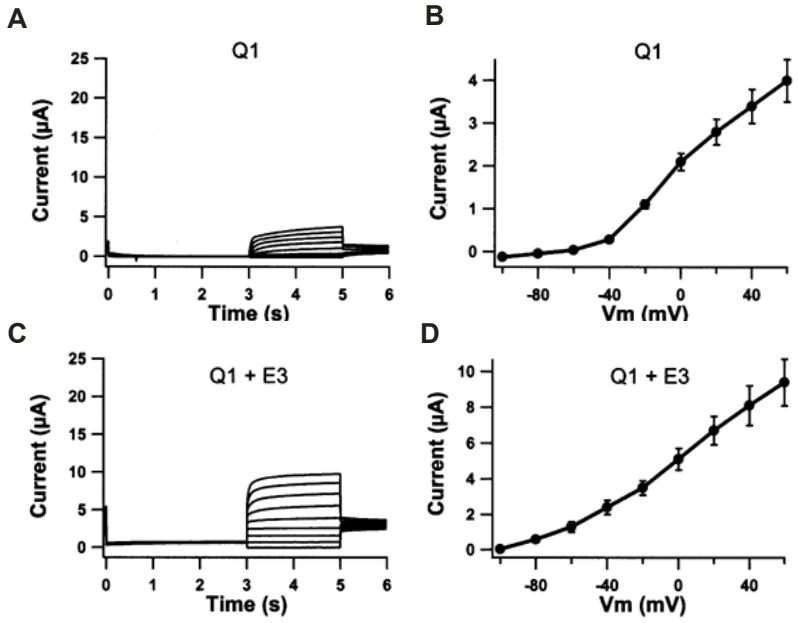


**Figure 2.5 Modification of KCNQ1 currents by KCNE3.** KCNQ1 (A and B) or KCNQ1/KCNE3 (C and D) currents recorded from *Xenopus* oocytes. Voltage was clamped from -100 to +60 mV in 20 mV increments. The corresponding averaged *I–V* curves are shown in B and D. KCNQ1/KCNE3 channel complex elicited enlarged, linear and voltage independent currents (adapted from Grunnet et al 2002).

KCNE3 for example had been speculated to associate with KCNQ1 in colonic crypts (Schroeder et al. 2000; Dedek and Waldegger 2001) and to be expressed in human skeletal muscle, where it was proposed to associate with Kv3.4 (Abbott et al. 2001). Some other reports had claimed KCNE3 expression in the mammalian brain, together with Kv2.1 and Kv3.1 (McCrossan et al. 2003) or kv3.4 (Pannaccione et al. 2007). KCNE3 expression was also observed in heart, by real-time quantitative RT-PCR and in situ hybridization experiments (Bendahhou et al. 2005; Lundquist et al. 2005; Lundquist et al. 2006), or in portal vein myocytes (Ohya et al. 2002), where it was proposed to associate with KCNQ1 or ERG channels respectively.

### 2.6.1.4 KCNE4

The physiological role of the KCNQ1/KCNE4 complex has not yet been clearly elucidated. Interestingly however, co-expression studies in heterologous systems have shown that KCNQ1/KCNE4 complexes are silent, suggesting that *in vivo* KCNE4 would inhibit KCNQ1 currents upon co-assembly (Grunnet et al. 2002) (Figure 2.6). These experimental evidences are however still speculative, since specie specific differences have been reported between rat and human: the rat KCNE4 protein would indeed silence KCNQ1, while the human version would just slow KCNQ1 activation kinetics (Teng et al. 2003).

In addition, KCNE4 has been shown to silence *in vitro* Kv1.1, Kv1.3 (Grunnet et al. 2003) and to regulate the cardiac Kv4.3 channel (Grunnet et al. 2002).

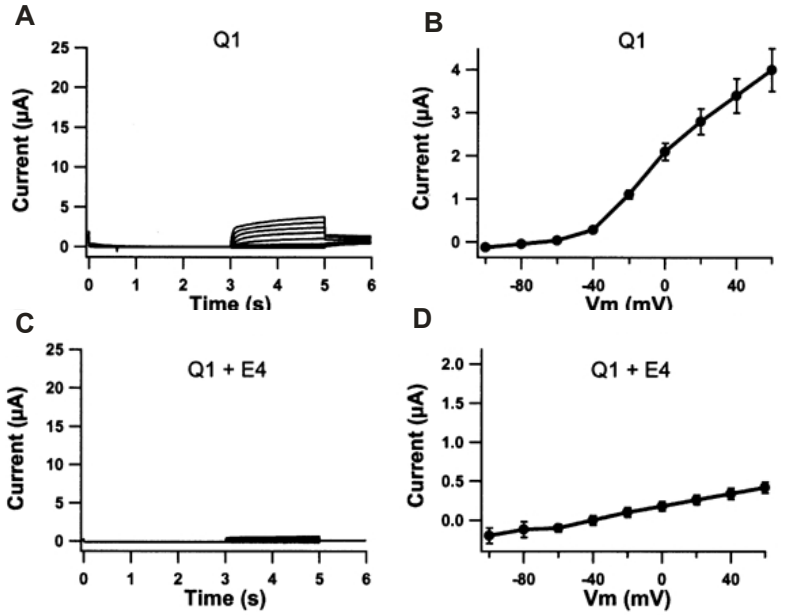


**Figure 2.6 Modification of KCNQ1 currents by KCNE4.** KCNQ1 (A and B) or KCNQ1/KCNE4 (C and D) currents recorded from *Xenopus* oocytes. Voltage was clamped from -100 to +60 mV in 20 mV increments. The corresponding averaged *I–V* curves are shown in B and D. Interestingly, KCNQ1/KCNE4 channel complex are electrophysiologically silent (adapted from Grunnet et al 2002).

### 2.6.1.5 KCNE5

Although its physiological function has not been clearly understood, the fact that KCNE5 shares its genomic location with several neuronal genes (Lundquist et al. 2006) all of which are deleted in the AMME syndrome, prompted the assumption that KCNE5 might also be involved in this pathological condition.

Overexpression studies in CHO cells have shown that KCNE5 coassembly with KCNQ1 leads to right shifting of its activation voltage (Angelo et al. 2002) (Figure 2.7), while a similar effect had not been observed in earlier experiments in *Xenopus* oocytes (Piccini et al. 1999). *In vitro* KCNE5 has also been reported to assemble with the cardiac Kv4.3 channel (Radicke et al. 2006).

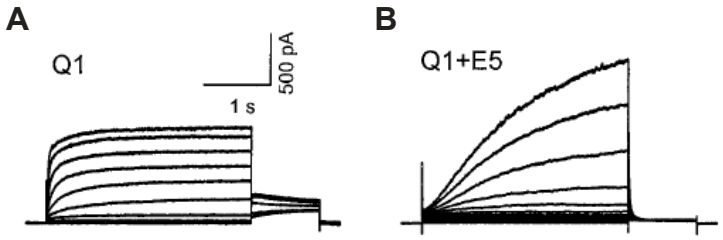


**Figure 2.7 Modification of KCNQ1 currents by KCNE5.** KCNQ1 (A) or KCNQ1/KCNE5 (B) currents recorded from *Xenopus* oocytes. Voltage was clamped from -100 to +40 mV in 20 mV steps. KCNQ1/KCNE5 channel complex elicited enlarged dependent currents. Interestingly, KCNQ1/KCNE5 channel complex behave similarly to KCNQ1/KCNE1 (adapted from Angelo et al 2002).

## 2.6.2 Glycosylation of KCNE Proteins

KCNE proteins have a single transmembrane domain, with intracellular C-terminus and extracellular N-terminus. The N-terminal contains consensus sequences for N-linked glycosylation, represented by N - X - T/S sequence motifs (N being an asparagine, X any amino acid but proline, and T or S a threonine or serine residue). It has been shown by several studies that these consensus sequences are effectively glycosylated in living cells (Gage and Kobertz 2004; Chandrasekhar et al. 2006).

The glycosylation process starts in the rough-ER with the covalent attachment of a branched saccharic chain to the peptide, either while it is being synthesized (co-translational glycosylation) or after the protein has been synthesized (post-translational glycosylation). The added oligosaccharide is composed by mannose and N-acetylglucosamine residues (ManNAc). After correct protein folding, the glycoprotein is exported to the Golgi where the glycosylation process is completed by further modifications of the sugar chain. N-linked glycoproteins are in fact immature when sitting in the ER and acquire complex additional modifications while traveling trough medial and *trans*-Golgi compartments.

N-glycosylation is important for protein folding, oligomerization and trafficking to the cell surface (Santacruz-Toloza et al. 1994; Khanna et al. 2001). Immature N-linked

glycans are common signals for ER retention. KCNE proteins in particular are also retained in the early steps of the secretory pathway until they are coassembled with Kv alpha subunits (Chandrasekhar et al. 2006). Assessing the glycosylation state of a protein has therefore been extensively used as a marker for its maturational state and to determine its "position" along the secretory pathway. In particular, two biomolecular tools allow differentiating whether a protein left or not the ER: Endoglycosidase H (EndoH), which selectively removes immature glycans; and PNGaseF glycosidase, which breaks up all kinds of N-linked oligosaccharides (immature and complex) from the peptide backbone (Lemp et al. 1990). The presence of glycans, which are not cleaved by the EndoH, but effectively removed by PNGaseF, indicates exit of the glycoprotein from the ER compartment.

## 2.7 KCNQ1/KCNE Complexes

### 2.7.1 Intracellular Trafficking of KCNQ1/KCNE Complexes

When studying KCNQ1 and KCNE partnering *in vitro*, it is of importance which heterologous system is chosen. The fact that some of them, *Xenopus* oocytes and HEK cells for example, already express endogenous KCNQ1, can lead to misinterpretation of the results. This is the case of some studies, which had erroneously concluded that assembly of KCNQ1 with KCNE1 takes place at the plasma membrane, and not in earlier steps of the exocytotic pathway (Romey et al. 1997; Grunnet et al. 2002). A later study however, performed in CHO and COS7 cells, which do not express endogenous KCNQ1, revealed that KCNE1 and KCNQ1 do not travel independently through the secretory pathway but assemble as a channel complex already in the ER (Chandrasekhar et al. 2006).

When overexpressed alone in CHO cells, KCNE1 does not progress past ER and *cis*-Golgi, while its co-expression with KCNQ1 leads to a robust KCNQ1/KCNE1 cell surface expression. Moreover, a specific mutation on the KCNE1 protein has been described which could retain KCNQ1 in the ER, further suggesting that both proteins first assemble in this intracellular compartment (Krumerman et al. 2004). Schroeder et al had reported a similar finding in 2000, where cotransfection of KCNE3 and KCNQ1, either alone or in combination, had shown that KCNE3 was not properly targeted to the

plasma membrane in absence of the alpha subunit, but was retained intracellulary in the ER compartment.

### 2.7.2 KCNQ1 and KCNE Assembly and Modulation

Although in recent years the exact location of the KCNE subunits within the KCNQ1 channel has been extensively investigated, broad consensus has not yet been reached. Early studies suggested that KCNE ancillary subunits are located in the periphery of the compact KCNQ1 homotetramer (Wang et al. 1996; Romey et al. 1997) or just across the S4 canal (Kurokawa et al. 2001). Other reports suggested KCNE1 subunits to be located inside the KCNQ1 pore domain, near the ion pathway (Tai and Goldstein 1998; Chen et al. 2003). This hypothesis has been however ruled out by more recent studies based on the crystal structure of Kv channels, which showed that the pore region is indeed too narrow to harbor a KCNE peptide. Moreover, the fact that KCNQ1/KCNE1 can assembly with different stoichiometries, as shown by targeted mutagenesis experiments (Wang et al. 1998b), does not support the hypothesis of KCNE subunits being located inside the channel pore.

More recent data have shown that KCNE1 and KCNE3 are able to interact with different segments of the KCNQ1 pore-lining S6 domain (Tapper and George 2001; Melman et al. 2004; Panaghie et al. 2006) (Figure 2.8), raising the possibility that mixed number of KCNE subunits might assemble at the same time within the KCNQ1 tetramer. Indeed Morin and Kobertz in 2008 described an elegant approach to determine the number of beta-subunits in ion channel complexes, and show that there are two KCNE subunits in a functioning tetrameric KCNQ1 channel.

Another study from the same group showed that key residues in the transmembrane domain of KCNE3 and KCNE1, called “activation triplet” (Figure 2.8), are able to modulate complex assembly and gating by direct interaction with the KCNQ1 pore lining region (Gage and Kobertz 2004). In addition to this regulatory mechanism, the KCNE C-terminus would be also involved in regulating KCNQ1 kinetics (Takumi et al. 1991; Tapper and George 2000).

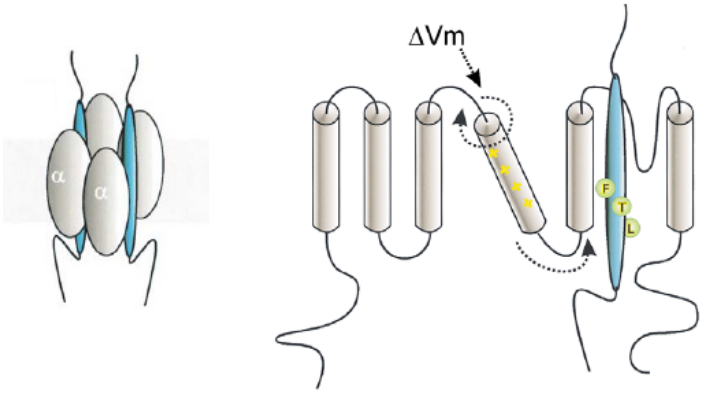


**Figure 2.8 KCNE and KCNQ1 association.** Left, Proposed association of 2 KCNE beta subunits with the Kv channel alpha subunit tetramer (though the stoichiometry and exact localization is not conclusively known). Right, KCNE interacting with the p-loop neighboring structures, the activation triplet is shown. The positive charged amino acids from the S4 voltage sensor domain are highlighted. The movement of the S4 under voltage changes (delta V) is depicted (adapted from Melman et al. 2002).

Concerning the molecular mechanism by which KCNE subunits could modify KCNQ1 kinetics, one possibility is that KCNE subunits are able to alter the behavior of the KCNQ1 voltage sensing S4 domain. This hypothesis has been directly tested for KCNQ1/KCNE1 and KCNQ1/KCNE3 complexes. In the case of the first complex, it has been shown that KCNE1 does not alter the behavior of the S4 domain during the transition from resting to active state. Therefore it was speculated that the slow activation of the KCNQ1/KCNE1 channel complex is probably due to slow opening of the intracellular gate (Nakajo and Kubo 2007; Rocheleau and Kobertz 2008). On the other hand, KCNE3 has been shown to alter the voltage-sensing domain S4, by uncoupling its movements from the intracellular gate opening, thereby facilitating the active state of the channel at hyperpolarizing potentials.

## 2.7.3 Functional Roles of KCNQ1/KCNE1

### 2.7.3.1 KCNQ1/KCNE1 in Heart

The cardiac action potential is comprised of four phases, each one characterized by specific ionic currents (Figure 2.9). During the first phase (phase 0) the cell passes from the resting membrane potential (close to the equilibrium potential for $K^+$, -84 mV) to a depolarized membrane potential due to the activation of fast $Na^+$ channels (SCN5A) which causes a rapid influx of $Na^+$ into the cell ($I_{Na}$).

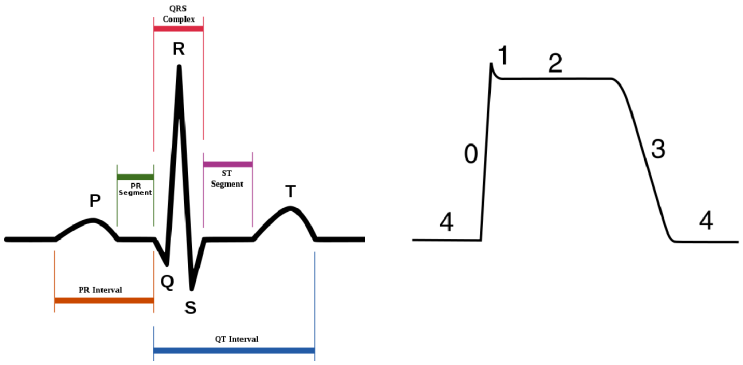


**Figure 2.9 Electrocardiogram and cardiac action potential. Left,** electrocardiogram showing the P wave (atrial depolarization), the QRS complex (reflects one heartbeat and corresponds to the depolarization of the right and left ventricles), the T wave is the repolarization of the ventricles, and the QT interval (measured from the beginning of the QRS complex to the end of the T wave). **Right,** cardiac action potential composed of 5 phases from 0 to 4 (a detailed description in the main text).

The next phase (phase 1) starts when $Na^+$ channels inactivate and outward $K^+$ currents, promoted by Kv4.2/4.3, get activated ($I_{to}$). During phase 2 there is a plateau, representing an ionic equilibrium between the inward movement of $Ca^{++}$ ($I_{ca}$) through L-type $Ca^{++}$ channels and outward movement of $K^+$ ions (slowly activating delayed rectifier $K^+$ current, $I_{ks}$) through the slow delayed rectifier KCNQ1/KCNE1 channel complex. In this phase also $Na^+/Ca^{++}$ exchanger current, $I_{Na,Ca}$ and the $Na^+/K^+$ pump current, ($I_{Na,K}$) are involved. In phase 3, there is a rapid membrane repolarization because L-type $Ca^{++}$ channels close while delayed rectifier KCNQ1/KCNE1 channel complex is still open, thereby it hyperpolarizes the cell membrane and activates rapid delayed rectifier hERG channels, probably co-assembled with KCNE2, and inward rectifying Kir2.1/2.2/2.3 channels ($I_{k1}$).

KCNQ1/KCNE1 channels close when the membrane potential is back to resting conditions (-80 mV). The Kir 2.1/2.2/2.3 are major players in phase 4, where resting conditions are maintained till the next stimulus comes and activates $Na^+$ channels, thereby reinitiating the cycle.

Both KCNQ1 and KCNE1 subunits are almost exclusively localized in atrial and ventricular myocytes, where they were shown to co-assemble into functional heteromeric complexes. The KCNQ1/KCNE1 function is essential to get the cell ready for the next stimulus, repolarizing the cell to its resting membrane potential values slow enough to allow the other $K^+$ channels (hERG and kir) to activate. KCNQ1

homotetramers could not perform this function alone since this complex would open and close too fast, thereby being unable to maintain the appropriate repolarization of cardiac myocytes. The modulatory role of the beta subunit KCNE1 is therefore essential for the physiological role of the complex.

Mutations that impair or modify KCNQ1/KCNE1 kinetics provoque a dramatic effect on cardiac activity, causing arrhythmias (irregular beat rhythmicity). Mutations on either KCNE1 or KCNQ1 extend the cardiac action potential, lengthening the so called "Q to T" interval (which represents the time in an electrocardiogram (ECG) recording for both ventricular depolarization and repolarization to occur, Figure 2.9), causing the „Long QT Syndrome" in humans (Wang et al. 1996). These mutations can be dominant or recessive, causing Romano-Ward Syndrome (RWS) (Chouabe et al. 1997; Wollnik et al. 1997), or Jervell-Lange Nielsen Syndrome (JLNS), respectively. KCNQ1 or KCNE1 recessive mutations in homozygosis provoque a total loss of the channel function. In this case, cardiac arrhythmia is also associated with congenital deafness (Vetter et al. 1996; Splawski et al. 1997).

### 2.7.3.2 KCNQ1/KCNE1 in Inner Ear

The cochlea contains the sensory organ of hearing, the organ of Corti. The KCNQ1/KCNE1 complex was identified in apical surfaces of marginal cells in the stria vascularis, a layer of epithelial cells on the outer wall of the cochlear duct (Neyroud et al. 1997). The stria vascularis maintains the special ionic composition of the endolymph, the liquid that fills the scala media, one of the three fluid-filled compartments of the cochlea. The high $K^+$ concentration present in the endolymph bathes the hair cells, the sensory receptors present on the basilar membrane in the organ of Corti. Under stimulation, $K^+$ and not $Na^+$, enters into the hair cell creating a depolarizing current called mechano-electric transduction current.

The KCNQ1/KCNE1 complex is involved in maintaining the elevated $K^+$ concentrations in the endolymph (Nicolas et al. 2001). Remarkably, KCNQ1 homomers alone are not able to perform this function, since the channel is inactivated and none conducting at the membrane potential of the marginal cells of the stria. Mutations on either KCNQ1 or KCNE1 produce severe deafness. KO mice models for either one the proteins show inner ear defects, resembling those observed in Jervell and Lange–Nielsen syndrome (JLNS) in humans.

### 2.7.3.3 KCNQ1/KCNE1 in Kidney

The nephron is the basic structural and functional unit of the kidney. Each nephron is composed of an initial filtering component (the glomerulus) and a tubule specialized for reabsorption and secretion (the renal tubule). The renal tubule itself is subdivided into several functional and structural parts, the proximal tubule being one of these components. Across the luminal membranes of proximal tubules electrogenic $Na^+$ coupled transport of substrates, such amino acids and glucose, depolarizes the membrane. In order to repolarize the membrane, slow conductance $K^+$ channels activate under depolarization (Lang et al. 1986; Lang and Rehwald 1992). Then, repolarization of the cell membrane is essential to maintain the negative voltages necessary for the $Na^+$ reabsorption.

Given the fact that KCNQ1 and KCNE1 are expressed in proximal tubules of the kidney (Sugimoto et al. 1990; Vallon et al. 2001) and that the channel complex is voltage dependent, led to the speculation that both proteins might be involved in proximal tubule membrane repolarization (Arrighi et al. 2001; Demolombe et al. 2001). Accordingly, mice lacking the KCNE1 protein suffer from increased renal excretion of $Na^+$ and glucose (Vallon et al. 2001; Warth et al. 2002a). However, *kcnq1*$^{-/-}$ animals do not show any impairment in renal transport under basal conditions, but only under substrate overloading (Vallon et al. 2005).

### 2.7.3.4 KCNQ1/KCNE1 in Pancreas

The pancreas is a gland organ in the digestive and endocrine system of vertebrates. It assolves both endocrine and exocrine functions, being responsible for producing several important hormones (including insulin, glucagon, and somatostatin), as well as secreting digestive enzymes into the small intestine. KCNQ1/KCNE1 complex is expressed in exocrine pancreas, where it regulates $Cl^-$ secretion, contributing to enzymatic granules release (Demolombe et al. 2001; Thevenod 2002). KCNQ1 seems to be also involved in regulating the membrane potential of insulin secreting cells (endocrine pancreas), since pharmacological inhibition of KCNQ1 led to increase in insulin secretion (Ullrich et al. 2005).

## 2.7.4 Functional Roles of KCNQ1/KCNE2

### 2.7.4.1 KCNQ1/KCNE2 in Stomach

The adult human body produces 2-3 liters of gastric juice per day. Gastric juice is strongly acidic liquid (pH around 1-2), whose major components HCl, KCl, NaCl and digestive enzymes. Gastric glands produce the gastric acid, while surface epithelial cells secrete alkaline mucus to protect the tissue from the acidic gastric juice. Deep in the gastric gland, three major cell types have been described: parietal, chief, and enterochromaffin-like cells. (Figure 2.10)

Upon food stimulus, parietal cells start to secrete $H^+$ and $Cl^-$ into the lumen of the gastric gland. Chief cells release pepsin protease precursors and are located at the base of the gland, while enterochromaffin-like cells have paracrine and endocrine roles and play important regulatory roles for the gastric secretory function.

The biophysical properties of KCNQ1/KCNE2 channel complex together with the pharmacological inhibition of acid gastric production by C293B, led to the hypothesis that KCNQ1/KCNE2 complexes are involved in gastric acid secretion (Grahammer et al. 2001a). KCNQ1 and KCNE2 form a functional complex characterized by voltage-insensitive background currents activated up on cAMP, $PIP_2$ or acidic pH stimulation (Tinel et al. 2000; Heitzmann et al. 2007).

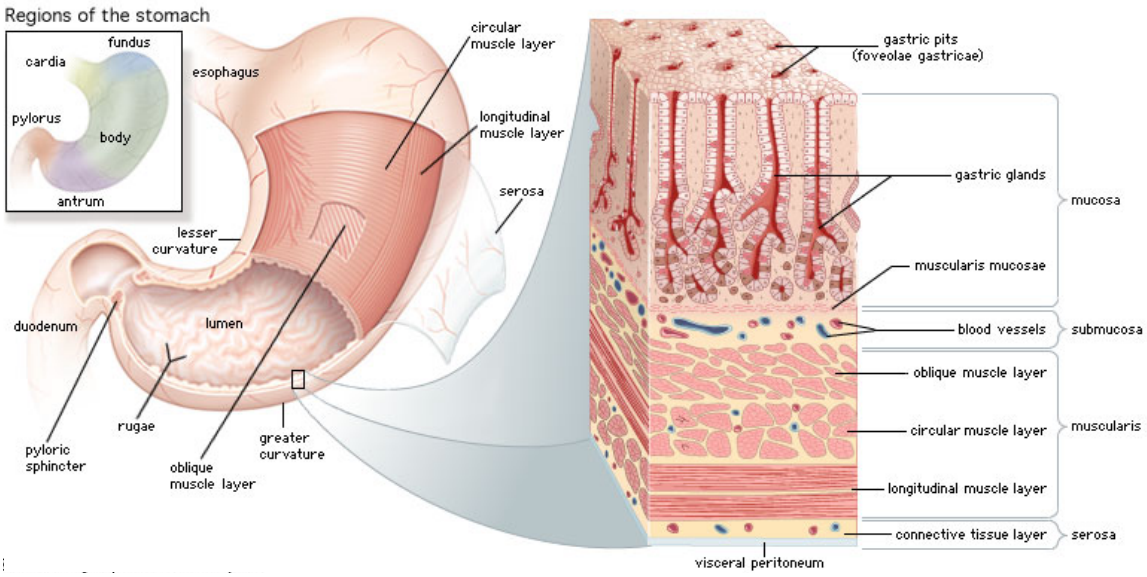


**Figure 2.10 Histology of the stomach.** On the left, gross stomach anatomy showing muscle layers, esophagus and the pyloric sphincter, as well as the lumen. On the right, a three-dimensional view of layers of the stomach. The stomach wall is composed of four layers: mucosa, submucosa, muscularis and serosal. The gastric glands are located in the mucosa and the gastric pits face the lumen of the stomach (adapted from Encyclopedia Britannica).

In the model described by Heitzmann et al., acid secreting parietal cells harbor two different populations of vesicles containing either $H^+/K^+$ ATPase or KCNQ1/KCNE2. Upon stimulus, both types of vesicles fuse to the large canaliculi, deep invaginations of the plasma membrane. $H^+/K^+$ ATPase import $K^+$ in, and pump $H^+$ out of the cell, whilst KCNQ1/KCNE2 lowers the intracellular $K^+$ concentration, building up luminal $K^+$, an absolute requirement for $H^+$ extrusion. In support of their functional involvement in gastric physiology, KCNQ1, KCNE2 or $H^+/K^+$ ATPase KO mice show gastric hyperplasia, as well as achlorhydria (Scarff et al. 1999; Lee et al. 2000; Roepke et al. 2006).

### 2.7.4.2 KCNQ1/KCNE2 in Thyroid

The thyroid gland secretes thyroxin (T4) and triiodothyronine (T3) hormones, which play a major role in the regulation of metabolism. These hormones (T4 is converted into the active form T3 in target tissues) are involved in diverse processes from bone growth, neuronal maturation to protein synthesis and acceleration of basal metabolism.

The synthesis of T4 hormones involves the attachment of iodine atoms (4 in T4) to the thyroglobulin, for this purpose iodide ions are actively loaded into the thyrocyte by the basolateral $Na^+$/iodide symporter NIS. This cotransport requires the $Na^+/K^+$ ATPase $Na^+$ efflux and probably KCNQ1/KCNE2 channel complex in the basolateral membrane, to recycle the $K^+$ back to the extracellular space (Roepke et al. 2009). Indeed, it has been recently reported that *kcne2*$^{-/-}$ animals suffer from hypothyroidism, dwarfism, alopecia and cardiac abnormalities due to the inability to produce T4/T3 hormones. These phenotypes were alleviated by complementing the diet with T3/T4 hormones.

### 2.7.4.3 KCNQ1/KCNE2 in Heart

KCNE2 has been reported to be expressed in heart and to interact with HERG (Abbott et al. 1999) and with KCNQ1 channels. Its malfunction has been associated with cardiac arrhythmias and atrial fibrillations (Yang et al. 2004). Moreover, *kcne2*$^{-/-}$ mice suffer from cardiac hypertrophy. It is however important to mention that the cardiac pathologies linked to KCNE2 deficiencies could be due to primary electrical defects in myocytes or to secondary effects of thyroid dysfunction (Roepke et al. 2009).

## 2.8 Putative Functional Roles of KCNE3

### 2.8.1 KCNE3 in Intestinal Tract

The small intestine is the organ where most of the digestion and absorption of nutrients takes place, and it is subdivided into duodenum, jejunum and ileum (Figure 2.11). The latter is followed by caecum and colon (Figure 2.12). The first literally refers to the "dead-end" structure connecting the ileum with the colon, which is found in herbivores and is needed to digest vegetal material, such as cellulose. In most carnivores, however a vermiform appendix replaces this structure. The final water and salt absorption takes place in the colon, where stools are dehydrated and finally expelled out of the intestinal tract.

At the microscopic level, a small intestine transversal section reveals a highly invaginated epithelia consisting of villi and crypts (Figure 2.11).

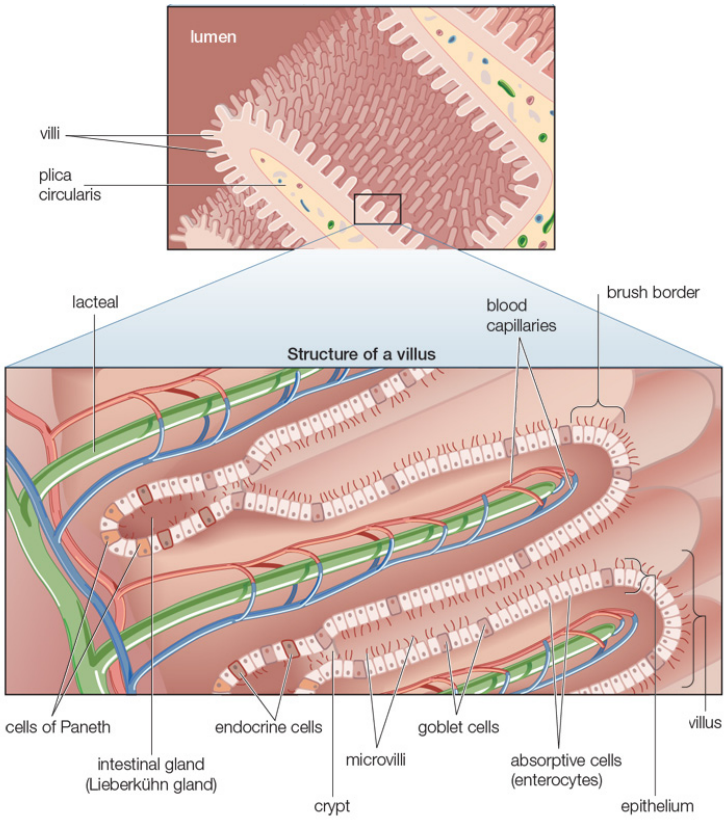


**Figure 2.11 Anatomy of the small intestine.** The upper picture displays a cross section of the small intestine lumen showing the tongue shaped structure called villi. The lower picture is a higher magnification of an intestinal crypt, showing the different cell population, the blood supply, and lymphatic system vessels (lacteal) (adapted from Encyclopedia Britannica).

The function of the villi and enterocyte microvilli is to increase the surface available for nutrients absorption. On the other hand, the colon is devoid of villi and instead presents large intestinal crypts (Figure 2.12).

Glucose and amino acid uptake is performed by the villi and it is coupled to $Na^+$ reabsorption. Basolateral $K^+$ channels, like KCNQ1, actively contribute to maintain the cell membrane potential at its resting value, thereby helping in substrate loading.

Although being mainly an adsorptive tissue, the intestine has also secretory properties, with $Cl^-$ and $HCO_3^-$ secretion taking place at intestinal crypts. $Cl^-$ is basolaterally imported into the cell through the 1 $Na^+$, 2 $Cl^-$ and 1 $K^+$ cotransporter NKCC1. $Cl^-$ leaves the cell apically by passing through the cAMP activated CFTR channel.

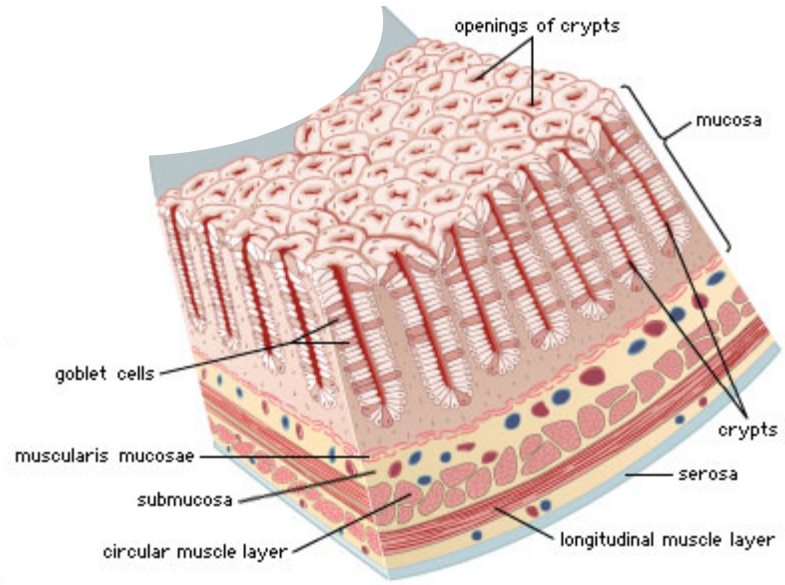


**Figure 2.12 Histology of the colon.** Three-dimensional view of layers of the colon. The Colon is composed of several layers: mucosa, muscularis mucosae, submucosa, two muscle layers, and the serosa. Note that in the colon the openings of the colon crypts face directly to the lumen of the colon (adapted from Encyclopedia Britannica).

The cAMP signaling cascade is activated by multiple stimuli: prostaglandin E2, serotonin, vasoactive intestinal polypeptide (VIP), pituitary adenylate cyclase-activating polypeptide (PACAP), and by bacterial toxins, e.g., cholera toxin. Remarkably, the effect of cholera toxin is not only on the enterocyte cAMP cascade, but it includes also increase in blood supply, immune system activation and enteric nervous system alterations (Nocerino et al. 1995; Farthing et al. 2004). These multiple synergistic effects are responsible for the overwhelming intestinal $Cl^-$ secretion and the dramatic water loss observed in patients affected by cholera.

It is important to mention that, since mucosal cells, lymphatic system, neurons, smooth muscle, blood vessels, immune system cells, and endocrine cells coordinate with the enterocytes to facilitate nutrient absorption and electrolyte secretion, it is not an easy task to study intestinal physiology, since *in vitro* and even *ex vivo* preparations will always lack one or several modulatory factors.

Basolateral activation of $K^+$ channels not only recycles $K^+$ to the extracellular space to fuel NKCC1 and $Na^+/K^+$ ATPase, but also hyperpolarizes the cell membrane. Both actions increase the driving force for apical $Cl^-$ exit (Schroeder et al. 2000; Dedek and Waldegger 2001; Kunzelmann et al. 2001; Matos et al. 2007). Interestingly, in duodenum another cAMP stimulated $K^+$ conductance has been observed, which differs from KCNQ1/KCNE3 channel complex in its large single channel conductance (McNicholas et al. 1994). This would explain why cAMP stimulated $Cl^-$ secretion is only partially abolished (50% of control levels) in KCNQ1-deficient small intestine (Vallon et al. 2005). In addition, $Ca^{++}$ activated KCNN4 $K^+$ channels are expressed in basolateral membranes of enterocytes in small intestine and colonic epithelia, and $Ca^{++}$ activated $Cl^-$ channels have been identified in goblet cells but not in enterocytes. KCNN4 would extrude $K^+$ upon intracellular $Ca^{++}$ increases, hyperpolarizing the cell membrane and thus helping $Cl^-$ leaving the apical membrane through CFTR. Intracellular $Ca^{++}$ waves would stimulate mucous secretion by goblet cells, as well as $Cl^-$ and water flush from basal crypt cells. Therefore, KCNN4 could possibly compensate for the loss of functional KCNQ1/KCNE3 complex in this tissue.

### 2.8.2 KCNE3 in Heart

Several reports have claimed that KCNE3 might play an essential role in cardiac physiology by assembling with diverse $K^+$ channels like KCNQ1, HERG, and Kv4.3. (Mazhari et al. 2002; Ohya et al. 2002; Lundby and Olesen 2006), although the precise function and kinetics remained unclear. In addition, several sequence variations in the KCNE3 gene have been linked to diverse cardiac pathologies like Long QT syndrome (Ohno et al. 2009), Brugada syndrome (Delpon et al. 2008) or atrial fibrillation (Lundby et al. 2008).

Ohno and coworkers in 2009 conducted a genetic screening in 485 Long QT syndrome (LQTS) probands and identified KCNE3 T4A, P39R, R99H sequence variations. This group suggested that KCNE3 would assembly with KCNQ1 modifying the slow

activated currents and the voltage dependence towards faster activation and voltage independency. The authors speculated that the lack of the KCNE3 subunit would reduce repolarizing $K^+$ currents in the myocardium. No direct evidence was provided to support this hypothetic function of KCNQ1/KCNE3 complexes in cardiac muscle, and it is still unclear how this complex would work in conjunction with KCNQ1/KCNE2 and KCNQ1/KCNE1 heterooligomers, which are also present in these cells.

To date only two single reports detected relatively low KCNE3 transcripts in human cardiac tissue by real time PCR experiments (Bendahhou et al. 2005) or in situ hybridization (Lundquist et al. 2005). Unfortunately, these studies lack of appropriate controls (e.g. KCNE3 deficient tissues and specific antibodies) and do not demonstrate the presence of KCNE3 protein in murine and human cardiac tissue.

### 2.8.3 KCNE3 in Airways

The pulmonary airway belongs to the respiratory system, conceptually beginning at the nose and mouth, and terminating in the alveoli. At the cellular level, the airway surface is populated by columnar ciliated, fluid secreting cells, non-ciliated cells, mucous secreting goblet cells, basal and Clara cells. Basal cells work as scaffold for the columnar cells (Shebani et al. 2005). Clara cells secrete multiple substances to protect airway epithelium and detoxify inhalated substances. Ciliated cells create a fluid layer (known as Airway Surface Liquid (ASL)) on top of the cilia, which helps the mucous to move upwards. CFTR channel localized primarily at the apical surfaces of epithelial cells lining the airway and in submucosal glands (Engelhardt et al. 1992; Kalin et al. 1999).

The ciliated cells carry out two important physiological functions: $Cl^-$ secretion and $Na^+$ absorption (Welsh 1987). Cl secretion provides the osmotic driving force for epithelial water secretion, since paracellular water movement accompanies $Cl^-$ secretion. $Cl^-$ may exit the apical membrane of ciliated cells through cAMP-activated channels (CFTR) or $Ca^{++}$ activated $Cl^-$ channels (CaCC) (Blouquit et al. 2006). In order for $Cl^-$ to be extruded from the cell, there must be an electrochemical gradient across the membrane, which drives its movement. Activation of basolateral $K^+$ channels, cAMP (KCNQ1) or $Ca^{++}$ activated (KCNN4), hyperpolarizes the cell membrane, counteracting the depolarizing effect of $Cl^-$ efflux, thus increases electrochemical driving force for apical $Cl^-$ secretion. Other proteins that play a role in $Cl^-$ secretion are: the $Na^+/K^+$ pump that

exchange intracelluar $Na^+$ for $K^+$ and, the NKCC1 that cotransports 1 $Na^+$, 2 $Cl^-$ and 1 $K^+$ ions simultaneously into the cell. In conclusion, basolateral $K^+$ channels are needed to recycle $K^+$ back to the extracellular space to avoid intracellular $K^+$ overloading. Hence, apical $Cl^-$ secretion is coupled to basolateral $K^+$ outward currents (McCann and Welsh 1990; Quinton 1990).

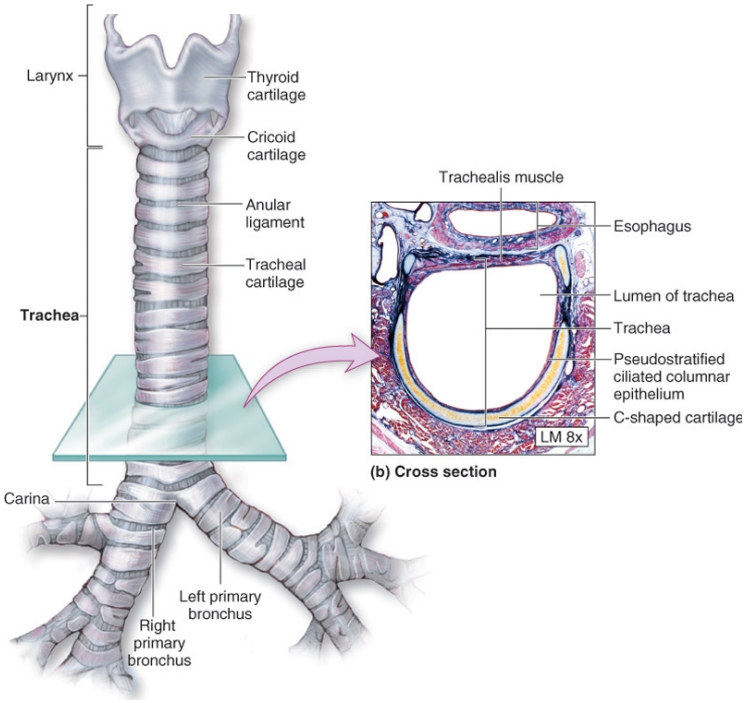


**Figure 2.13 Anatomy of the upper airways.** On the left, gross anatomy of the airways showing the larynx, trachea and main primary bronchi. On the right, cross section of the trachea showing a detailed histology, where the ciliated and columnar epithelium can be seen (adapted from Encyclopedia Britannica).

Regarding the molecular identity of basolateral $K^+$ channels, KCNQ1 has been detected in trachea and has been described as the dominant $K^+$ conductance in basolateral membranes of ciliated cells (MacVinish et al 1998, Mall et al 2000, Grahammer et al 2001). The fact that KCNE3 mRNA was detected in trachea led to the speculation that KCNQ1/KCNE3 complexes would be directly involved in cAMP-stimulated $Cl^-$ secretion. Besides, also KCNN4 was reported to play a role in tracheal basolateral $K^+$ transport (Devor et al. 1996; Ishii et al. 1997; Grahammer et al. 2001b).

CFTR mutations, which are the cause of cystic fibrosis in humans, lead to excessive $Na^+$ absorption and lack of $Cl^-$, bicarbonate and water secretion from respiratory tissues. This chain of events leads to dehydrated mucous, acidic ASL, and consequently compromised mucociliary clearance and lung defense. Because of the severe impairment in respiratory tissue physiology, Cystic Fibrosis causes progressive disabilities and early death.

In mice however, CFTR deletion did not result in any obvious respiratory complication. This is probably due to, first, the different anatomy of the airways, and second, to the fact that murine upper airways do not only express CFTR as apical $Cl^-$ conductance, but also a $Ca^{++}$ activated $Cl^-$ channel (CaCC), which might compensate for the loss of CFTR (Clarke et al. 1994; Grubb et al. 1994).

### 2.8.4 KCNE3 in Central Nervous System

KCNE3 has been reported to be broadly expressed in brain together with Kv2.1 and Kv3.1 to alter neuronal excitability (McCrossan et al. 2003). KCNE3 would slow Kv3.1 gating, broading the action potential and lowering the maximal firing frequency in selected neuronal subpopulations. Besides, in hippocampus and other regions, KCNE3 would downregulate the Kv2.1 delayed rectifier currents and slow its deactivation, producing a delayed repolarization.

Alzheimer disease is the most common of dementia in humans. This disease has been associated with apoptotic neuronal cell death triggered by deposits of amyloid peptide in the brain of affected patients. Pannaccione et al. in 2007 reported that expression of the Kv3.4/KCNE3 complex is upregulated by the amyloid peptide. Kv3.4 is expressed in neurons of the adult dentate gyrus and in the mossy fibers terminals of the hippocampus, where it regulates action potential length and membrane repolarization in axons and pre-synaptic terminals (Heinemann et al. 1996; Rudy et al. 1999). According to the hypothesis of Pannaccione and collaborators, beta amyloid peptide would upregulate Kv3.4/KCNE3 expression in plasma membrane, leading to increased $K^+$ outward currents, which would then lower $K^+$ intracellular concentrations and directly promote cell death (Pannaccione et al. 2005; Pannaccione et al. 2007).

### 2.8.5 KCNE3 in Skeletal Muscle

Myocytes, the cellular units of skeletal muscle fibers, are excitable cells that transduce the chemical signal of neuromuscular synapses into electrical membrane potential depolarizations and mechanical contraction.

Kv3.4/KCNE3 heteromeric $K^+$ channels have been suggested to set the resting membrane potential of skeletal myocytes (Abbott et al. 2001; Abbott et al. 2006). Abbott et al reported a prominent KCNE3 expression in human muscle tissue, and suggested that KCNE3 would assembly with Kv3.4, alter the dependence of this $K^+$

channel on voltage and intracellular pH, accelerate its recovery from inactivation, and increase its single channel conductance.

Moreover, a sequence variant on KCNE3 gene (R83H) was reported to decrease $K^+$ currents upon co-expression in heterologous cells in a dominant negative manner (Abbott et al. 2001). Importantly, the R83H sequence abnormality was found in patients from two families with periodic paralysis and was absent in 120 unaffected individuals, leading to the conclusion that mutations in *kcne3* might underlie some forms of this genetically heterogeneous human disease. Periodic paralysis is an hereditary disease that leads to frequent muscle feebleness, debility and even paralysis after exercise, fasting, high carbohydrate intake or emotional stress. Three distinct types of periodic paralysis have been classified according to the conditions under which muscle cell irresponsiveness becomes manifest: the hypokalemic-type, where muscular deficit is promoted by low blood levels of $K^+$; the hyperkalemic-type, by high blood levels of $K^+$; the paramyotonia congenital-type, where muscle contractures are present either in low or high levels of $K^+$ in the bloodstream. KCNE3 R83H would provoke an abnormal positive skeletal muscle membrane potential, causing irresponsiveness of the muscular cell to the contracting stimulus. These data have been however heavily disputed, since several other groups have found KCNE3 R83H in healthy humans suggesting that it is a benign polymorphism (Sternberg et al. 2003; Jurkat-Rott and Lehmann-Horn 2004).

## 2.9 Aim of the Study

When overexpressed in heterologous systems, KCNE3 is able to interact with several pore-forming $K^+$ channel alpha subunits greatly modifying their currents. Based on these *in vitro* evidences, KCNE3 has been proposed to serve different roles in multiple tissues, including brain, heart, muscle, colon and kidney (McCrossan and Abbott 2004). Additional reports have also linked sequence variations in the KCNE3 gene to cardiac (Delpon et al. 2008; Lundby et al. 2008; Ohno et al. 2009) and skeletal muscle pathologies in human (Abbott et al. 2001). Based on the literature, the overall picture of KCNE3 physiological function is rather complex and heterogeneous, and its direct involvement in pathologies is still speculative and far from being conclusively proven.

In order to study the physiological role of KCNE3 *in vivo* and to address its potential pathological implications, we generated *kcne3*$^{-/-}$ mice. Although this approach has been often criticized (Routtenberg 1995), we believe that reverse genetics, in particular the

KO approach, is an invaluable tool to define or clarify the *in vivo* function of the protein of interest. In addition, tissues from KO animals, which are completely devoid of the protein of interest, provide the most specific and valuable controls to study protein localization by conventional biochemical and immunohistochemical techniques. For these reasons, we undertook a genetic approach to study KCNE3 expression pattern and its function *in vivo*.

# 3 MATERIALS

## 3.1 Chemicals and Enzymes

Unless otherwise specified, standard chemicals companies BioRad (Hercules, USA), Boehringer (Mannheim), Fluka (Neu-Ulm), Merck (Darmstadt), Roth (Karlsruhe), Riedel de Haen (Seelze), Serva (Heidelberg) and Sigma ( Munich, Germany).
Restriction enzymes were purchased from New England Biolabs (Schwalbach / Taunus), Invitrogen (Eggenstein) and Fermentas (St. Leon-Rot). The oligonucleotides were synthesized by the company Biomer (Ulm).

## 3.2 Buffers and Solutions

| | |
|---|---|
| DEPC water | 900µl diethylpyrocarbonate in 450ml $H_2O$. Incubate stiring overnight at 37 ° C, and autoclave |
| Dextran solution | Add some Dextran granules in $H_2O$;take 250µl and add to 15ml of 100% EtOH |
| DNA loading buffer (10x) | 0.25% (w / v) bromophenol blue, 0.25% (w / v) Xylencyanol, 30% (w / v) glycerol |
| Fixation buffer | 4% PFA in PBS |
| Homogenization buffer (Membrane prep) | 140mM NaCl, 20 mM Tris, pH 7.4, 5 mM EDTA; 1xComplete (Roche). |
| IF pre treatment trachea | 0.05% trypsin in 0.1% $CaCl_2$, 0.05 M Tris, pH 7.8 |
| IF block solution | 2% normal goat serum (NGS), 1% bovine serum albumin (BSA), 0.05% Tween, and 0.2% Triton X100 in PBS |
| Ketamine-Rompun mixture | 120µl Ketamin10; 80µl 2% Rompun; 800µl PBS |
| Lysis buffer (mem.prep) | 50 mM Tris pH 6.8, 5mM EDTA, 2% SDS and Complete® protease inhibitor (Roche) |
| Lysis buffer (ES cells) | 0.1% SDS, 14 mg / ml proteinase K |

| | |
|---|---|
| Lysis buffer (tail cuts) | 50 mM Tris, 100 mM EDTA, 100 mM NaCl, 1% SDS, pH8, 0.5 mg / ml proteinase K |
| Low-TE buffer | 10 mM Tris pH 7.5, 0.1 M EDTA pH 8, pH 7.1 with HCl |
| $Na^+$-phosphate buffer | Na-phosphate buffer (50 mM, pH 7.4), 1% NP40 and PNGase F 0.5 U/25 µg of total protein (Roche) |
| PBS | 137mM NaCl, 7.4 mM Na 2 HPO 4, 2.7 mM KCl, 1.5 mM KH 2 PO 4, pH 7.4 |
| Ponceau Red (10x) | 2 g Ponceau S, 30 g trichloroacetic acid, sulfosalicylic 30g; to 100ml water |
| Protein Transfer Buffer | 25mM Tris, 200mM glycine, pH 8.3 with HCl, 20% methanol |
| RNase buffer | 0.5 M NaCl, 0.01 M Tris pH 7, 1 mM EDTA, 0.02 mg / ml RnaseA |
| SB-hybridization buffer (Speed-hybrid 2) | 7% SDS, 10% polyethylene glycol, 1.5 x SSPE |
| SB-Wash buffer A | 0.5% SDS, 2% SSC |
| SB-Wash buffer B | 0,1% SDS; 0,2% SSC 0.1% SDS, 0.2% SSC |
| Separating gel buffer | 1.5 M Tris, 0.4% SDS, pH 8.8 with HCl |
| SDS (10%) | Heat 100 g SDS in 900 ml of H 2 O at 68 ° C, adjusted to pH 7.2 with HCl, to replenish 1L with H 2 O |
| SDS-PAGE running buffer (10x) | 250mM Tris, 2M glycine, 1% SDS |
| SDS-PAGE sample buffer (5x) | 250mM Tris, 10% SDS, 0.5% bromophenol blue, 50% glycerol solution, at 50 ° C (+5% β-mercaptoethanol for reducing conditions) |
| Sequencing buffer | 5 mM MgCl 2, 200mM Tris, pH 9 |
| SSC (20x) | 3M NaCl, 0.3 M sodium citrate, pH 7 |
| SSPE (20x) | 3M NaCl, 0.2 M NaH 2 PO 4, 20 mM EDTA, pH 7.4 |
| Stacking gel buffer (4x) | 0.5 M Tris, 0.4% SDS, pH 6.8 |
| TAE buffer (50x) | 0.2 M Tris-acetate, 10 mM EDTA pH 7.4 |
| TBS buffer (10x) | 1.37M NaCl, 27 mm KCl, 250mM Tris, pH 7.4 with |

| | |
|---|---|
| | HCl |
| Toluidine Blue Stock | Toluidine blue O (Sigma) 1 g ;70% alcohol 100 ml |
| Toluidine Blue working | Toluidine blue stock solution 5 ml; 1% Sodium chloride, pH 2.3 45 ml |
| Trypsin / EDTA | 0.25% trypsin, 0.02% EDTA in PBS |
| WB-block buffer | 5% skimmed milk powder, 0.1% NP-40 in TBS |
| WB-wash buffer | 0.1% NP40 in 1xTBS |

## 3.3 Bacterial Culture

### 3.3.1 Media

| | |
|---|---|
| LB medium | 0.5% NaCl, 0.5% yeast extract, 0.1% glucose, pH 7 |
| LB-amp medium | 100µg/ml ampicillin in LB medium |
| LB-amp plates | 15g Agar in 1000 ml LB-Amp medium |
| LB agar | LB medium with 1.5% agar |
| LB-Amp agar | LB agar with 100µg/ml ampicillin |
| Top Agar | LB medium with 0.7% agarose |

## 3.4 Cell Culture of Embryonic Stem Cells

| | |
|---|---|
| R1 ES cells | Murine embryonic stem cell line (Nagy et al., 1993) |

### 3.4.1 Media and Solutions

| | |
|---|---|
| DMEM (+ Glutamax) | Gibco # 61965026 |
| Fetal calf serum (FCS) | Gibco # 10270106 |
| MEM amino acid cocktail | Gibco # 11140035 |
| Penicillin / streptomycin | Gibco # 15070022 |
| DMEM | Gibco # 42430025 |
| Glutamine | Gibco # 25030024 |
| Sodium pyruvate | Gibco # 11360039 |
| 2-mercaptoethanol | Gibco # 31350010 |
| Geniticin (G418, Neomyzin) | Gibco # 10131019 |
| Trypsin / EDTA (for MEF) | Gibco # 25300054 |

| | |
|---|---|
| Trypsin / EDTA (for ES cells) | Gibco # 25200056 |
| PBS | Gibco # 18912014 |
| Oil | Sigma # M-8410 |
| 0.1% gelatin | Sigma # G-1890 |
| Mitomycin C | Sigma # M-0503 |
| MEF medium | DMEM + Glutamax, 9% FCS, 1x MEM, 1x Pen / Strep |
| ES medium | DMEM, 15% FCS, 2 mM glutamine, 1x MEM, 1x Pen / Strep, 1x Nukleosidmix, 1x sodium pyruvate, 0.1 mM 2-mercaptoethanol, 1000 U / ml LIF |
| ES-selection medium | ES-medium, 200-300 µg / ml G418 |
| Electroporation buffer | 20 mM Hepes, 137 mM NaCl, 5 mM KCl, 0.7 mM Na 2 HPO 4, 6 mM glucose, pH 7.5 |
| ES-freezing | 50% FCS, 40% ES medium, 10% DMSO |

## 3.5 Plasmids

| | |
|---|---|
| pBluescript SK + | From Stratagene, the vector contains an f (1) - and a *ColE1-origin of replication* (ORI), ampicillin resistance, a bacterial lacZ gene, and a multiple cloning site |
| pcDNA3 | Mammalian plasmid from Invitrogen, contains a CMV promoter, a f (1) - and a *ColE1-origin of replication* (ORI), ampicillin resistance, and a multiple cloning site |

## 3.6 Oligonucleotides

| **Purpose** | **Sequence (forward/reverse)** |
|---|---|
| Genotyping | CGCAAGCTTGTCATGGAGACTACCAATGGAACG/ CGCGGTACCTTAGATCATAGACACACGGTTC |
| Southern blot 5’ probe | CACTCTGGGTCTTTTGAATCC/ CCACATCCAAATTGTTTCTGA |

| | |
|---|---|
| Southern blot 3'probe | CAAAGAAGGAGGAAAAGGAA/<br>ATAAAGGGCTGGCTCTGAAA |
| Northern KCNE3 probe | CACATTCCAGCTCTTCCCATACC/<br>CACATCAGATCATAGACACACGG |
| Northern beta actin probe | TTCTTTGCAGCTCCTTCGTTGCCG/<br>TGGATGGCTACGTACATGGCTGGG |

## 3.7 Antibodies

### 3.7.1 Primary Antibodies

| **Antibodies** | **Species** | **Dilution** | **Company** |
|---|---|---|---|
| Actin | Rabbits polyclonal | 1:1000 (WB) | Sigma |
| $H^+/K^+$ ATPase beta | Mouse | 1:500 | Dianova |
| KCNQ1 | Rabbit polyclonal | 1:300 (WB)<br>1:500 (IF) | Jentsch lab |

## 3.8 Electrophysiology

### 3.8.1 Chemicals

All compounds (carbachol, ATP, 3-Isobutyl-1-Methylxanthine (IBMX), forskolin, amiloride, indomethacin were of highest available grade of purity and were from Sigma (Taufkirchen, Germany). 293B was gifts from Aventis Pharma (Frankfurt,Germany).

### 3.8.2 Solutions

| | |
|---|---|
| Ice cold buffer solution 1 | (in mM) NaCl 145, $KH_2PO_4$ 0.4, $K_2HPO_4$ 1.6, d-glucose 6, $MgCl_2$ 1, Ca-gluconate 1.3, pH 7.4 |
| Ice cold colon solution | (in mM) NaCl 127; KCl 5; Na-pyruvate 5; D-glucose 5; HEPES 10; $MgCl_2$ 1; $CaCl_2$ 1.25, pH 7.4. |
| $Ca^{++}$ free solution | (in mM) NaCl 127; KCl 5; Na-pyruvate 5; D-glucose 5; HEPES 10; $MgCl_2$ 1; EDTA 5, pH 7.4 |
| Pipette solution | (in mM): K-gluconate 95; KCl 30; $NaH_2PO_4$ 1.2; $Na_2HPO_4$ 4.8; $CaCl_2$ 0.73; $MgCl_2$ 2.38; EGTA 1; D-glucose 5; ATP 3. |
| Bath solution | (in mM): NaCl 145; $K_2HPO_4$ 1.6; $KH_2PO_4$ 0.4; $CaCl_2$ 1.3; $MgCl_2$ 1; D-glucose 5; HEPES 5, pH 7.4 |

# 4 METHODS

## 4.1 Microbiological Methods

### 4.1.1 Electroporation of Plasmid DNA into Competent Bacteria

A 50 µl aliquot of freshly thawed electrocompetent cells was mixed with an appropriate amount of DNA (1 µl of ligation reaction or 1 µl of 1/1000 dilution of a plasmid preparation) and poured into a chilled electroporation cuvette. Electroporation was conducted using a Gene Pulser (BioRad) at 2.5 kV. Then, 0.9 ml LB medium were added immediately to the cuvette, the mixture was transferred in a new tube and allowed to recover for 1 hour, at 37°C in a shaking hot plate. After recovery, the cells were carefully centrifuged and the pellet resuspended in 100 µl of LB-medium and plated on selection agar plates.

## 4.2 Molecular Biological Methods

### 4.2.1 DNA Plasmid "Mini" Preparation

This method from Holmes et al. (1981) is used for the quick analysis of clones after transformation to determine the success of transfer of the plasmid DNA into the bacterial cells, e.g. after ligation. Single colonies were chosen and incubated over night at 37°C in 2 ml selection tubes. The DNA of this culture was purified using the EZNA plasmid Miniprep Kit I (Peqlab Biotechnology) according to the manufacturer handbook.

### 4.2.2 Preparation of Plasmid DNA from 50 ml Cultures (Midiprep)

Preparations from 100 to 200 µg plasmid DNA from 50 ml cultures were done using the Jet Star plasmid purification system (Genomed). The process was carried out as described by the manufacturer, with the digestion of the bacteria is done by alkaline lysis.

### 4.2.3 Isolation of Genomic DNA from ES Cells

Confluently grown ES cells were washed twice with PBS. Then 100 µl of lysis buffer was added and were incubated overnight at 55 °C in a moist chamber. Subsequently, 10 µl LiCl (8 M) and 100 µl isopropanol were added and incubated over night in a shaking moist chamber. Afterwards, the plates were centrifuged 30 minutes at 3800 rpm. The DNA pellet was washed twice with 70% ethanol, dried at 37 °C and resuspended in 100 µl low TE.

### 4.2.4 Genomic DNA Isolation from Mouse Tail Samples

Quick isolation of genomic DNA from mouse-tails was performed using either the Invisorb kits (Invitek) according to the manufacturer's guidelines or by phenol chloroform precipitation (DNA for Southern blots).

For the phenol-chloroform precipitation the tissue was lysed with 0,5 ml tail biopsy lysis buffer in a shaking hot plate set at 55 °C overnight. Subsequently, 500 µl of 25:24:1 phenol-chloroform-isoamyl alcohol were added and the mixture was incubated 45 minutes at RT in a shaking overhead. After 30 minutes centrifugation at 14000 rpm, the upper phase was transferred into a new tube and the DNA was precipitated by 500 µl lithium chloride / isopropanol addition. Light shaking of the tubes evidenced the genomic DNA as a white filamentous precipitate. The DNA was then pelleted by 30 minutes centrifugation at 14000 rpm. The supernatant was removed and the pellet washed with 400 µl 70% ethanol. After 30 minutes centrifugation at 14000 rpm, the supernatant was again removed and the pellet air-dried. The dry pellet was resuspended in 100 µl low TE buffer and stored at 4 ° C.

### 4.2.5 Digestion of DNA by Restriction Endonucleases

Restriction enzymes were purchased together with the appropriate 10 x concentrated buffer for optimal reaction conditions. Restriction digests of plasmid DNA were performed by incubating restriction reaction mixtures for 1.5 to 2 hours at the enzyme specific temperature. Preparative restriction mixes were prepared as follows:

| Preparative Restriction Mix | |
|---|---|
| Plasmid DNA | 1-2 µg |
| Restriction Buffer 10x | 10 µl |
| Restriction Enzyme | 1.5 µl |
| (BSA 10x) | 10 µl |
| To 100 µl final volume with water | |

### 4.2.6 DNA Agarose Gel Electrophoresis

Agarose gel electrophoresis was used to separate, identify and purify negatively charged DNA fragments based on their size. DNA bands were made visible with ethidium bromide, and could be photographed in UV-Light (254 or 314 nm). Usually 0.7 to 2% gels were used. Agarose was dissolved by heating in 100 ml of the required 1x TAE buffer, and 0.5 mg/ml Ethidium Bromide was added. Samples were mixed with 10x DNA loading buffer to a final 1x concentration, and loaded into the wells. DNA fragments are separated at constant voltage (80-120 V) in TAE running buffer.

### 4.2.7 Isolation of DNA Fragments from Agarose Gels

Single electrophoretic DNA bands can be excised from the gel and the containing DNA can be eluted and used for further applications. For this purpose, the High Pure PCR Product Purification Kit (Roche) was used. The protocol, outlined in the handbook for purifying PCR fragments, was provided by the producers.

### 4.2.8 DNA Sequencing

The DNA sequence analysis was performed by chain termination method by Sanger (Sanger and Brownlee 1970). The 20 µl PCR mixture for sequencing contained 0.5-1 µg DNA, 4 µl ABI premix (ABI Prism Dye Terminator Cycle Sequencing Ready Reaction Kit, Applied Biosystems), 4 µl Sequecing buffer and 1 µl primer. The PCR program used consisted of a first step of 3 minutes at 96 °C, followed by 28 cycles comprised of 15 seconds at 96 °C, 20 seconds at 60 °C and 4 minutes at 60 °C, and terminated by a last step of 7 minutes 60 °C. To precipitate the DNA produced, 90 µl of sodium acetate (3 M) were added to the mixture and transferred together with 250 µl of 100% ethanol

into a new tube, to improve the visibility of the pellets dextran blue was added After repeated inversion, the DNA was pelleted by 15 minutes centrifugation at 14000 rpm. The pellet was washed with 70% ethanol, dried and resuspended in 20 µl Template Suppressor Reagent (Applied Biosystems). The resuspended DNA was sequenced in an ABI Prism 310 Genetic Analyzer (Perkin Elmer). The analysis of the sequences was carried out with the bioinformatics program DNASTAR.

### 4.2.9 Measuring DNA Concentrations

Nucleic acids concentration was determined by Gene Quant II photometer (Pharmacia). Briefly, 1 OD measured at 260 nm corresponds to 50 µg/ml double-stranded DNA, 40 µg/ml single-stranded DNA or RNA and 33 µg/ml oligonucleotides. As an indicator of sample purity the ratio of the OD at 260 nm and the OD at 280 nm was given, being 1.8 for pure nucleic acid solutions.

### 4.2.10 Polymerase Chain Reaction (PCR)

*In vitro* enzymatic DNA amplification is achieved via PCR (Mullis et al., 1992). The PCR reaction mix included double-strand template DNA, single-strand primers, deoxyribonucleosides (dNTPs), Taq-polymerase, buffer and salt. Reaction mixes were as follows:

| **PCR reaction** |
|---|
| 50 ng of cDNA template |
| 1 µl 5’ Primer (10 pmol) |
| 1 µl 3’ Primer (10 pmol) |
| 1 µl dNTP-Mix (2.5 mM each) |
| 5 µl 10x Polymerase Buffer |
| 2 µl $MgCl_2$ 25 (mM) |
| 1 U Taq Polymerase (Invitrogen) |
| Final volume to 50 µl with $H_2O$ |

Basic PCR cycling parameters were as follows:

Step 1: 95°C for 5 minutes

Step 2: 95°C for 30 seconds

Step 3: Annealing temperature for 30 seconds

Step 4: 72 °C for extension time (30-40 cycles from step 2)

Step 5: 72°C for 10 minutes

#### 4.2.10.1 Genotyping PCR

KCNE3 genotyping was performed on mouse genomic DNA by separate amplification of wild-type and knock-out alleles. The wild-type and knock-out alleles were amplified with primers listed in materials. Amplification conditions used were identical for both amplifications, detailed above.

### 4.2.11 RNA Preparation

The RNA was extracted from WT and KO animals, in order to compare gene expression in both genotypes. The mice were killed by cervical dislocation, and the desired tissues were removed and weighed. All tissues but stomach and intestine were immediately frozen in liquid nitrogen. Colon, small intestine and stomach were cut open lengthwise to clean all contents before freezing. The frozen tissues were crushed in a nitrogen-filled mortar with a pestle. Then, 1 ml of Trizol per 70 mg of starting tissue was added to the powder and the mixture was homogenized using a glass douncer. 200 µl of chloroform per 1 ml Trizol were added and shaken vigorously for 15 seconds. After 5 minutes incubation at RT the mixture was centrifuged at 10,000 rpm (4 °C) for 15 minutes. The upper phase was transferred into a fresh reaction vessel, mixed with 500 µl of isopropanol per 1 ml Trizol, vortexed and incubated for 10 min at RT. A further 10 min centrifugation at 10,000 rpm (4 ° C) served to pellet the RNA. The pellet was washed first with 1.5 ml ice-cold 70% ethanol and then centrifuged 5 minutes at 7500 rpm. Afterwards, 1.5 ml of ice-cold 80% ethanol and further 5 minutes centrifugation at 14,000 rpm (4 ° C). Finally, the supernatant was removed and the pellet dried. The dry pellet was dissolved, depending on the amount in 50-500 µl DEPC water.

### 4.2.12 Purification of RNA

Freshly isolated and DNase digested RNA samples were filled with DEPC water to 100 µl and purified according to the manufacturer's instructions using RNeasy columns (Qiagen). The RNA was eluted with 35 µl DEPC water from the columns and then the concentration determined photometrically.

### 4.2.13 cDNA Synthesis

After measuring the purified RNA concentration and verify their integrity by agarose gel electrophoresis, 1 to 5 µg of RNA were used for cDNA synthesis. First, the RNA was filled up with DEPC water to 9 µl, 1 µl oligo dT primer (500 µg/ml) (Roche) was added and the mixture was incubated for 10 min at 65 °C. The samples were briefly chilled in ice, and the following ingredients were added: 4 µl of 5x first-strand-reaction buffer (Superscript II kit, Invitrogen), 2 µl DTT (0.1 M), 2 µl dNTP mix (10 mM) and 1 µl RNase inhibitor (RNaseOUT 40 U/µL, Invitrogen). The mixture was gently mixed and incubated for 2 min at 42 °C before 1 µl Superscript II RT (200 U/µL) (Invitrogen) was added. The negative control "- RT " samples instead received 1 µl DEPC water. The synthesis reaction was terminated after a 60 minutes at 42 ° C by a heating step of 15 minutes at 70 °C.

### 4.2.14 Southern Blot

Digested genomic DNA (~ 10 µg) was separated on an agarose gel at 4 V/cm. 10 min incubation with HCl (0.25 M) was necessary to depurinate and cleave the DNA in the agarose gel, as an indicator the bromophenol blue turned yellow/green. Subsequently, the gel was washed briefly with $ddH_2O$ and incubated for 30 minutes with NaOH (0.4 M) at RT, in order to denature the DNA present in the gel. The transfer to a positively charged nylon membrane (Hybond N +, Amersham Biosciences) was performed by capillarity in a NaOH (0.4 M) bath for at least 12 hours. The membrane was moistened before use with $ddH_2O$ and equilibrated 15 minutes in transfer buffer (0.4 M NaOH). For the transfer, the gel was placed on three layers of Whatman 3 MM paper equilibrated with transfer buffer, both extremes soaked also in transfer buffer. On top of the gel, the nylon membrane, several layers of Whatman 3 MM paper equilibrated in transfer buffer and a stack of dry cellulose towels below 1kg weight. After the blotting,

the membrane was washed with 2 x SSC and dried. The nylon membranes were backed for 2 hours at 80°C in order to permanently link the DNA to the membrane.

### 4.2.15 Northern Blot

Total RNA was prepared from various mouse organs using Trizol reagent (Gibco-Invitrogene, Karlsruhe, Germany) according to the manufacturer's instructions, as described above. MOPS, formamide and formaldehyde were added to 30 µg of total RNA. The samples were load into denaturing formaldehyde agarose gel with MOPS running buffer. The transfer to a positively charged nylon membrane (Hybond N +, Amersham Biosciences) was performed by capillarity using 20×SSC buffer. After transfer, the RNA was covalently link to the membrane by UV irradiation. All the solutions were done with DEPC-H2O.

### 4.2.16 Radioactive Labeling of DNA Samples

cDNA probes were labeled with $^{32}P$ by random priming with the RediprimeII kit (Amersham Biosciences). 25 ng of DNA denatured for 5 minutes at 100 °C and rapidly cooled in water ice, to prevent rehybridization of the individual strands. The denatured DNA was added to the reaction mix provided by RediprimeII kit and well mixed before adding 50 mCi $^{32}P$-dCTP. The final mixture was incubated 30 minutes at 37 °C. The purification of the radiolabelled DNA was carried out with Quick Spin Columns (Roche) according to the manufacturer's specifications.

### 4.2.17 Hybridization of Genomic DNA

After capillary transfer, Northern blot membranes were incubated with Ultrahyb buffer (Ambion) in a glass tube in a rotating oven set at 42°C for 30 minutes. While Southern blot membranes were incubated at 65°C with 20 ml Speed Hybrid II and 200 µg/ml denatured herring sperm DNA for 1 hour. Afterwards the buffer was discarded and new hybridization buffer added. Subsequently, the radioactive cDNA probe was added to the hybrization solution and left overnight in the rotating oven set at 42°C (Northern blotting) or 65°C (Southern blotting). After hybridization, the membrane was wash in solution A for about 30 min a nd with solution B for 10 min. The membrane was

repetitively washed till the radioactivity was only slightly above normal background activity. The membrane was then wrapped in a moist plastic film (Saran paper) and exposed for 1 to 12 hours on imaging plates (Fuji Imaging Plate). Afterwards, signals were detected using a PhosphoImager Bas-1500 (Fuji, USA).

## 4.3 Protein Biochemical Methods

### 4.3.1 Membrane Preparation

Mice were perfused transcardially with PBS to remove blood. Organs were dissected, snap-frozen in liquid $N_2$, minced in a mortar, transferred into ice-cold homogenization buffer (140 mM NaCl, 20 mM Tris pH 7.4, 5 mM EDTA and protease inhibitor (Complete®; Roche)) and homogenized in a glass douncer. Membranes were pelleted from post-nuclear supernatants (~100.000 x g for 30 minutes at 4°C) and resuspended in lysis buffer (50 mM Tris pH 6.8, 5mM EDTA, 2% SDS and Complete® protease inhibitor (Roche)).

### 4.3.2 Lysates of Transfected Cells

COS7 transfected with an expression plasmid (pcDNA3 from invitrogen) containing the human KCNE3 cDNA downstream of an HA-tag fused in frame. Were harvested after ~40 hours of expression, cells were detached mechanically in $Ca^{++}$-free phosphate buffered saline (PBS) and cell membranes were prepared as described above for tissue membrane preparation.

### 4.3.3 Deglycosylation of Membrane Bound Proteins

For deglycosylation, membrane preparations (described above) were denatured for 10 minutes at 95°C, diluted in $Na^{+}$-phosphate buffer (50 mM, pH 7.4), 1% NP40 and PNGase F 0.5 U/25 µg of total protein (Roche). After incubation for 2 hours at 37°C, samples were diluted in Laemmli sample buffer and incubated for 12 minutes at 55°C.

### 4.3.4 Determination of Protein Concentrations

The determination of protein concentrations was carried out using the BCA protocol, and following the instructions provided by Protein Assay from Uptima-Interchim. This assay is based on $Cu^{+2}$ reduction and the selective colorimetric detection of the cuprous cation ($Cu^{1+}$) by Bicinchoninic acid.

### 4.3.5 Sodium-Dodecyl-Sulfate-Polyacrylamide Gel Electrophresis (SDS-PAGE)

In SDS polyacrylamide gel electrophoresis, proteins are separated based on their molecular size as they migrate in an electrical field through pores in the gel matrix towards the anode. Pore sizes decrease with increasing acrylamide concentrations.

### 4.3.6 SDS-PAGE gel Composition

| | **Separation Gel (for 2 gels)** | **Stacking Gel (for 2 gels)** |
|---|---|---|
| Acrylamide | X ml (for desired gel %) | 0.4 ml |
| Buffer | 2.5 ml | 0.75 ml |
| $H_2O$ | 10 ml | 1.85 ml |
| 10% APS | 60 µl | 60 µl |
| TEMED | 6 µl | 6 µl |

### 4.3.7 Preparation of SDS-PAGE Gels

After pouring the separation gel, the surface was covered with isopropanol to obtain a smooth surface of the gel. After polymerization of the gel, the isopropanol was removed and the remaining volume above the gel was filled with stacking gel solution and the comb was inserted. After the gel was polymerized, the protein samples were mixed with SDS sample buffer and warmed at 55°C for 12 minutes before loading on the 15% gel. As molecular weight marker, the stained Protein Standard Benchmark (Invitrogen) was used. The gel chamber was filled with SDS running buffer and the electrophoresis was performed at constant voltage of 90-120V.

### 4.3.8 Western Blotting

Western Blotting (or immunoblotting) is used to identify specific antigens on proteins separated by SDS-PAGE and transferred to nitrocellulose membranes. The identification relies on the specificity of antibody-antigen reactions. Proteins were first separated by SDS-PAGE, and the antigens were electrophoretically transferred at 250 mA for 2 hours, or overnight at 40 mA, to a nitrocellulose membrane. The process was subsequently monitored by reversible Ponceau staining. The transferred proteins bound to the surface of the membrane, providing access to reactions with immunodetection reagents.

### 4.3.9 Immunostaining of Blots and Visualisation

For immunoblotting, a primary antibody was used which recognizes a specific epitope on the protein of interest. Unspecific binding was inhibited additionally by the use of blocking solution containing either protein or detergent blocking agents. To detect the antigen-antibody reaction, a horseradish peroxidase (HRP)-labeled secondary antibody was used, which binds to the first unlabelled antibody (indirect staining method). The active components of the ECL system are luminol and $H_2O_2$. The peroxidase reduces the hydrogen peroxide, and the resulting oxygen oxidizes the luminol, which releases light. Western Lightning Chemiluminescence Reagent (Perkin Elmer) was used for the detection. The chemiluminescence is then enhanced through appropriate enhancers and visualized using a Peqlab dark chamber connected to LVDS camera and the Chemi-Capt 5000 software from Viber Lourmat.

| **Number of washes** | **Buffer** | **Time (min)** |
|---|---|---|
| 1 | Blocking Buffer | 30 (or overnight at 4°C) |
| 1 | Blocking Buffer and 1° Ab | 60 (or overnight at 4°C) |
| 4 | Blocking Buffer | 5 |
| 1 | Blocking Buffer and 2° Ab | 60 |
| 3 | Blocking Buffer | 5 |
| 3 | Washing Buffer | 5 |
| 2 | TBS 1x | 5 |

The above incubations were done at room temperature under moderate shaking. Occasionally, blocking or incubation with primary antibody were performed overnight at 4°C. After the last washing step of the above protocol, the membrane was placed on a glass plate and ECL signal development was performed according to the manufacturer's instructions. A clean transparency was placed on top of the membrane and the membrane was visualizedo using a Peqlab dark chamber connected to LVDS camera and the Chemi-Capt 5000 software from Viber Lourmat

## 4.4 Cell Biological Methods

The ES cell culture was carried out in the Transgenic Mouse Facility of the ZMNH with the help of Dr Irm Hermans-Borgmeyer.

### 4.4.1 Culture of Murine Embryonic Fibroblasts

Murine embryonic fibroblasts (MEF) cells are required to support embryonic stem cells growth, since they work as feeder cells. MEF cells were cultured at 37 °C in 7.5% $CO_2$ humidified air (Heraeus incubators). Media and solutions were warmed at 37 °C before use.

### 4.4.2 Trypsinization of Embryonic Fibroblasts

The medium from a 150 mm plate with MEF cells was removed; the fibroblasts were washed twice with PBS and then incubated with 3 ml trypsin/EDTA for 3-5 minutes at 37 °C Addtion of MEF medium stopped the reaction and the fibroblasts were isolated with a Pasteur pipette. Afterwards, the trypsinized cells were seeded in the desired density and the medium changed after 6-8 hours.

### 4.4.3 Inactivation of Embryonic Fibroblasts

The MEF cells were inactivated with mitomycin (MMC, Sigma) before using them as a substrate for embryonic stem cells. MMC cross-linked the DNA strand, therefore blocked further cell cycle and stopped the MEF cells from further dividing. Confluent 150 mm MEF cell plate were incubated 2-3 hours at 37 °C after 15 ml of fresh medium

and MMC (10 µg/ml final concentration) addition. Subsequently, the medium was aspirated, the cells washed twice with PBS and trypsinized (see above). The inactivated fibroblasts were seeded on gelatinized cell culture dishes at the desired density (5 x $10^4$ cell/$cm^2$). The plates were used for embryonic stem cells (ES cells) culture after 12-24 hours.

### 4.4.4 Culture of Murine Embryonic Stem Cells

Murine embryonic stem cells were cultured on gelatinized (0.1% gelatin) MEF-coated cell culture dishes at 37 °C in 7.5% $CO_2$ humidified air (Heraeus incubators). The ES cell medium was changed every 24 hours. In order to identify recombinant clones, copies of these cell colonies were grown for DNA extraction on gelatinized plates without MEF cells. All media and solutions were pre warmed at 37 ° C before use.

### 4.4.5 Trypsinization of Embryonic Stem Cells

ES medium was removed; the cells were washed twice with PBS and then incubated with 3 ml trypsin/EDTA for 3-5 minutes at 37°C. Addition of ES medium stopped the reaction and the ES cells were isolated with a Pasteur pipette. Trypsinized ES cells were seeded in the desired density on gelatinized (0.1% gelatin) MEF-coated cell culture dishes.

### 4.4.6 Freezing Embryonic Stem Cells

a) Freezing cells in cryovials

Embryonic stem cells grown in 24 - and 6-well plates were washed, trypsinized, isolated and frozen in cold cryovials (NUNC) at -80 °C. After several days, the tubes were transferred into a liquid nitrogen tank.

b) Freezing the cells in 96-well

For temporary storage of frozen isolated ES cell clones 96-well plates were frozen. Consequently, the ES cells grown in the 96-well plates were first washed with PBS/EDTA, then trypsinized with 40 µl 0.25% trypsin and resuspended in 60µl ES medium. Afterwards, 100 µl of cold 2x freezing medium was added and mixed

carefully, finally a drop of mineral oil was put on top of the mixture. The storage was for a maximum of 4 weeks at -80 °C.

## 4.5 Generation of Transgenic Mice

### 4.5.1 Electroporation of Embryonic Stem Cells

800 µl electroporationbuffer containing 1 x $10^7$ embryonic stem cells (R1) were placed in a 0.4 cm gap electroporation cuvette (suitable for Biorad Electroporator). 25-50 µg of the linearized target vector DNA were added to the electroporation mixture. Two consecutive short pulses of 800 V and 3µF, and 240 V and 500µF were applied. After electroporation, the cells were plated into several 10 cm cell culture dishes in varying densities and incubated at 37 ° C. The cell culture dishes were previously coated with gelatin and contained inactivated embryonic fibroblasts, which serve to support ES cells growth.

### 4.5.2 Selection and Isolation of ES Cell Clones

In order to positively select the recombinant cells, the ES-cell medium was enriched with Genicitin (150-300 g / ml, G418, mixed Gibco) 2 days after transfection and until the isolation of individual colonies. Every 24 hours the ES cell medium was changed After 6-8 days of in vitro culture, colonies that were round but not flat and sharply defined with a smooth surface were lifted with yellow pipette tips and transferred from the cell culture dish to a 96-well with round bottoms containing 40 µl of trypsin. Once 2-3 rows of the 96-well plate were filled with colonies, the plate was incubated 3 min at 37 °C, after carefully pipetting up and down 100 µl ES medium were added. These ES cell clones were afterwards transferred in gelatinized 96-Well with flats bottoms containing inactivated MEF cells, again the medium was changed every 24 h. After 2-3 days, the ES cells were trypsinized again in order to get multiple copies of individual clones. Therefore, the ES medium was removed, the colonies washed with 200 µl PBS/EDTA and incubated with 40 µl trypsin in PBS at 37 °C for 3 min. Cells were resuspended with 80 µl medium and splitted (1:4 ratio) in 4 different 96-well plates, 2 gelatinized containing a MEF cell monolayer and 2 without. Cells on gelatinized plates

(without MEF cell monolayer) were digested to isolate genomic DNA. Southern blot was performed to genotype the DNA of the cell clones.

### 4.5.3 Blastocyst Injection

For blastocyst injection positive ES cell clones were carefully thawed at 37 °C and mixed with 200 µl ES medium. In order to expand clones, they were transferred from the initial 96-well MEF plates to 24-well MEF plates and then to 6-well MEF plates. It is important that the culture never reach confluence, otherwise the ES cells would start to differentiate. The ES medium was changed 2 h before the injection. For the injection, the cells were washed with PBS, trypsinized, resuspended into 3-5 ml of ES medium and centrifuged for 4 min at 1000 rpm, after that the pellet was taken up in 500 µl ES medium. The injection into blastocysts, was carried out by the facility. The blastocysts (C57BL/6J line) were taken 2.5 days after fertilization. 10-16 ES cells were injected in each blastocyst using a micromanipulator (Eppendorf). Afterwards the injected blastocysts were implanted in the uterus of pregnant foster mothers.

## 4.6 Histological Methods

### 4.6.1 Mice Perfusion

For histological and immunohistochemical studies, mice were transcardially perfused first with PBS to washout red cells and then with the fixative PFA to better preserve tissue structures. The mice were anesthetized by injecting a ketamine-Rompun mixture (100 µl /10 g body weight) before its chest was cut opened. The heart was exposed and a cannula introduced into the left ventricle and a small incisure was performed in the vena cava. First, 0.01% heparin in PBS (pH 7.4) were pumped into the heart at a constant pressure of 180 mmHg for 1-3 min pumped in order to prevent clotting of blood and flush the blood out of the body (through the cut vena cava). Then 4% PFA in PBS (pH 7.4) was pumped in the heart and fixate the body tissues. After perfusion, the tissues were dissected and incubated in 4% PFA in PBS (pH 7.4) for 2 hours at 4°C.

### 4.6.2 Paraffin Sections

The organs were removed after perfusion and passed through an ascending Isopropanol row (2 h 60%, 3 h 75%, 3 h 90%, 4 h 100%), then incubated for 12 h at 63 ° C in an isopropanol/paraffin mixture (1:1) and then left in pure paraffin for at least 6 hours. Tissues were embedded with liquid paraffin in small metallic containers and placed at 4°C O/N. Afterwards the paraffin block was hard enough to be removed from its container. The block was then sectioned in 6-micron thick slices using a microtome. The paraffin sections floating in a 50 °C warm water bath were mounted on microscope slides and dried. They were stored at room temperature until further processing.

### 4.6.3 Hematoxylin-Eosin (HE) Staining

Using this staining, nuclei appear blue-violet by hematoxylin and cytoplasms are stained pink by eosin. Paraffin sections were first deparaffinized in 10 min Histoclear (or xylene) following short incubations in descending ethanol series. The sections were then incubated for 10 min in hematoxylin solution and then washed with running tap water. In order to remove the excess of staining the section were briefly rinsed with 70% EtOH/1% HCl. Staining with 0.3% eosin solution (with a few drops of acetic acid) was then perfomed. Short incubations in ascending ethanol row (50%, 70%, 100%) removed the excess of staining and prepared the section for the final dehydration step 6 min in xylene (Histoclear) and the mounting in DPX (Histokitt).

### 4.6.4 PAS (Periodic Acid Schiff) Staining

The staining was used to detect excess of glycogen and mucin in mucous secreting tissues such as small intestine and airways. The glycogen and mucin will be stained pink-purple. Paraffin-embedded tissue sections were first deparaffinized in 10 min Histoclear (or xylene) following short incubations in descending ethanol series and then hydrated to water. The sections were oxidize in 0.5% periodic acid solution for 5 minutes, rinsed in distilled water, and incubated for 15 minutes in Schiff reagent (sections become light pink color during this step). Wash in lukewarm tap water for 5 minutes (immediately sections turn dark pink color). Afterwards, short incubations in ascending ethanol row (50%, 70%, 100%) prepared the section for the final dehydration step 6 min in xylene (Histoclear) and the mounting in DPX (Histokitt)

### 4.6.5 Toluidine Blue Staining

Mast cells play a key role in inflammatory process, defense against pathogens and, wound healing. Therefore they were used as a marker of tissue integrity.. They are found in the connective tissue and their cytoplasm contains granules (metachromatic) composed of heparin and histamine. Toluidine blue stained mast cells red-purple and the background blue (orthochromatic staining).

Paraffin-embedded tissue sections were first deparaffinized in 10 min Histoclear (or xylene) following short incubations in descending ethanol series and then hydrated to water. The sections were then stained with toluidine blue working solution for 2-3 minutes, washed 3 times with distilled water and quickly dehydrated through 95% and 2 changes of 100% ethanol (these changes in alcohol were fast enough to avoid stain to diffuse away). Sections were then incubated twice in xylene for 3 minutes each, and then mounted in DPX (Histokitt).

### 4.6.6 Immunofluorescence

Paraffin embedded sections of stomach; small intestine and colon were boiled for 10 minutes in a microwave in 10 mM citrate buffer (tracheal sections only 3 minutes). The sections were cooled down slowly and washed twice with PBS and then incubated in PBS, 1% SDS for 15 minutes. Tracheal sections were incubated at room temperature with trypsin solution for 10 minutes. After 1 hour in blocking solution, sections were incubated with primary antibodies (diluted in blocking solution) overnight at 4°C. The rabbit antibody against KCNE3 was used at 1:1000 dilution, and the KCNQ1 antibody at 1:500 dilution. Sections were then incubated with goat-anti-rabbit IgG coupled to Alexa Fluor 488 (absorbance maximum approx. 495 nm, emission maximum 519 nm;Molecular Probes, Mo Bi Tec, Göttingen, Germany) and the nuclear stain Topro-3 1:5000 (absorbance maximum approx. 642 nm, emission maximum 661; Invitrogen). Analysis was by confocal microscopy (Zeiss LSM 510 META, Germany) using sequential excitation for double-labeled preparations.

## 4.7 Animal Experiments

### 4.7.1 KCNE3 Antibody Generation

Dr. M. Beyermann (FMP) synthesized a peptide representing the entire cytoplasmic C-terminus of mouse KCNE3 (RSRKVDKRSDPYHVYIKNRVSMI) that was coupled via maleimidobenzoic acid-N-hydroxysuccinimide ester to keyhole limpet hemocyanine using a cysteine residue added to its N-terminus. Antisera were obtained from rabbits injected 6 times within 90 days (Pineda Antikörper-Service, Berlin) with the carrier-coupled peptide and were purified by affinity against the peptide. One of the purified antisera showed specificity in Western blots of transfected COS-7 cells and WT/KO colon membrane preparations and recognized KCNE3 (at 1:1000 dilution) in immunofluorescence in intestinal and tracheal tissue sections. Staining was specific as revealed by the absence of signals in KO tissues.

### 4.7.2 Serum, Feces and Urine Analysis

Blood was drawn from the heart of WT and KO mice under isoflurane anesthesia and and stored until the clot at 4 ° C. The cellular components were pelleted by Centrifugation at 14,000 rpm (4 ° C) for 10 min and the serum stored until analysis at -80 ° C. Mice were kept in metabolic cages (Phymep, Paris, France) for 6 days. Weight, food and water intake were controlled daily. Urine and feces were collected daily. Feces were dried at 95°C for 3 hours, weighed, and dissolved in 0.75 M HNO3 at room temperature overnight. After homogenization in a glass douncer and centrifugation to remove insoluble material, the electrolyte composition of the supernatant was analyzed by flame photometry (IL 943 Flame Photometer, Instrumentation Laboratory). Concentrations of creatinine, glucose, proteins or and urine electrolytes were determined by Dr. D. Becker (Institut für Labormedizin, Helios Klinikum Berlin-Buch).

### 4.7.3 Measurement of Intestinal Fluid Secretion *in vivo*

Wild type or KCNE3 knockout mice (body weight 20-22 g) were deprived of food 24 h prior to prior to the experiment. Briefly, animals were placed in an anesthetic chamber and exposed to isoflurane using the Univentor 400 anesthesia unit (airflow rate 400 - 500 mL/min, 4% isoflurane). Afterwards, anesthetized mice were placed in the modifies heating plate (set at 38°C) in order to maintain body temperature. Mice were kept

anaesthetized by exposure to 2% isoflurane using a mask and a constant flow rate (150 - 250 ml/min). A small abdominal incision was made to expose the small intestine. Ileal tissue proximal to the caecum was exteriorized and isolated, and 2-3 loops (~20 mm each) were tide up. The closed loops were then injected with 100 µl of PBS alone or 100 µl PBS containing 0.5 µg CTX (Gentaur). The wound was sutured and mice were allowed to recover. After 6 h, mice were sacrificed, intestinal loops removed, weighed with and without fluid contents, and their length measured.

### 4.7.4 Rotarod Performance

Ability to maintain balance and movement agility on a rotating rod apparatus (TSE accelerating rotarod) was assessed for each genotype and condition in adult mice. 8 WT and 8 KO animals were first kept for 15 days under hypokalemic diet, in the control group 8 WT and 8 KO animals were kept under standard diet. Animals from both groups were randomly observed several times a day, no signs of periodic paralysis were observed during these 15 days in WT neither in KO mice. On day 16th, animals were accustomed to the rotating rod apparatus (TSE Systems, Inc. Chesterfield, MO, USA accelerating rotarod) by placing them on the rod at the lowest speed (4 rpm) for 3 minutes. After some rest (5 minutes) the animals were test in an accelerating mode rotarod (4 to 40 rpm); the average time to fall (latency) was measured from three trials and analyzed.

### 4.7.5 Measurement of Mucociliary Clearance

Dr. Rainer Schreiber carried out these experiments in the lab of Prof. Kunzelmann. Dept. of Physiology at the University of Regensburg

Tracheas were mounted with insect needles onto an extra thick blot paper (Bio-Rad, Germany) and transferred into a humid chamber at 37°C. The filter paper was perfused with buffer solution at a rate of 1 ml/min and at 37°C. Polystyrene black dyed microspheres (diameter 6.51 ± 0.58 µm, Polybead®, Polyscience Inc., Warrington, PA, USA) were washed with buffer solution (± ATP 10 µM), twice. Particle solution (10 µl with around 0.5% Latex) was added onto the surface of the trachea, without and subsequently with ATP (10 µM). Carbachol (100 µM) was applied from the basolateral side. The particle transport was visualized by taking pictures every 15s for 10 min using

the Zeiss stereo microskope Discovery.V12 with PlanS objective (1.0x, FWD 81 mm), Zeiss digital camera AxioCam ICc1 and the software AxioVision (Release 4.6.3, Zeiss, Göttingen, Germany). 5 to 8 moving particles of different regions of the trachea were selected and the transport was calculated by measuring the distance per time (µm/min) using the AxioVision Software (Release 4.6.3, Zeiss, Göttingen, Germany).

## 4.8 Electrophysiological Experiments

### 4.8.1 Ussing Chamber: Colonic Epithelia

Experiments done under Dr. Dorothee Guenzel supervision in Prof. Fromm's lab (Dept of clinical Physiology at the Charité Berlin).

The Ussing chamber was invented by Hans Ussing in the 1950s to measure the net ion transport taking place across an epithelium clamped between two reservoirs are filled with symmetrical solutions. The equal charges in both sites of the epithelia result in an initial equilibrium at the set up potential of 0 mV. Ions that move through paracellular pathways, tight junctions or across the cell generate a voltage difference among chambers. Addition of specific drugs will promote or inhibit channel activity and modify the ionic conductances, thereby changing the voltage. The amount of current injected to clamp the voltage to 0 mV is called short circuit current ($I_{sc}$) and is the measure of net ion transport across the epithelium.

Briefly, in our set up the current was applied by two silver/silver chloride (Ag/AgCh) electrodes (one for each tank,) placed in a vessel filled with KCl. Agar bridges (filled with KCl) connected the electrode vessel with the Ussing chamber and allow homogeneous current distribution. They were placed at the same distance of the epithelium in each of the two halves of the Ussing-chamber. Similarly, electrodes placed in KCl filled vessels, also connected to the Ussing chamber by KCl filled agar bridges, measured the transepithelial voltage.

This method very valuable to measure ionic permeability (conductance or resistance) and active ion transport (short circuit current, Isc).

### 4.8.1.1 Procedure

Mice were anesthetized and killed by inhalation of 100% CO2 . Late distal colon was dissected, cut open along the mesenteric insertion and partially stripped, where, the lamina muscularis propria was removed. The partial 'stripping' allows assessment of the epithelium contribution by removal of all subepithelial elements. The epithelium (lamina propria mucosae) was then clamped in the Ussing chamber. The epithelium was stretched over a silicon ring of 0.05 $cm^2$, fixed with a tissue adhesive to a plastic container and then placed into the chamber. The two reservoirs were filled with 10 ml ringer solution warmed up by a closed water circuit (at 37°C) and gassed with carbogen (95% O2, 5% CO2, to maintain pH 7.4). This bubble lift facilitated the continuous chamber perfusion, and proper mix of the solution. Addition of 50 mg/l Piperacillin (Hexal AG, Holzkirchen, Germany) and 10 mg/l Zienam (MSD Sharp & Dohme GmbH Haar, Germany) effectively inhibited bacterial growth. TTX (serosal, 1 µM), indomethacin (mucosal and serosal, 10 µM) and amiloride (mucosal, 10 µM) were applied to inhibit neuronal activity, prevent prostaglandin release, and block apical $Na^+$ channels (ENaC), respectively.

Prior to each experiment, the resistance of the bath solution between the voltage-sensing electrodes was determined and taken into account.

### 4.8.1.2 Measurement of Voltage, Resistance and Short Circuit Current

The transepithelial resistance was calculated following the Ohm's Law taking the transepithelial potential differences ($V_1$ and $V_2$) and the current injected by the pulse generator (I1-I2). $R_{te} = (V_1-V_2)/(I_1-I_2)$. For the correct calculation of transepithelial resistance, the area of the tissue being studied (A=0,05 $cm^2$) and the resistance of the empty removable disk or of the blank filter, were taken into account The short circuit current was calculated as the ratio between voltage and resistance, where the transepithelial resistance is known and the transepithhelial voltage is directly measured. $Isc = V_{te}/R_{te}$.

### 4.8.2 Ussing Chamber: Tracheal Epithelia

Dr. Ousingsawat carried out these experiments in the lab of Prof. Kunzelmann. Dept. of Physiology at the University of Regensburg

Tracheas were dissected, opened longitudinally on the opposite side of the cartilage free zone and were transferred immediately into an ice cold buffer solution 1 containing amiloride (10 μM). Stripped colon was put into ice-cold buffer containing amiloride (10 μM) and indomethacin (10 μM). Tissues were mounted into a micro-perfused Ussing chamber with a circular aperture of 0.785 $mm^2$. Luminal and basolateral sides of the epithelium were perfused continuously at a rate of 5 ml/min. Bath solutions were heated to 37 °C, using a water jacket. Experiments were carried out under open circuit conditions. Data were collected continuously using PowerLab (AD-Instruments, Australia).

Values for transepithelial voltages ($V_{te}$) were referred to the serosal side of the epithelium. Transepithelial resistance ($R_{te}$) was determined by applying short (1s) current pulses ($\Delta I$ = 0.5 μA). $R_{te}$ and equivalent short circuit currents ($I_{SC}$) were calculated according to Ohm's law ($R_{te} = \Delta V_{te}/\Delta I$, $I_{SC} = V_{te}/R_{te}$).

### 4.8.3 Patch Clamp of Mouse Colonic Crypt Cells

Experiments done in collaboration with Prof. Warth. Dept. of Physiology at the University of Regensburg

In this technique, the membrane potential is held constant ("clamped") while the current flowing through the membrane is measured. Technically, a patch pipette with a tip diameter of approximately is placed in contact with the plasma membrane. When little negative pressure is applied from the interior of the pipette, a very high resistance seal (Giga-seal – resistance typically 50 GΩ) develops between the membrane patch and the glass of the pipette ("on-cell" configuration). Rupture of the membrane patch underlying the electrode surface (whole-cell configuration) allows direct communication between the interior of the electrode (filled with so called "internal solution") and the intracellular space. Voltage-clamp of the cell, which consists in maintaining membrane voltage at a constant fixed value, is then achieved using a negative feedback loop through a high-gain differential amplifier (Hodgkin and Huxley, 1952).

Mice were killed by cervical dislocation. A 3 cm piece of mouse distal colon was everted and rinsed with ice-cold “colon” solution. Both ends were tied to obtain a sac preparation. This sac was filled with a “$Ca2^{+}$-free” solution and then incubated in “$Ca2^{+}$-free” solution for 11 min at 37° C. Isolated crypts were obtained by shaking these sacs in “colon” solution.

For patch clamp experiments, crypts were transferred into a bath chamber mounted on the stage of an inverted microscope. The crypt under study was held by a suction pipette. All experiments were performed at 37° C. Individual cells were approached on the basal cell pole (crypt base and crypt middle cells) by patch pipettes with a mean resistance of 6-10 MΩ. The patch pipettes solution and bath solution compositions are detailed in electrophysiology materials. The recordings reported here were obtained in whole-cell mode using an EPC7-like amplifier (U. Fröbe, Freiburg, Germany).

# 5 RESULTS

## 5.1 Generation of *kcne3*$^{-/-}$ Mouse

In order to investigate the function of the KCNE3 subunit, we generated the *kcne3*$^{-/-}$ mouse by homologous recombination in mouse embryonic stem (ES) cells.

Figure 6.1A depicts the targeting vector that contained a DNA sequence of the initial intronic sequence and the first 3 exons of the KCNE3 gene, which are part of the 5'untranslated region (UTR), and exon 4, which contains the entire coding region for KCNE3 (Lundquist et al. 2006). Exon 4 was flanked with LoxP sites in order to allow its selective removal by using the Cre/LoxP-recombinase system (see below).

In addition, three selectable genes have been introduced in the targeting construct in order to select for the desired recombination product (Figure 5.1A): the neomycin resistance (neo) gene for positive selection, which allows cells to survive in the presence of the antibiotic neomycin, the diphtheria toxin (dta) gene and the herpes simplex virus type 1 Thymidine Kinase gene (tk). Dta and tk genes are used for "positive-negative" selection in case of random integration of the targeting vector in the murine genome. Those cells in which random integration has occurred retain the dta or the tk gene and thus will be specifically eliminated by expression of the dta protein or by the antiviral agent ganciclovir.

As seen in figure 5.1A, both the dta and the tk genes were placed outside the homologous region (5' of the short arm and 3' of the long arm of the vector, respectively). In this configuration, if homologous recombination occurs between the targeting construct and the native KCNE3 gene, both the dta and the tk genes will be excluded.

To exclude possible undesired effects due to the insertion of the neomycin cassette into the mouse genome, the neomycin resistance cassette was also flanked by 2 loxP sites to allow its removal by the Cre-recombinase.

ES cell clones that incorporated the recombined allele in the desired fashion were expected to be resistant to neomycin. To further test the specificity of the clones which survived positive selection, we employed a Southern blotting analysis of genomic DNA. Following BglI enzymatic restriction digestion, genomic DNA was probed with the 5'

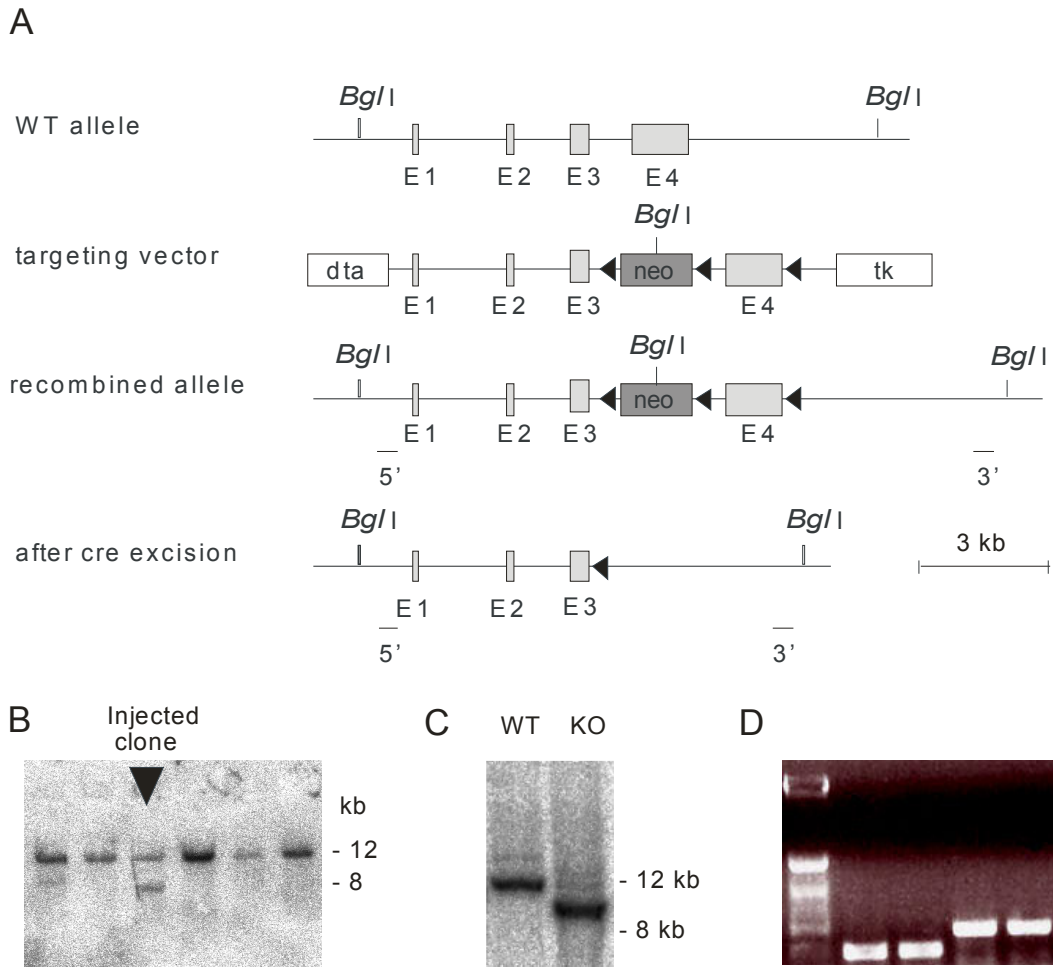


**Figure 5.1. Generation of *kcne3*$^{-/-}$ mice**. **A,** strategy for disruption of the KCNE3 gene. *Top*, wild type allele showing exons 1-3 (UTR), 4 (CDS, Exon 4 contains the entire coding region) depicted as boxes and unique 12 kb Bgl1 restriction fragment. *Middle upper,* targeting vector. The neomycin cassette (neo) inserted for positive selection, introduced a new Bgl1 restriction site. Diphteria toxin (dta) and Thymidine Kinase (tk) gene located outside the homologous region were used for negative selection. The neomycin cassette was flanked by loxP sites (◄). A third loxP site was inserted after exon 4. *Middle lower*, recombined allele after successful homologous recombination, Bgl1 enzymatic digestion produces a 6 and 8 Kb restriction fragments, detected in Southern blot analysis by the probes indicated as bold bars labeled as 5' (detected 6 kb Bgl1 restriction fragment) or 3' (detected 8 kb Bgl1 restriction fragment). *Bottom*, KO allele after Cre excision. The neocassette and exon 4 (CDS) were removed by cre recombinase leaving instead 1 loxP sites (◄). The 9,5 Kb BglI restriction fragment was detected with either 5' or 3' probe (bold bars) by Southern blot (see C). **B**, Southern blot analysis of embryonic stem cells showing the wild type band (12 kb) and the successfully recombined band detected with probe 3' (8 kb). The positive clone was afterwards injected into a blastocoele. **C,** Southern blot analysis of tail DNA from WT (12 kb) and KO (9.5 kb) mice. **D**, PCR for routine genotyping showing the wild type and *kcne3*$^{-/-}$ bands .

or 3' probes. As shown in figure 5.1B, the wild type allele was identified by a sharp band about 12 kb, whilst the recombinant allele band was about 6 kb for the 5' probe or 8 kb for the 3' probe.

Positive clones were injected into the blastocoele cavity of C57BL/6 embryos and transferred to a pseudo pregnant foster mother. Offspring showing more than 80%

chimerism were bred to C57BL/6 females. Successful germ line transmission and hence transfer of the modified ES cell genome to their offspring, was determined by Southern blotting. Subsequently, the selected offspring was crossed with Cre-deleter mice (Schwenk et al. 1995) (in C57BL/6J background) to excise the neomycin selection cassette and the KCNE3 coding region (exon 4).

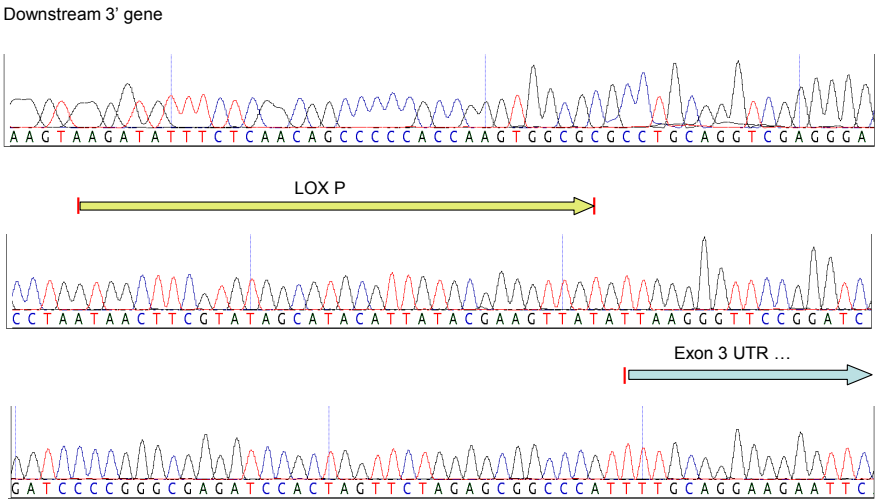


**Figure 5.2. Modified KCNE3 gene region sequence.** The modified KCNE3 gene fragment was first amplified by PCR from the *kcne3*$^{-/-}$ mouse genome and then subjected to sequencing. The nucleotide sequence with the respective color codes are shown, corresponding to the 334 bp covering KCNE3 exon 3 downstream the 3' end of the KCNE3 gene. As expected, in the *kcne3*$^{-/-}$ mouse, exon 4 (containing the whole coding region for KCNE3) has been removed, leaving instead a single loxP sequence (the 34 bp loxP sequence is highlighted). Moreover, also neomycin cassette has been deleted from the recombined allele.

Cre-deleter mice ubiquitously express high levels of cre-recombinase, an enzyme that catalyzes site-specific recombination of floxed DNA segments, meaning that fragments between loxP sites in the same orientation will be deleted.

As a result, KCNE3 gene was permanently modified in the knock-out (KO) allele, leading to a constitutive deletion of *kcne3* expression. As shown by Southern blotting analysis performed from homozygous offspring, KO allele was identified by a specific 9,5 kb after BgII digestion (Figure 5.1C). Afterwards, the presence of the KO allele was routinely checked by genotyping PCR (Figure 5.1D).

Further sequencing of the *kcne3*$^{-/-}$ genomic DNA confirmed that the Cre-recombinase excised both the neocassette and exon 4 (Figure 5.2), leaving instead a unique loxP site in the KO allele.

*Kcne3*$^{-/-}$ mice resulting from interbreeding heterozygous animals were obtained at the predicted Mendelian frequency, were viable, superficially indistinguishable from their wild type littermates and showed no obvious phenotypic changes in the cage environment.

## 5.2 Analysis of KCNE3 Expression Pattern in Murine Organs

The expression profile of the KCNE3 protein has been studied in recent years by several groups. However, given the lack of the *kcne3*$^{-/-}$ tissues, which would serve as the most ideal and specific control to reliably study the expression pattern of the gene, these studies have been source of many controversies. A number of contradictory datasets has accumulated, which report KCNE3 expression in brain, skeletal muscle, kidney and heart, besides epithelial secretory tissues like trachea and intestine.

To address KCNE3 tissue distribution and better understand its physiological role, we performed an extensive analysis of KCNE3 expression at the mRNA and protein level in several wild type tissues. Northern blotting analysis was employed to study mRNA expression pattern, while Western blots and immunohistochemistry were used to analyze protein distribution and subcellular localization. Most importantly, our data in wild type animals have been routinely validated by employing KCNE3 deficient tissues from *kcne3*$^{-/-}$ littermates as negative controls.

### 5.2.1 Analysis of KCNE3 mRNA Distribution

Northern blot analysis was carried out to investigate KCNE3 mRNA expression pattern in murine organs. Total RNA (30 μg) was extracted from skeletal muscle, lung, heart, brain, kidney, caecum, colon, ileum, jejunum, duodenum and stomach. Small aliquots of these samples were pre-run in a standard agarose gel containing ethidium bromide, ribosomal 28S and 18S RNA were clearly visible assuring the quality and integrity of the total RNA extracted.

As shown in figure 5.3B, a strong KCNE3 band at 1.5 kb was detected all along the gastrointestinal tract of wild type mice. KCNE3 transcript signals were found in wild type stomach, duodenum, jejunum, ileum, caecum and colon (Figure 5.3A and B). Northern blot analysis revealed prominent KCNE3 expression in colon. No KCNE3 mRNA was detected in the respective *kcne3*$^{-/-}$ tissues, proving the specificity of our

probe and providing additional confirmation for the disruption of the KCNE3 gene in *kcne3*$^{-/-}$ animals (Figure 5.3A). KCNE3 transcripts were not detectable in brain, heart, kidney, lung and skeletal muscle (Figure 5.3A).

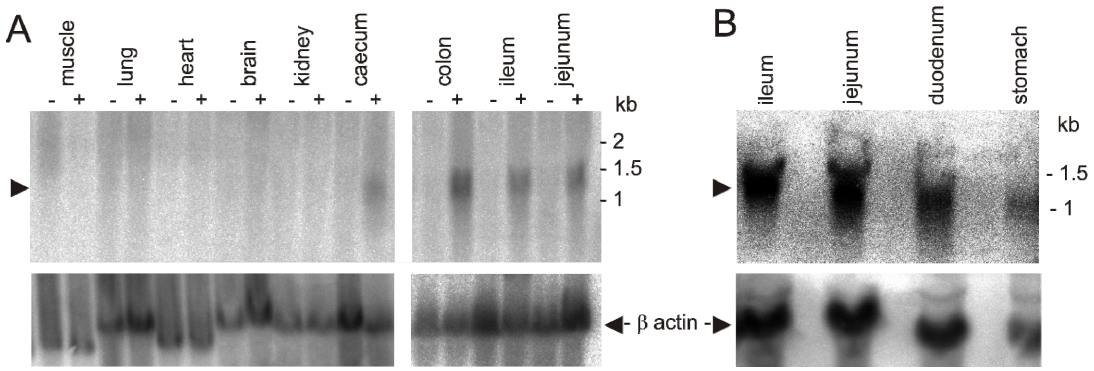


**Figure 5.3. KCNE3 mRNA expression. A**, Northern blot analysis of total RNA (30 µg per lane) from wild type (+) and *kcne3*$^{-/-}$ (-) tissues. KCNE3 probe (354 bp) contained the coding region (part of exon 4) as described in Experimental Procedures. A KCNE3 specific band was detected at ~1-1.5 Kb in wild type caecum, colon, ileum and jejunum. This signal was absent from *kcne3*$^{-/-}$ tissues. KCNE3 mRNA was not detected in muscle, lung, heart, brain and in kidney total RNA. Beta actin was used as RNA loading control (band runs at 2 kb). Note that muscle and heart present different beta actin mobilities. 1.6 kb and 1.4 kb respectively (Zhang et al. 2006). **B**, Northern blot analysis of total RNA (30 µg / lane) from upper gastrointestinal tract of wild type animals. KCNE3 mRNA is present in stomach, duodenum, jejunum and ileum. The hybridization probe (354 bp) contained the coding region (part of exon 4). Beta actin was used as RNA loading control.

In addition to mRNA, total RNA also contains ribosomal and transfer RNA, in a proportion that is tissue specific. Therefore, although the same amount of total RNA was loaded in all wells, relative mRNA levels might change depending on the specific organ of origin. Hence, an internal standard was needed to prove that uniform amounts of mRNA were present in each lane.

Beta actin is a housekeeping gene commonly used as a control, and has been extensively evaluated throughout the years (Zhang et al 2006). Beta actin is a highly conserved isoform of actin, which carries on cytoskeletal functions in all tissues, and it is constitutively expressed with several transcribed but not translated pseudo-genes (Vaarala et al. 2001; Bas et al. 2004).

When probed for beta-actin, the tissues analyzed displayed a 2 kb band corresponding to beta actin (Figure 5.3A and B). Heart and skeletal muscle displayed bands lower than 2 kb, 1.4 kb and 1.6 kb respectively (Zhang et al. 2006; Vaarala et al. 2001). In conclusion, mRNA levels were indeed in a similar range within all wild type and *kcne3*$^{-/-}$ tissues analyzed in our Northern blotting analysis.

Altogether, our analysis on the expression pattern of KCNE3 mRNA revealed that KCNE3 is expressed in gastrointestinal tissues. Although KCNE3 had been previously reported to be expressed in skeletal muscle, heart, kidney and brain, we did not observe any detectable signal in these tissues. Furthermore, compared to the studies which have been published previously, our data on the expression pattern of KCNE3 in wild type tissues included an additional level of specificity, provided by the use of *kcne3*$^{-/-}$ tissues from control littermates. Our data are therefore extremely useful to clarify the contradictory expression patterns reported in the recent years (Abbott et al. 2001; McCrossan et al. 2003; Lundquist et al. 2006)

### 5.2.2 Anti-KCNE3 Antibody Generation

In order to study KCNE3 expression at the protein level, and given the current lack of a reliable and specific anti-KCNE3 antibody, a novel anti-KCNE3 antibody was generated. Anti-KCNE3 antisera was raised in rabbits, against a 23 residues peptide corresponding to the KCNE3 cytoplasmic carboxy-terminus (Figure 5.4A) (see methods for further details).

To assess the specificity of the immunopurified antibody, HA-tagged KCNE3 cDNA was heterologously expressed in COS7 cells. As shown in figure 5.4B, Western blot analyis of KCNE3-transfected cells shows that anti-KCNE3 and anti-HA antibodies specifically detected several bands between 19 and 25 kDa (Figure 5.4B and D). These multiple bands, which appear around the expected molecular weight of the KCNE3 protein, have been previously suggested to represent differentially glycosylated KCNE3 species (Gage and Kobertz 2004).

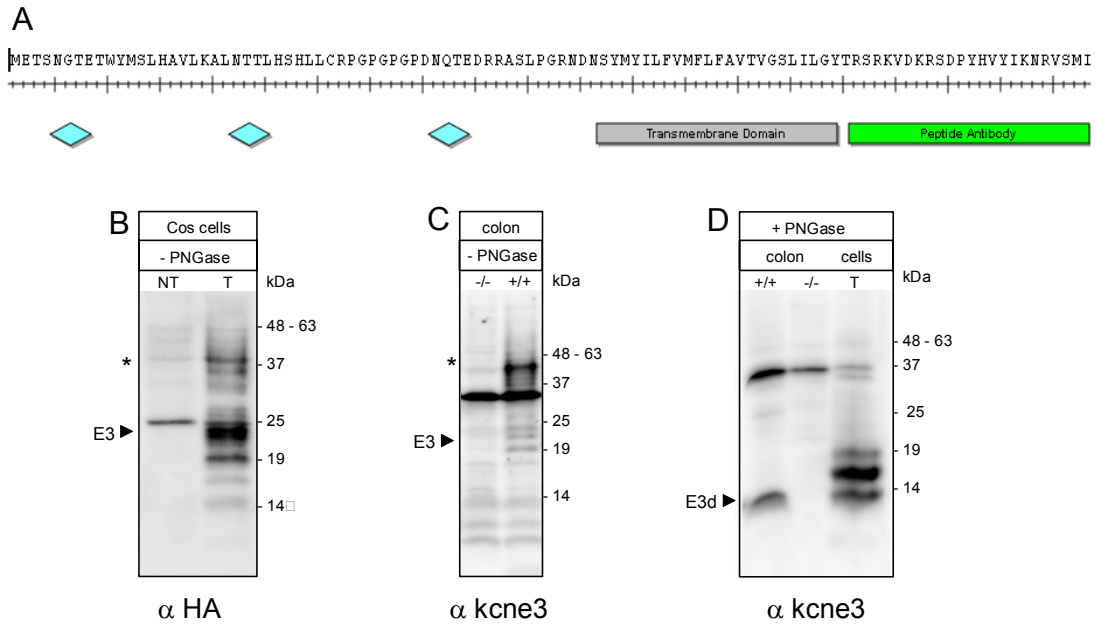


**Figure 5.4. Specificity of the newly generated anti-KCNE3 antibody. A,** the 103 amino acid sequence of the KCNE3 protein is depicted. The anti-KCNE3 antibody was raised against a 23 amino acid peptide representing the whole C-terminal domain of KCNE3 (depicted as filled green box). The N-terminal presents 3 putative N-glycosylation sites indicated by blue diamonds and the transmembrane domain is shown by the filled grey box. **B,** Western blot analysis from lysates of COS-7 cells overexpressing N-terminally HA-tagged version of KCNE3. The anti-HA antibody detected a 3 band pattern (between 19 and 25 kDa, filled arrowhead) (*lane T*), which were absent from the non-transfected COS-7 cells (lane NT). **C,** a faint but similar band pattern was detected in a membrane fraction preparation of wild type colonic tissue, and it was absent from *kcne3*$^{-/-}$ tissues. Asterisk indicates a KCNE3-immunoreactive, high-molecular weight band, which might represent SDS-resistant KCNE aggregates. **D,** after deglycosylation by PNGase, the newly generated KCNE3 antibody recognized a single band (~14 kDa arrowhead) in membrane preparation of wild type colon (*WT lane*). No specific signal was detected in *kcne3*$^{-/-}$ tissue (*KO lane*). As a positive control, total lysate of COS-7 cells overexpressing HA-KCNE3 was used (*T lane*), where different glycosylation states of HA-KCNE3 were still observed. The presence of several bands in the latter lane might be owed to incomplete deglycosylation caused by the N-terminal HA tag. Please note that when blot with anti-KCNE3 antibody, independently of the genotype an unspecific band at 30 kDa was homogenously labeled in all tissues and cell lysates.

As it has been previously reported, KCNE3 undergoes posttranslational modifications and contains three putative glycosylation sites on its N-terminal (Gage and Kobertz 2004). To test whether the posttranslational added sugar chains accounted for the migration shifts and the multiple band pattern observed in our Western blot in figure 5.4B-D, lysates from transfected cells were treated with Peptide N-glycosidase F (PNGaseF) prior to loading. Under these conditions, only three specific prominent bands at approx. 14, 17, and 19 kDa were detected with anti-KCNE3 antibody (Figure 5.4D last lane). These bands correspond to the expected molecular weight of non-glycosylated HA-tagged KCNE3 (14 kDa) and to incomplete glycosylated forms (aprox. 17 and 19 kDa). Interestingly, these last incompletely deglycosylated bands were commonly seen in HA-KCNE3 transfected cell lysates, but it never appeared when

the untagged KCNE3 protein was probed in native tissue after PNGaseF treatment (Figure 5.4D, first lane; Figure 5.5). Chandrasekhar et al in 2006 have also reported a very similar incomplete PNGaseF-mediated deglycosylation of HA-tagged KCNE1. I therefore assume that the N-terminal position of the HA tag of KCNE3 might have provided steric interference with the PNGaseF mediated deglycosylation reaction, thereby preventing efficient removal of one of its sugar chains.

As it was shown in figure 5.3, KCNE3 mRNA was abundant in the gastrointestinal tract, particularly in colon. To further characterize the specificity of our anti-KCNE3 antibody in native tissue, we prepared membrane-bound protein fractions from wild type and *kcne3*$^{-/-}$ colon. Similar to what it was previously observed in Western blot analysis of HA-tagged KCNE3 transfected cells (Figure 5.4B and D), lysates from wild type colon which were not treated with the deglycosylating enzyme PNGaseF also exhibited a similar band pattern between 19-25 kDa (Figure 5.4C). Besides, in these samples an additional KCNE3-immunoreactive band was detected around 40 kDa (marked with asterisk (*) in Figure 5.4C). This additional band observed in wild type colon lysates might represent SDS-resistant KCNE3 aggregates that run at higher molecular weights, a common phenomenon that had been previously reported for several other membrane-associated proteins (Sagne et al. 1996). However, Chandrasekhar et al in 2006 when blotting against KCNE1 protein also described the same additional band at 40 kDa, and claimed that it was instead due to posttranslational KCNE modifications.

On the other hand, PNGaseF treatment resulted in a shift of the apparent molecular mass of the glycosylated species, which migrated now as a single visible band at 14 kDa (Figure 5.4D, first lane).

Taken together, these data lead us to conclude that first, KCNE3 undergoes N-linked glycosylation in heterologous expression and in native tissue. As expected, the presence of complex oligosaccharides increased the molecular weight of the KCNE3 protein, producing several KCNE3 immunoreactive bands in Western blot analysis. Similar to KCNE1 (Chandrasekhar et al. 2006), deglycosylation with PNGaseF was necessary to detect a single KCNE3-specific band at the expected molecular weight of 14 kDa in wild type tissues, which was absent in *kcne3*$^{-/-}$ controls (Figure 5.4D). In particular, our newly generated anti-KCNE3 antibody was able to recognize both glycosylated and non-glycosylated forms of the KCNE3 protein, in either heterologous expression or

native tissues, thereby proving an extremely useful tool for further investigations (Figure 5.4C and D).

### 5.2.3 Analysis of KCNE3 Protein Distribution

In order to study more extensively the tissue distribution of KCNE3 at the protein level, we performed a Western blot analysis from a wide number of wild type tissues, using KCNE3 deficient tissues as controls for the specificity of the assay. Membrane-bound protein fractions from wild type and *kcne3*$^{-/-}$ tissues were deglycosylated and probed for KCNE3 (Figure 5.5).

Clear specific bands at the expected KCNE3 molecular weight (14 kDa) were detected in wild-type jejunum, ileum, caecum, and colon (Figure 5.5A and C). A KCNE3 specific band in stomach and trachea was only visible after longer exposures of the blots (Figure 5.5D). KCNE3 immunoreactive bands were absent in *kcne3*$^{-/-}$ tissues, confirming the specificity of our newly generated antibody (Figure 5.5A-D).

Consistent with our data on KCNE3 mRNA expression (Figure 5.3), our Western blot analysis also confirmed the presence of the KCNE3 protein in intestine, while no KCNE3 specific signals were observed in brain, kidney, heart and skeletal muscle (Figure 5.5). Our results are in accordance with previously published data on KCNE3 expression in gastrointestinal epithelia (Schroeder et al. 2000). Altogether, our data show KCNE3 expression to be restricted to the secretory epithelia, namely gastrointestinal tract and trachea.

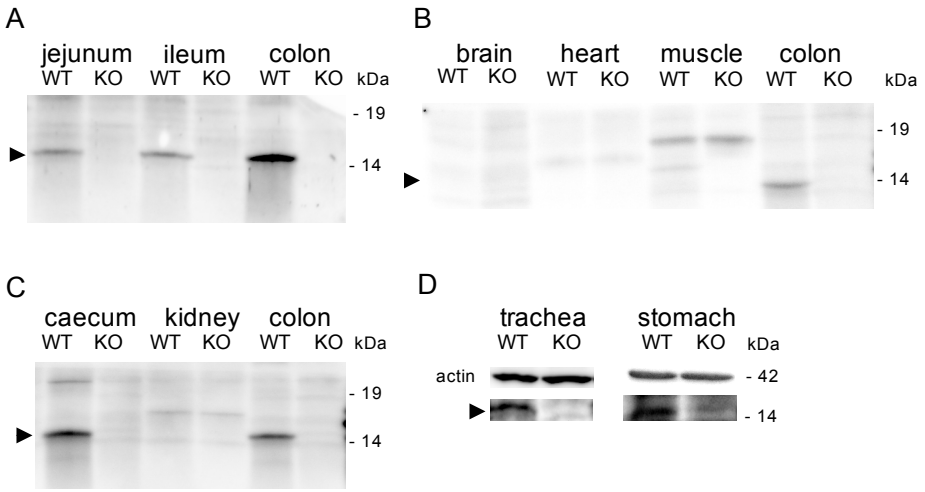


**Figure 5.5. KCNE3 protein distribution in wild type tissues. A-D,** Western blot analysis of KCNE3 expression in wild type and *kcne3*$^{-/-}$ tissues. After deglycosylation by PNGase, a single KCNE3-immunoreactive band (~14kDa) was specifically detected in wild type membrane fractions from jejunum, ileum and colon (A) and caecum (C). This band was not detected in wild type brain, heart, muscle (B) and kidney (C). KCNE3 band was absent in all *kcne3*$^{-/-}$ samples (A-D). **D**, Western Blots showing KCNE3 band in wild type trachea and stomach after long exposure. *Kcne3*$^{-/-}$ samples were devoid of KCNE3 signal (~14kDa). Beta actin (~ 42 kDa) was used as a loading control.

## 5.2.4 Subcellular Localization Studies of KCNQ1 and KCNE3

### 5.2.4.1 Immunolocalization of KCNE3 and KCNQ1 in Stomach

Since our Northern blot analysis revealed moderate KCNE3 transcript levels in the stomach (Figure 5.3), we analyzed in more detail the KCNE3 localization at the subcellular level in this tissue.

For this aim, we first compared the general morphology and integrity of the gastric epithelia in wild type and *kcne3*$^{-/-}$ littermates by standard histological techniques. No significant changes in gastric tissue organization were observed in *kcne3*$^{-/-}$ mice compared to controls (Figure 5.6). This is in contrast to the disruption of *kcne2* or *kcnq1* genes, which lead to gastric glandular hyperplasia (Roepke et al. 2006, Lee et al. 2000) and impaired acid secretion. This dramatic phenotype relies on the presence of KCNQ1/KCNE2 heteromeric channels in parietal cells (Lee et al. 2000; Dedek and Waldegger 2001; Heitzmann et al. 2004). We can therefore conclude that KCNE3 deletion did not result in any detectable alteration in gastric epithelia morphology and cytoarchitecture.

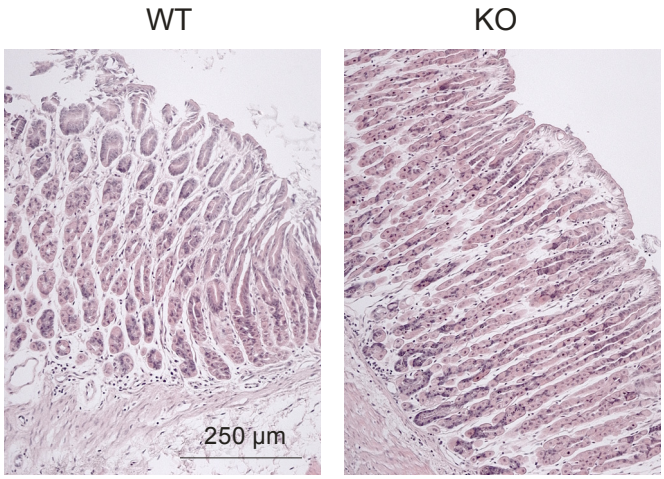


**Figure 5.6. Stomach morpholo gy.** Histological analysis of Hematoxylin/eosin (H/E) stained stomach sections from 1 year-old wild type and *kcne3*$^{-/-}$ mice. Scale bars denote same lengths for *kcne3*$^{-/-}$ and wild type. No obvious morphological diffe-rences were observed between tissues from the two genotypes.

Next, we performed an immunohistochemical analysis on wild type and *kcne3*$^{-/-}$ stomach. As shown in figure 5.7A, C and D, *kcne3*$^{-/-}$ controlled staining showed that KCNE3 was present in basolateral membranes of epithelial cells at the bottom of gastric glands. Interestingly, anti-KCNQ1 antibody yielded a similar basolateral staining pattern at these positions both in wild type or *kcne3*$^{-/-}$ stomach sections (Figure 5.7G-I). Additionally however, anti-KCNQ1 antibody strongly labeled cell bodies of other cells located closer to the opening of the gland (Figure 5.7G). As described previously (Grahammer et al. 2001a; Heitzmann et al. 2004), KCNQ1 co-localized in these latter cells with the $H^+/K^+$ ATPase (Figure 5.7H and I), identifying them as parietal cells.

Parietal cells are acid-secreting cells, that express KCNE2 as well as KCNQ1 and $H^+/K^+$ ATPase (Dedek and Waldegger 2001; Grahammer et al. 2001a; Heitzmann et al. 2004). Our data show that cells stained for KCNE3 were not positive for the $H^+/K^+$ ATPase (Figure 5.7A-D). Sections of wild type stomach showed basolateral KCNE3 staining of cells restricted to the lowest segment of the gastric gland. In particular, KCNE3 was present only in basolateral membranes of chief cells and other epithelial cells found deep down the gastric gland in the proliferative zone (Figure 5.7A, C and D). This staining was completely absent in *kcne3*$^{-/-}$ tissues (Figure 5.7E and F), providing further confirmation for the specificity of the signal.

Altogether our results indicate that, although KCNE2 is coexpressed in the gastric tissue (Dedek and Waldegger 2001) with KCNE3 , they are not expressed in the same cell type.

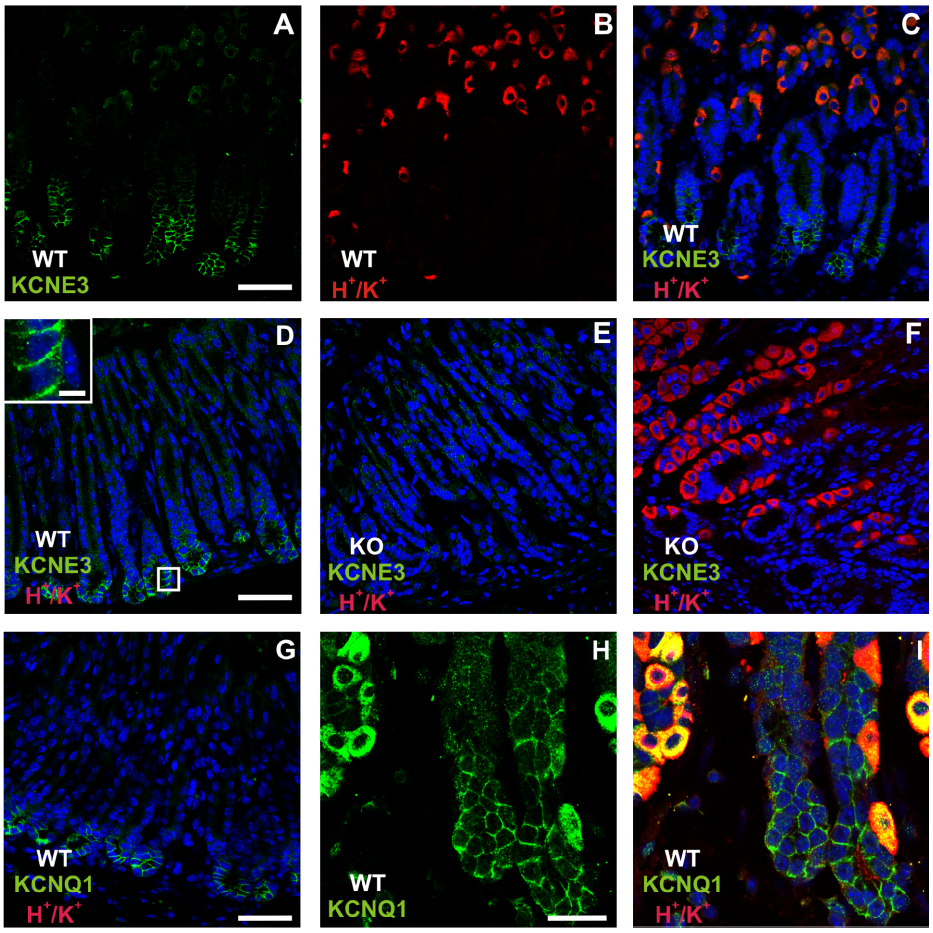


**Figure 5.7. Immunolocalization of KCNE3 in stomach**. **A-D,** immunolocalization of KCNE3 (green) and $H^+/K^+$ ATPase (B-D; red) in stomach. KCNE3 expression was restricted to the basal region of the gastric glands which are devoid of the $H^+/K^+$ ATPase. KCNE3 is expressed both in regions with a prominent presence of $H^+/K^+$ ATPase-expressing parietal cells (A-C), and in regions lacking those cells (D). **E – F,** *kcne3*$^{-/-}$ controls for specificity of KCNE3 staining in areas lacking (E) or expressing (F) the $H^+/K^+$ ATPase. G-I. Immunolocalization of KCNQ1 (green) and $H^+/K^+$ ATPase (red) in regions lacking (G) or expressing (H, I) the ATPase. KCNQ1 and the ATPase co-localize in parietal cells in a staining pattern broadly covering the cytoplasm. KCNQ1 is additionally present at the bottom of gastric glands in basolateral membranes of cells lacking $H^+/K^+$ ATPase (G). These cells express KCNE3 (A-D). KCNQ1 staining was similar in *kcne3*$^{-/-}$ stomach. Counterstaining by Topro-3 (blue) was performed to identify cell nuclei. Inset scale bar in (D), which shows higher magnification of marked area, is 5 µm. Lower right scale bar in (D) represents 50 µm and also applies to (E, F).

While KCNE2 is expressed in $H^+/K^+$ ATPase-positive parietal cells located apically in the gastric gland axis (Heitzmann et al. 2004, Roepke et al. 2006), we found KCNE3 to be present in more basal gastric gland cells (Figure 5.7A,C and D). This in an important piece of evidence that suggests possible differential functional roles of the two KCNE isoforms in the stomach.

### 5.2.4.2 Immunolocalization of KCNE3 and KCNQ1 in Small Intestine

Next, we focused on the small intestine and analyzed its morphology in the *kcne3*$^{-/-}$ mouse. Hematoxilin-eosin stained sections of *kcne3*$^{-/-}$ small intestine did not show any sign of morphological abnormality and appeared indistinguishable from control wild type tissues (Figure 5.8). Transversally and longitudinally cut villi appeared normal in *kcne3*$^{-/-}$ sections, they were not overgrown or damaged, and crypts were tightly packed as in wild type tissues (Figure 5.8).

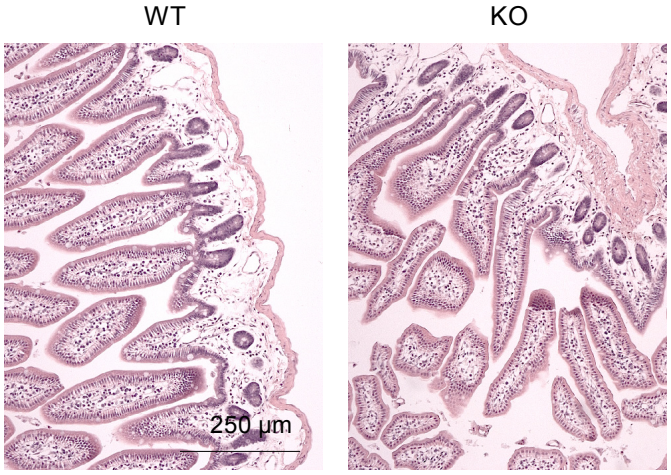


**Figure 5.8. Small intestine morpho logy.** Hematoxylin/eosin (H/E) stained small intestine sections from 1 year-old wild type and *kcne3*$^{-/-}$ mice. Scale bars denote same lengths for *kcne3*$^{-/-}$ and wild type. No obvious morphological differences were observed between tissues from the two genotypes.

In small intestine, we also analyzed in more detail the subcellular localisation of the KCNE3 protein by immunohistochemical methods. The anti-KCNE3 antibody labeled only intestinal crypts cells, whith no signal being observed in apical surface or villi (Figure 5.9A). On the other hand, *kcne3*$^{-/-}$ sections of the same organ from control littermates did not show any signal (Figure 5.9B).

Resembling KCNE3 staining and consistent with previous work (Schroeder et al. 2000; Warth et al. 2002a), we also detected KCNQ1 in wild type intestinal crypts with our anti-KCNQ1 antibody (Figure 5.9C). Similar to what we have previously shown in the stomach (Figure 5.7), *kcne3*$^{-/-}$ sections of small intestine also exhibited typical KCNQ1 expression and localization (Figure 5.9D) indistinguishable from control tissues.

Taken together, our data indicate that in wild type small intestine, KCNE3 is selectively expressed in basolateral membranes of intestinal crypts cells. Furthermore, like in the stomach (Figure 5.7), in KCNE3-deficient small intestine the localization of the KCNQ1 alpha subunit was not altered.

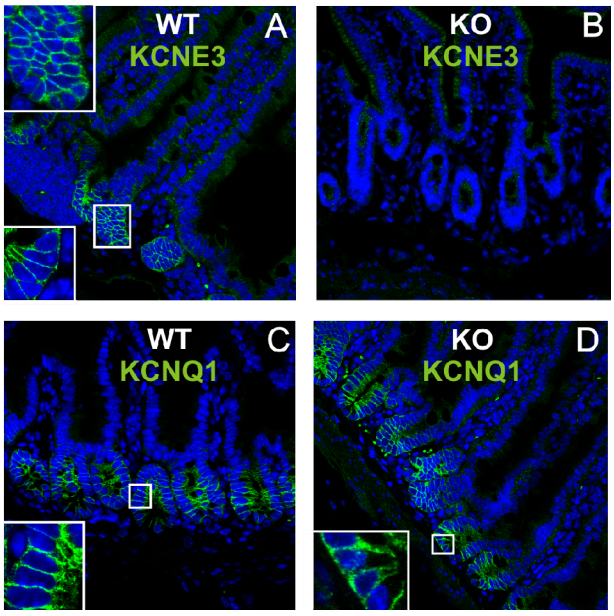


**Figure 5.9. Immunolocalization of KCNE3 in small intestine. A,** in small intestine, KCNE3 expression (green) was restricted to the basolateral membrane of crypt cells. **B**, KCNE3 staining in *kcne3*$^{-/-}$ intestine shows complete absence of specific immunoreactive signal. **C** and **D**, immunolocalization of KCNQ1 (green) in wild type (C) and *kcne3*$^{-/-}$ (D) small intestine. Basolateral KCNQ1 distribution was not altered in the *kcne3*$^{-/-}$ intestinal tissue. Nuclei are shown by Topro staining (blue). Insets show higher magnifications of regions shown in frames, except for the lower left inset of (A) that is from a different section and highlights KCNE3 expression in basolateral membranes Scale bars are 50 µm. Inset bar is 5 µm.

### 5.2.4.3 Immunolocalization of KCNE3 and KCNQ1 in Colon

Both our Northern blot (Figure 5.3) and Western blot analysis (Figure 5.5) revealed that KCNE3 expression is highest in colonic tissue. We therefore extensively investigated the general morphology of this organ in *kcne3*$^{-/-}$ animals (Figure 5.10). H-E stained colonic sections from *kcne3*$^{-/-}$ animals were indistinguishable from wild type control littermates (Figure 5.10A and B). Close examination did not reveal any aberration, obstruction or tissue damage in *kcne3*$^{-/-}$ colonic tissue. In addition, Periodic Acid Staining (PAS), which is conventionally used for staining structures containing a high proportion of carbohydrate macromolecules, showed that mucous density and accumulation were similar in both genotypes (Figure 5.10C and D). Toluiden blue staining, which selectively stains mast cells commonly found in connective tissue, did not detect infiltration of immune cells or other signs of inflammation in the *kcne3*$^{-/-}$ colon (Figure 5.10E and F).

Altogether, these data indicate that overall morphology and general function of colonic tissue in *kcne3*$^{-/-}$ animals were normal and comparable to their wild type littermates (Figure 5.10).

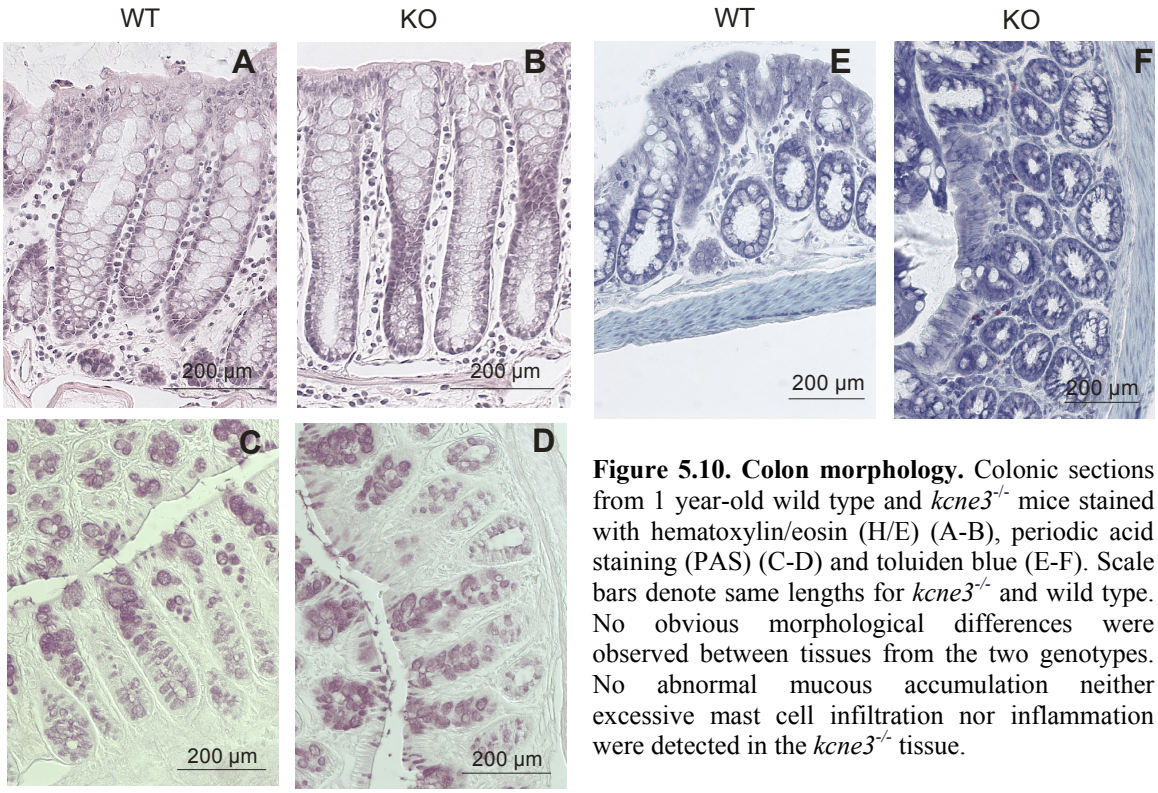


**Figure 5.10. Colon morphology.** Colonic sections from 1 year-old wild type and *kcne3*$^{-/-}$ mice stained with hematoxylin/eosin (H/E) (A-B), periodic acid staining (PAS) (C-D) and toluiden blue (E-F). Scale bars denote same lengths for *kcne3*$^{-/-}$ and wild type. No obvious morphological differences were observed between tissues from the two genotypes. No abnormal mucous accumulation neither excessive mast cell infiltration nor inflammation were detected in the *kcne3*$^{-/-}$ tissue.

Next, we analyzed the localization of KCNE3 in wild type colon. Immunohistochemical analysis revealed a prominent KCNE3 staining in the middle lower part of colonic crypts (Figure 5.11A). Consistent with other published studies focusing on KCNE3 localization in rat and guinea pig colon (Liao et al. 2005), our anti-KCNE3 antibody labeled basolateral membranes of murine colonic crypt cells. KCNE3 antibody failed to detect any protein in the *kcne3*$^{-/-}$ sections, confirming again the specificity of our signals (Figure 5.11B).

Our data therefore indicate that KCNE3 is selectively expressed in secretory regions of the colonic tissue (the crypts) all along the proximal and distal colon (Figure 5.11A). In those areas we could also identify KCNQ1 protein (Figure 5.11C and D). Anti-KCNQ1 antibody stained basolateral membranes of colonic crypts cells, overlapping perfectly to the KCNE3 localization (Figure 5.11A and C). As we have described above for *kcne3*$^{-/-}$ stomach (Figure 5.7G-I) and *kcne3*$^{-/-}$ small intestine (Figure 5.9C and D), also in *kcne3*$^{-/-}$ colonic epithelia KCNQ1 localization was unchanged (Figure 5.11C and D).

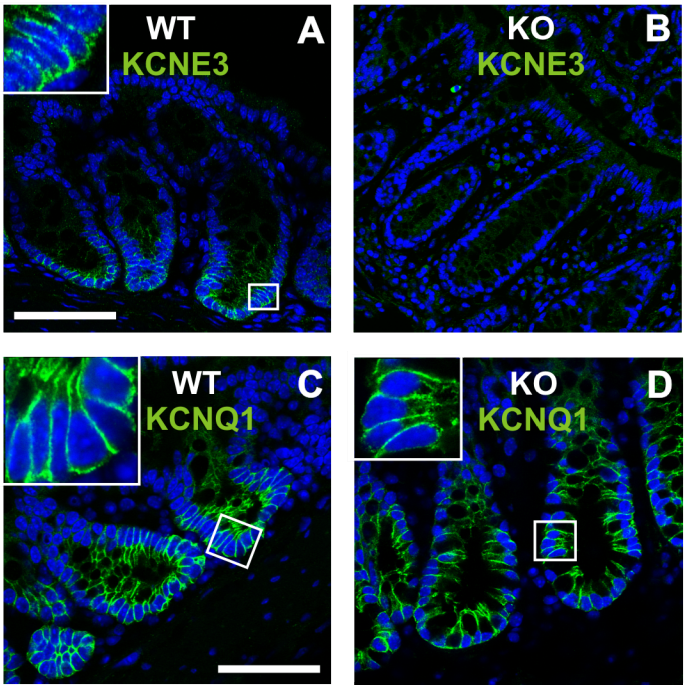


**Figure 5.11. Immunolocalization of KCNE3 in colonic epithelia. A** and **B**, KCNE3 localization (green) in the basolateral membrane of wild type colonic crypt cells (A), and absence of specific immunoreactive signal in *kcne3*$^{-/-}$ colonic tissue (B). **C** and **D**, immunolocalization of KCNQ1 (green) in wild type (C) and *kcne3*$^{-/-}$ (D) colonic tissue. Basolateral KCNQ1 distribution was not altered in the *kcne3*$^{-/-}$ tissue. Nuclei are shown by Topro staining (blue). Insets show higher magnifications of regions shown in frames. Scale bars are 50 µm. Inset bar is 5 µm.

### 5.2.4.4 Immunolocalization of KCNE3 and KCNQ1 in Trachea

Since RT-PCR experiments had previously reported KCNE3 mRNA expression in trachea, together with KCNQ1, KCNN4 and CFTR (Grahammer et al. 2001b; Cowley and Linsdell 2002) we next focused our analysis on tracheal tissue, by first analyzing the morphology of tracheal tissue in *kcne3*$^{-/-}$ animals (Figure 5.12). H/E staining revealed that the general morphology was preserved in KCNE3-deficient tracheas (Figure 5.12A-D). In addition, PAS staining of tracheal sections showed that overall physiology was conserved, since no abnormal mucous density or altered mucosal gland distribution could be observed (Figure 5.12E and F).

Next, in order to examine in more detail tracheal KCNE3 expression, we performed Western blot and immunohistochemical analysis. After long exposure of the blot, our Western blotting revealed KCNE3 expression in wild type tracheal epithelium, (Figure 5.5D), indicating that KCNE3 protein is indeed present in upper airways tissue as it was suggested previously (Grahammer et al. 2001b; Cowley and Linsdell 2002).

Furthermore, by immunohistochemical approach we were able to pin down KCNE3 localization to the lining epithelial layer in wild type trachea. As shown in Figure 5.13, KCNE3 was clearly localized at the membranes of the epithelial cells found in tracheal epithelium. Specificity of KCNE3 localization pattern was confirmed by absence of detectable signal in *kcne3*$^{-/-}$ trachea sections (Figure 5.13B).

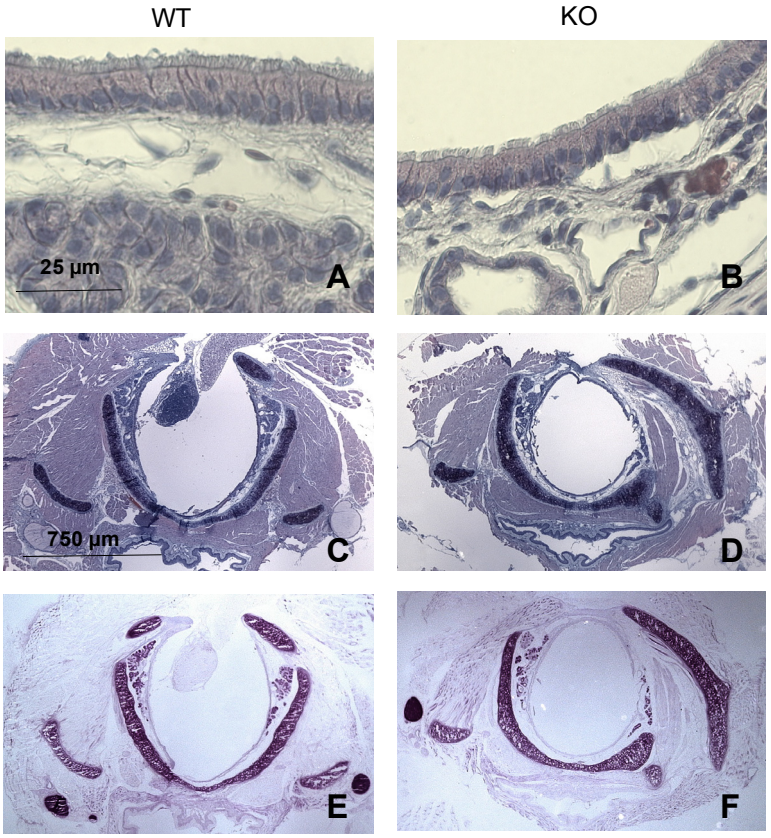


**Figure 5.12. Trachea morphology.** Histological analysis of tracheal tissue from 1 year-old wild-type and *kcne3*$^{-/-}$ mice. **A-D** hematoxylin/eosin (H/E) stained tracheal sections shown at 2 different magnification levels, from wild type (A and C) and *kcne3*$^{-/-}$ (B and D) mice. Periodic acid staining from wild type (E) and *kcne3*$^{-/-}$ (F) mice. Scale bars denote same lengths for *kcne3*$^{-/-}$ and wild type. At higher magnification, no obvious morphological differences in the tracheal lining epithelium are evident, while the lower magnification shows unaltered general morphology of tracheal tissue in *kcne3*$^{-/-}$ mouse.

Interestingly, KCNQ1 had been previously shown to localize in basolateral membranes of the epithelial airway (Grahammer et al. 2001b), the same compartments where we have observed KCNE3 expression (Figure 5.13A). These data provide the first indication for a possible interaction of KCNE3 and KCNQ1 outside the gastrointestinal tract.

In conclusion, our data indicate that KCNE3 is expressed in basolateral membrane compartment of epithelial cells in tracheal tissue. Together with the previously reported localization of KCNQ1 in the same compartments, these data suggest a possible role of the KCNQ1/KCNE3 complex to sustain cAMP stimulated $Cl^-$ secretion through CFTR in tracheal tissue.

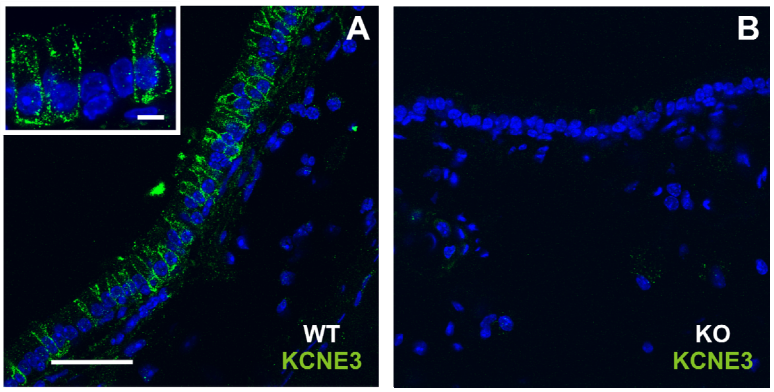


**Figure 5.13. Immunolocalization of KCNE3 in upper Airways. A,** KCNE3 localization (green) in the basolateral compartment of the lining epithelia of wild type trachea. Inset shows a magnification of the indicated area. **B,** complete absence of KCNE3 immunoreactive signal in *kcne3*$^{-/-}$ tracheal sections. Nuclei are shown by Topro staining (blue). Scale bars are 50 µm. Inset bar is 5 µm.

## 5.3 KCNQ1 is not Altered in the *kcne3*$^{-/-}$ Mouse

*In vitro* studies have shown that KCNE3 needs KCNQ1 to be efficiently transported to the plasma membrane (Schroeder et al. 2000). To test if the KCNE3 deletion resulted in altered KCNQ1 localization, we performed immunohistochemistry analysis on wild type and *kcne3*$^{-/-}$ stomach (Figure 5.7), small intestine (Figure 5.9) and colon (Figure 5.11). As discussed in previous sections, the KCNQ1 protein was expressed properly localized and did not show any abnormal distribution in both genotypes.

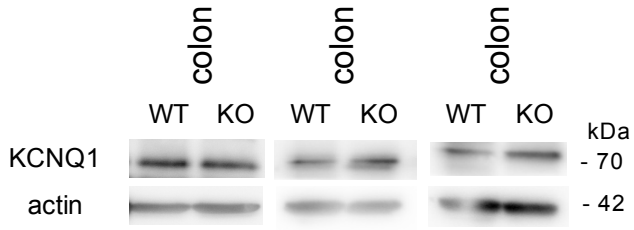


**Figure 5.14. KCNQ1 is not altered in *kcne3*$^{-/-}$ tissues.** Western blot from colonic membrane preparations shows no difference in KCNQ1 protein amount between wild type and *kcne3*$^{-/-}$ mice. Colonic membranes from 3 different wild type and *kcne3*$^{-/-}$ littermates are shown. Equal amounts of proteins (~50 µg) were loaded and α-actin served as loading control.

Furthermore, we tested if KCNQ1 expression levels were changed upon KCNE3 deletion in *kcne3*$^{-/-}$ mice. For this reason, we prepared membrane-bound protein fractions from colon of three wild type and three *kcne3*$^{-/-}$ animals, and analyzed them by Western blotting for the presence of KCNQ1. As shown in Figure 5.14, wild type and *kcne3*$^{-/-}$ fractions did not exhibit any compensatory change in KCNQ1 expression levels. Taken together, these results indicate that KCNE3 deletion did not result in any compensatory change in expression levels of the alpha-subunits. Furthermore, the subcellular localization of KCNQ1 in gastrointestinal epithelia was also unaffected by KCNE3 deletion.

## 5.4 Analysis of Metabolic Parameters in *kcne3*$^{-/-}$ Mouse

Our data indicate that KCNE3 is expressed in several epithelial tissues with absorptive and secretory function. In order to investigate in more detail the physiological implications of KCNE3 deletion, *kcne3*$^{-/-}$ and control mice were subjected to metabolic cage experiment.

| | | *KCNE3* $^{+/+}$ | *KCNE3* $^{-/-}$ |
|---|---|---|---|
| Urine (n=6 per genotype) | Creatinine mM | 2.6 ± 0.5 | 3.1 ± 0.31 |
| | K/creatinine (mmol/mmol) | 112.2 ± 5.7 | 104.3 ± 6.1 |
| | Na/creatinine (mmol/mmol) | 39 ± 1.7 | 37.6 ± 2.5 |
| | Cl/creatinine (mmol/mmol) | 75.6 ± 3.8 | 68.8 ± 2.9 |
| | Ca/creatinine (mmol/mmol) | 0.8 ± 0.1 | 1.2 ± 0.6 |
| | Mg/creatinine (mmol/mmol) | 8.6 ± 0.6 | 7.7 ± 1.2 |
| | Pi/creatinine (mmol/mmol) | 14.8 ± 2.1 | 14 ± 1.7 |
| | Protein/creatinine (mg/mg) | 29.6 ± 2.7 | 28.5 ± 2.2 |
| Feces (n=4 per genotype) | Na µmol/ gr dry | 40.7 ± 10.2 | 28 ± 8.5 |
| | K µmol/ gr dry | 137.6 ± 32.2 | 81.9 ± 25.7 |
| Serum (n= 8 per genotype) | K (mM) | 7.2 ± 0.8 | 6.3 ± 1 |
| | Na (mM) | 131.2 ± 5.6 | 126.7 ± 2.3 |
| | Cl (mM) | 96.8 ± 3.8 | 93.4 ± 2.7 |
| | Ca (mM) | 1.9 ± 0.1 | 2.1 ± 0.1 |
| | Mg (mM) | 1.3 ± 0.1 | 1.3 ± 0.1 |
| | Protein (g/dL) | 3.8 ± 0.2 | 3.9 ± 0.1 |
| | Phosphorus (mM) | 3.6 ± 0.3 | 3.1 ± 0.1 |
| | Glucose (mM) | 16.4 ± 1.7 | 14.9 ± 1.5 |
| | ALP IU/L | 71.3 ± 0.8 | 62.4 ± 3.5 |

**Table 5.1. Urine, feces, and serum parameters from wild type and *kcne3*$^{-/-}$ mice.** *Urine*, electrolyte and protein levels were normalized to the creatinine values. *Feces,* $Na^+$ and $K^+$ concentrations assessed in fecal water were normalized to their dried weight. *Serum*, electrolytes and protein content are indicated as mM concentrations. No statistically significant difference was observed between wild type and *kcne3*$^{-/-}$ mice in any of the measured parameter in urine, feces and serum. Each urine and feces sample consisted of 1 day of recollection from N animals (6 recollection days in total). The number of animals is indicated in brackets. Data are shown as mean ± SEM.

This approach allows monitoring of mice under standardized conditions, collecting urine and feces as well as tracking of food and water intake to analyze general ion homeostasis and renal function. Animal weight, food and water intake were monitored every 24 hours in *kcne3*$^{-/-}$ mice and their wild type control littermates. The biochemical analysis of serum, urine and feces did not reveal any statistically significant difference between *kcne3*$^{-/-}$ and wild type littermates (table 5.1).

These results conclude that *kcne3* disruption in the gastrointestinal system did not impair $Na^+$ absorption or $K^+$ secretion. Although KCNE3 had been previously reported be expressed in human kidney (Schroeder et al. 2000), we did not detect KCNE3 mRNA nor protein in the murine kidney samples analyzed (Figure 5.3A and 5.5C). Moreover, all the metabolic parameters measured from urine samples of *kcne3*$^{-/-}$ animals were within the normal range, further indicating that kidney function in the *kcne3*$^{-/-}$ mouse was not altered.

## 5.5 Analysis of the Secretory Function in *kcne3*$^{-/-}$ Intestinal Epithelia

Hans Ussing invented the Ussing chamber in the 1950s to measure the net ion transport taking place across an epithelium clamped between two chambers that are filled with Ringer solution. Ions that move through paracellular pathways, tight junctions or across the cell generate a voltage difference among chambers. Addition of specific drugs will promote or inhibit channel activity and modify the ionic conductances, thereby changing the voltage. The amount of injected current (called short circuit current, $I_{sc}$) necessary to clamp the voltage to 0 mV is the measure of net ion transport taking place across the epithelium.

To study the secretory functions of *kcne3*$^{-/-}$ colonic epithelia, we performed Ussing chamber experiments from colonic tissue preparations.

### 5.5.1 Role of KCNQ1/KCNE3 $K^+$ Channels in Colonic Chloride Secretion

Based on the biophysical and pharmacological properties of KCNQ1/KCNE3 heteromers, it has been previously postulated that KCNQ1/KCNE3 channels might be involved in increasing the driving force for apical $Cl^-$ exit by hyperpolarizing the apical membrane and recycling basolateral $K^+$ (Greger et al. 1997; Schroeder et al. 2000).

To determine whether cAMP-stimulated $Cl^-$ secretion was impaired in the *kcne3*$^{-/-}$ intestine, colonic samples were mounted in Ussing chambers, and both basal and drug stimulated secretion were measured under short-circuit current ($I_{sc}$) conditions (Figure 5.15).

To avoid stimulation of colonic transport by prostaglandins that may be generated and liberated from submucosal tissue and to inhibit action potentials of attached neurons, indomethacin (10 μM) and tetrodotoxin (1 μM), respectively, were present throughout these experiments. For better isolation of $Cl^-$ currents, apical ENaC $Na^+$ channels were inhibited by 10 μM amiloride (Figure 5.15).

First, we investigated the effects of forskolin addition (10 μM) on net ion flux in colonic tissues from *kcne3*$^{-/-}$ and wild type littermates. Forskolin is a natural medicinal component, produced by the plant *Coleus forskohlii*, which activates adenylate cyclase thereby stimulating cAMP production. Forskolin application leads to CFTR and KCNQ1/KCNE3 activation.

The addition of 10 μM forskolin, evoked a large and sustained anion secretion ($I_{sc}$ 156.8 ± 21.7 μA/cm$^2$, n=7) seen by a peak in the recorded $I_{sc}$ in wild type colonic tissue (Figure 5.15A and C). In addition, this current component could be efficiently inhibited by 10 μM chromanol 293B, a $K^+$ channel inhibitor that preferentially inhibits KCNQ1-containing channels (Figure 5.15A and C) with an $IC_{50}$~1-10 μM. In wild type samples, the remaining current after chromanol 293B application was 51.3 ± 11.5 μA/cm$^2$. In contrast to wild type, forskolin-stimulated current was almost abolished in *kcne3*$^{-/-}$ colon ($I_{sc}$ = 34.1 ± 5.4 μA/cm$^2$, n=6) and the application of chromanol 293B had no effect (Figure 5.15B).

Additionally, carbachol was used to stimulate muscarinic $Ca^{++}$ dependent $Cl^-$ secretion, and led to increases in $I_{sc}$ that were on average indistinguishable between wild type and *kcne3*$^{-/-}$ tissue (Figure 5.15A-C; $I_{sc}$ WT 95.7 ±16.6 μA/cm$^2$ ; $I_{sc}$ KO 112.9 ± 24.1 μA/cm$^2$).

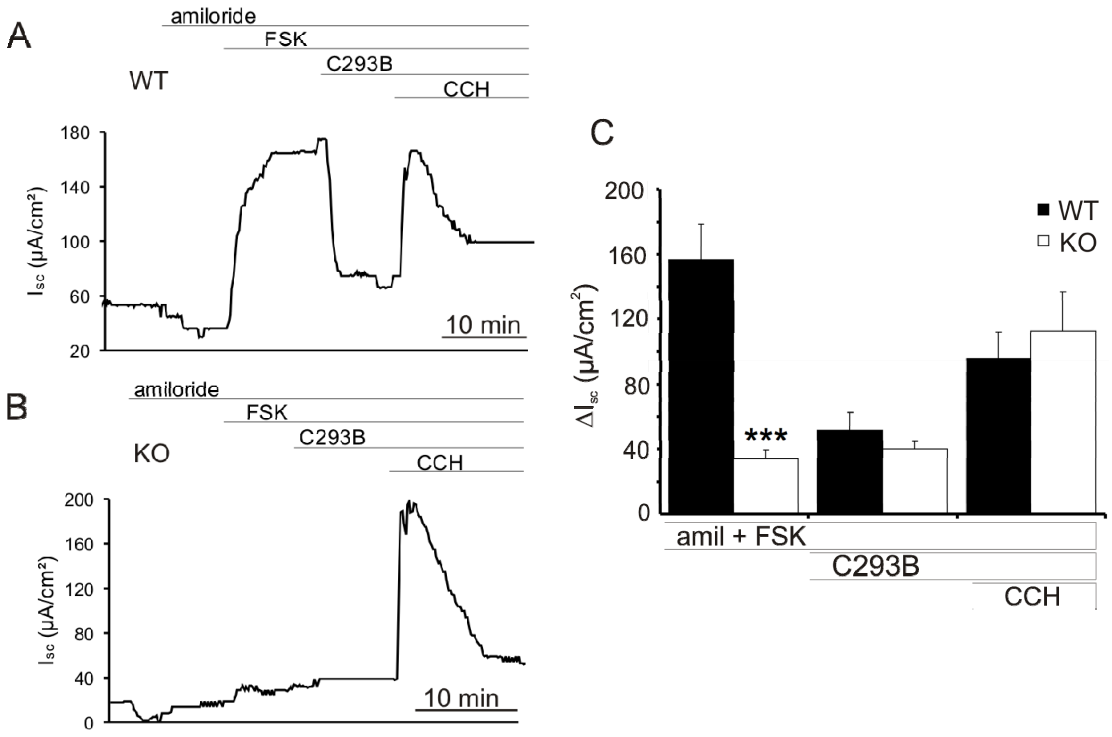


**Figure 5.15. Transepithelial transport across intestinal epithelia of wild type and *kcne3*$^{-/-}$ mice.** **A** and **B,** representative traces of short-circuit current (Isc) recordings performed with Ussing Chamber from wild type (A) and *kcne3*$^{-/-}$ (B) distal colon clamped to 0 mV. Luminal amiloride (10µM), serosal forskolin (FSK; 10 µM), serosal chromanol 293B (C293B, 10 µM), and serosal carbachol (CCH, 100 µM) applications are shown above the traces. **C.** Bar graph summarizing the mean of ΔIsc under different conditions (WT, n = 7; KO, n = 6). Data are means ± SEM. (*) Indicates the level of significance of p<0.0005. The resistance of the colonic tissues was 66.8 ± 5.2 (WT) and 68.4 ± 5.0 (KO) Ω cm2, . The resistance of the fluid amounted to 19 - 25 Ω cm2.

Carbachol binds to muscarinic acetylcholine receptors, activating a G-protein (Gq/11) cascade that stimulates phospholipase C that in turn hydrolyzes phophatidyilinositol ($PIP_2$) to diacyl glycerol (DAG) and inositol triphosphate ($IP_3$). The latter will release the $Ca^{++}$ from the endoplasmatic reticulum (ER), by acting on $IP_3$ receptors bound to the ER membrane.

Increases in cytosolic $Ca^{++}$ promote a $K^+$ efflux at the basolateral membrane due to KCNN4 activation. Simultaneous increase of intracellular cAMP and $Ca^{++}$ will promote a synergistic acute effect on anion secretion, as seen in figure 5.15A-C for both genotypes. Since the recorded carbachol stimulated $I_{sc}$ were within the normal range (Strabel and Diener 1995; Warth et al. 1999b) for both genotypes, carbachol was a suitable test for tissue viability, and was used at the end of every experiment.

Similar results were obtained with tissue samples taken from the proximal, middle and distal parts of the colon.

Taken together, these results clearly demonstrate the dependence of the cAMP-stimulated $Cl^-$ secretion pathway on the KCNE3 subunit. Membrane hyperpolarization and $K^+$ recycling via the KCNQ1/KCNE3 is therefore a key pathway to sustain cAMP-activated $Cl^-$ secretion all along the colonic tissue. Interestingly, the response to carbachol was not affected in *kcne3*$^{-/-}$ tissues (Figure 5.15B and C), indicating that cAMP and $Ca^{++}$ stimulated $Cl^-$ secretion do not crosstalk and function independently one from the other in the murine colon.

## 5.5.2 Whole Cell Recordings of Colonic Crypt Cells

The results obtained with the Ussing chamber technique, were further supported by electrophysiological data of whole cell recordings from intact murine colonic crypts (please see material and methods for additional details).

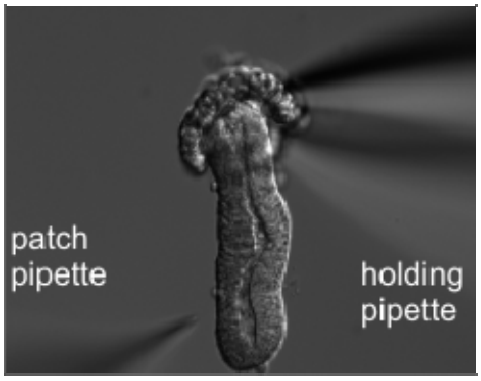


**Figure 5.16. Colonic crypt.** Picture showing a colonic crypt under the electrophysiological recording configuration. The holding pipette stabilizes the crypt, while the recording patch-pipette is approaching. One cell per colonic crypt was patched. All the recorded cells were from the lower part of the colonic crypt.

Colonic crypt cell patching is a challenging technique where cells from the mid-basal crypt are patched while the upper part of the crypt is smoothly sucked by holding pipette (Figure 5.16). Patches lasted from 5 to 10 minutes, long enough to apply a voltage step protocol ranging from -95 mV to +25 mV under the 3 following solutions: (1) control, (2) control + forskolin, and (3) control + forskolin + chromanol 293B. As described in the previous section, forskolin will raise intracellular cAMP and consequently $Cl^-$ will be secreted apically through CFTR, thus increasing the total currents.

Addition of chromanol 293B, will specifically inhibit KCNQ1/KCNE3 currents ($IC_{50}$ = 1-10 μM), affecting the driving force for $Cl^-$ and its secretion. There has not been yet published any study regarding murine colonic crypt patching, but the existence of the

chromanol 293B sensitive whole cell current component had been reported for rat colonic crypts (Diener et al. 1996; Schroeder et al. 2000).

Our experiments demonstrated that also murine wild type colonic crypt cells exhibited a $K^+$ conductance sensitive to chromanol 293B (Figure 5.17E and F), that was absent in *kcne3*$^{-/-}$ colonic cells.

Under control conditions both, wild type and *kcne3*$^{-/-}$ colonic crypt cells displayed whole-cell currents that depended almost linearly on voltage (Figure 5.17A, B and D). Consistent with a reduced $K^+$ conductance, currents from *kcne3*$^{-/-}$ cells were about 30% smaller than those from wild type cells and reversed at a slightly more positive voltage.

In the presence of forskolin (Figure 5.17B, C and D), currents from both wild type and *kcne3*$^{-/-}$ crypt cells reversed at more positive potential (WT control is -75 mV and WT FSK -45 mV; KO control is -70 mV and KO FSK is -35 mV), compatible with a prominent $Cl^-$ current component carried by CFTR in cells from both genotypes. Under our ionic conditions, the $Cl^-$ reversal potential is calculated to -37 mV. Again, currents of *kcne3*$^{-/-}$ cells showed a more positive reversal potential that is compatible with a partial loss of a $K^+$ conductance.

Surprisingly, even though cAMP should increase total currents through CFTR and KCNQ1/KCNE3 (Figure 5.17B, C and D), the whole cell conductance was not increased by forskolin (at 25 mV: WT control 131.7 ± 13.7 pF/pA, WT FSK: 112.5 ± 21.5 pA/pF, and KO control 91.9 ±15.1 pF/pA, KO FSK: 61.9 ± 4.5 pA/pF, n= 9). It is worth to mention that another group obtained similar results in similar an experimental configuration (Diener et al. 1996).

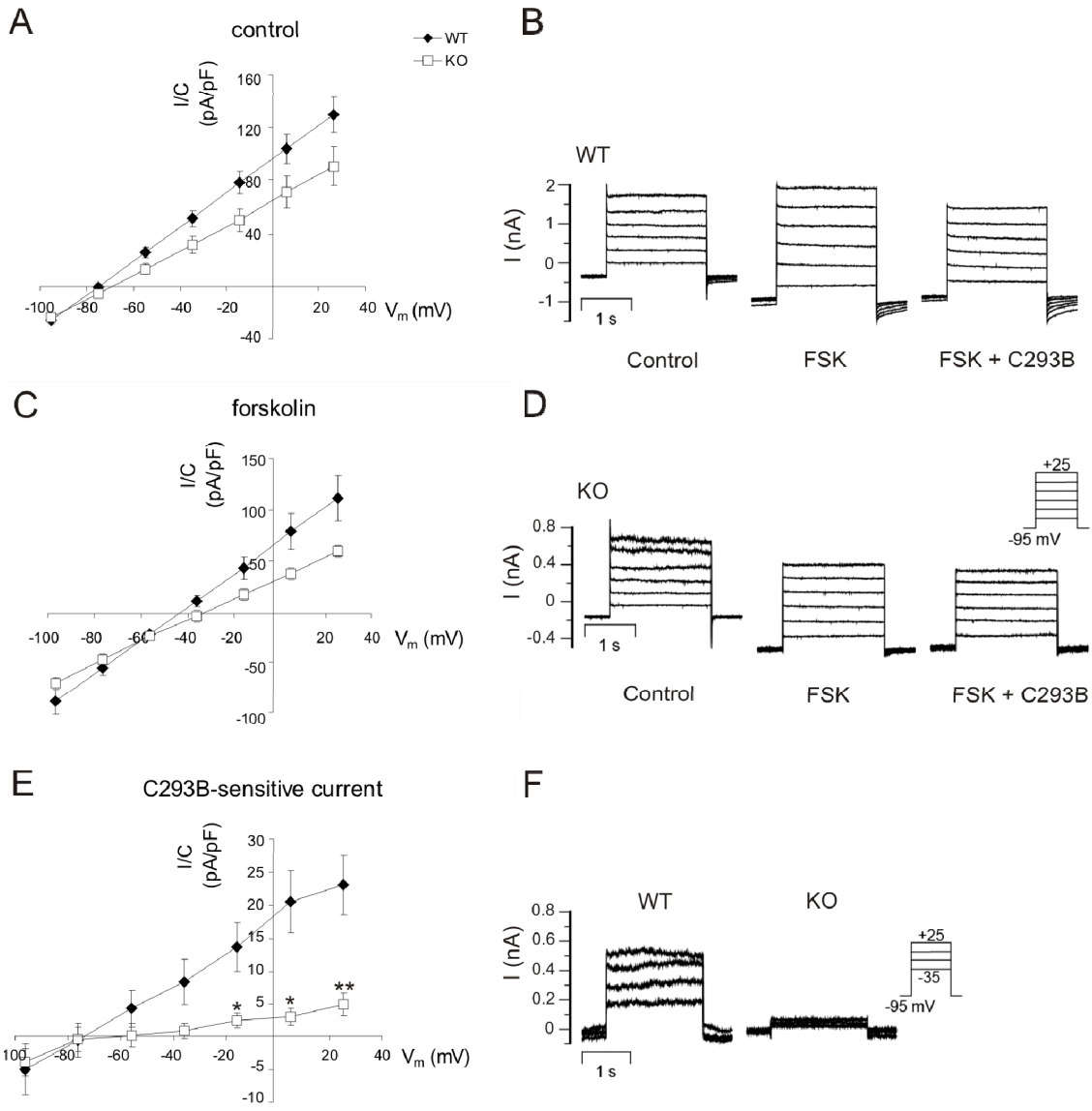


**Figure 5.17. Whole-cell recordings from wild type and *kcne3*$^{-/-}$ colonic crypt cells**. **A** and **C,** current/voltage relationship of WT (♦) and KO (□) colonic crypt cells under control conditions (A) and after addition of 10 µM forskolin (C). Number of cells: (A), 10 WT, 9 KO; (C) 10 WT, 7 KO. **E,** C293B-inhibitable current component of wild type (♦) and *kcne3*$^{-/-}$ (□) colonic crypt cells obtained by subtracting currents recorded in the presence of FSK from those in the presence of both FSK and C293B (10 WT and 7 KO) cells). **B** and **D,** representative current traces recorded from wild type (B) and *kcne3*$^{-/-}$ (D) colonic crypts during superfusion with control- (left), FSK- (middle) and FSK + 293B-containing solutions (right). From a holding potential of -95 mV, the voltage was clamped for 2 s to values between -95 and +25 mV (voltage-step protocol shown as inset in figure D). **F,** representative traces of 293B-sensitive currents recorded from wild type and *kcne3*$^{-/-}$ crypt cells. Recorded cells were located at the lower third of an isolated crypt. Voltage-step protocol is shown in the inset. Mean values ± SEM are shown.*, $p<0.05$. **, $p<0.005$.

This result can be explained either by a concomitant downregulation of apical $Na^+$ absorption (by ENaC), or by a deactivation of $K^+$ outward currents, e.g. carried out by KCNN4. Increases of cytosolic cAMP may switch off the $Ca^{++}$ activated $K^+$ conductances, producing a slight decrease in total currents.

Nonetheless, *kcne3*$^{-/-}$ cells exhibit lower whole cell currents under forskolin compared to wild type cells (Figure 5.17C), probably due to the lack of the basolateral hyperpolarizing KCNQ1/KCNE3 $K^+$ channel complex, which lowered the driving force for $Cl^-$ to exit apically the cell.

We next evaluated the chromanol 293B-sensitive current after stimulation by forskolin (Figure 5.17E). This current was obtained by subtracting the chromanol 293B remaining currents from the forskolin induced currents (WT chromanol 293B sensitive 22.9 ± 4.6 pA/pF, n = 10; *kcne3*$^{-/-}$ chromanol 293B sensitive 4.3 ± 1.7 pA/pF, n = 7; p-value=0.003). The chromanol 293B sensitive current component, which accounts for about 20% of whole cell current under our experimental conditions, was totally abolished in *kcne3*$^{-/-}$ crypt cells (Figure 5.17 E and F).

The reversal potential of the inhibited current is about -75 mV, which is close to the $K^+$ reversal potential (-86.2 mV with 140 mM in the pipette and 5.6 mM in the bathing solution). Wild type cells clearly showed a $K^+$ current, which was absent in *kcne3*$^{-/-}$ cells (Figure 5.17E and F).

As a conclusion, these results show that first, whole cell currents from *kcne3*$^{-/-}$ crypt cells were 30% smaller compared to wild type controls, corresponding to a partial loss of the $K^+$ conductance. Second, consistent with the lack of a basolateral hyperpolarizing $K^+$ channel, forskolin stimulated currents from *kcne3*$^{-/-}$ cells reversed at more positive potentials. Third, *kcne3*$^{-/-}$ cells show a nearly totally abolished chromanol 293B sensitive current, indicating that KCNQ1/KCNE3 mediates the bulk of chromanol 293B sensitive current.

### 5.5.3 Analysis of Cholera Toxin Mediated Intestinal Fluid Secretion *in vivo*

At the molecular level, we have shown that KCNE3 and KCNQ1 were both expressed (Figure 5.5 and 5.14) in basolateral membranes of gastrointestinal tissues (Figure 5.7, 5.9 and 5.11). At the functional level, we demonstrated that *ex vivo* colonic tissues from *kcne3*$^{-/-}$ animals were unable to secrete $Cl^-$ in response to an increase in intracellular cAMP levels (Figure 5.15). Next, we decided to test *in vivo* the effect of cholera toxin on intestinal fluid secretion in the *kcne3*$^{-/-}$ mouse.

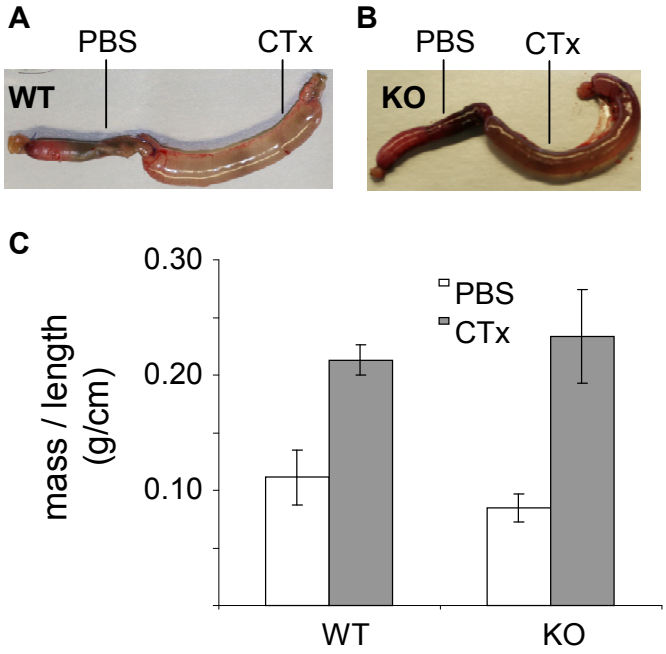


**Figure 5.18. *Kcne3*$^{-/-}$ mice show no difference from wild type in CTx-mediated small intestine fluid secretion. A** and **B,** representative ileal loops 5 h after luminal injection of PBS alone (left ligated loop) and PBS + cholera toxin (CTx; 0.5 µg per loop) (right ligated loop) in wild type (A) and *kcne3*$^{-/-}$ mice (B). **C,** bar graphs showing averaged loop mass/length from wild type and *kcne3*$^{-/-}$ mice 5 h after PBS (white bar) and PBS + CTx (grey bar) injections. Data are shown as mean ± SEM, n=3 each. There are no statistically significant differences between the two genotypes.

Injection of cholera toxin into intestinal closed-loops induces an acute luminal fluid accumulation, due to a dramatic $Cl^-$ secretion in the intestinal lumen (Richardson et al. 1984). Consequently, net increase in gut weight (weight of maximally stimulated minus weight of unstimulated loops) can be taken as an estimate for the cholera toxin effect on fluid secretion (Banwell et al. 1970).

In our experiments (Figure 5.18), examination of the averaged gut mass/length indicated that *kcne3*$^{-/-}$ mice were able to secrete fluid as efficiently as their wild type littermates (CTx KO 0.23±0.04; PBS KO 0.084±0.012; CTx WT 0.213±0.013; PBS WT 0.111±0.02).

In *kcne3*$^{-/-}$ mice we could not observe the expected reduction in intestinal fluid loss after *in vivo* cholera toxin injection. Cholera toxin promoted an acute and dramatic $Cl^-$ secretion also in the *kcne3*$^{-/-}$ gastrointestinal tissue (Figure 5.18).

## 5.6 Analysis of the Secretory Function in *kcne3*$^{-/-}$ Airway Epithelia

In ciliated cells of the airways lining epithelia there are two main ion fluxes: $Cl^-$ secretion (through CFTR and $Ca^{++}$-activated $Cl^-$ channel CaCC) and $Na^+$ absorption through ENaC.

In human airways CFTR is the main player for $Cl^-$ secretion, as mutations in CFTR lead to a dramatic pathology, Cystic Fibrosis, where inappropriate $Cl^-$ secretion unbalances

the airway surface liquid (ASL). In murine airways however, there seem to be at least an equal contribution from CaCC and CFTR, since *cftr*$^{-/-}$ mice did not suffer of any kind of airway complication. Although, it is important to notice that the different tracheal morphology might also account for the discrepancies between human and murine studies.

To study the secretory functions of *kcne3*$^{-/-}$ tracheal epithelia, we performed Ussing chamber experiments from tracheal tissue preparations. In addition, to study the impact of the KCNE3 deletion on tracheal tissue function, we performed mucociliay clearance experiments.

### 5.6.1 Role of KCNQ1/KCNE3 in Tracheal Chloride Secretion

Since KCNE3 is expressed in trachea (Figure 5.13), we studied short-circuit currents ($I_{sc}$) of tracheal preparations in Ussing chamber experiments to assess the contribution of KCNE3 to epithelial transport in upper airways.

Consistent with the notion that KCNQ1/E3 support $Cl^-$ secretion but not $Na^+$ absorption in epithelial cells, basal and amiloride-sensitive currents (Figure 5.19A and C) showed no significant difference between wild type and *kcne3*$^{-/-}$ tissues (WT amiloride -48.37 ± 11.73 µA/cm$^2$ n=12; KO amiloride -82.55 ± 16.98 µA/cm$^2$ n=11; p=0.2).

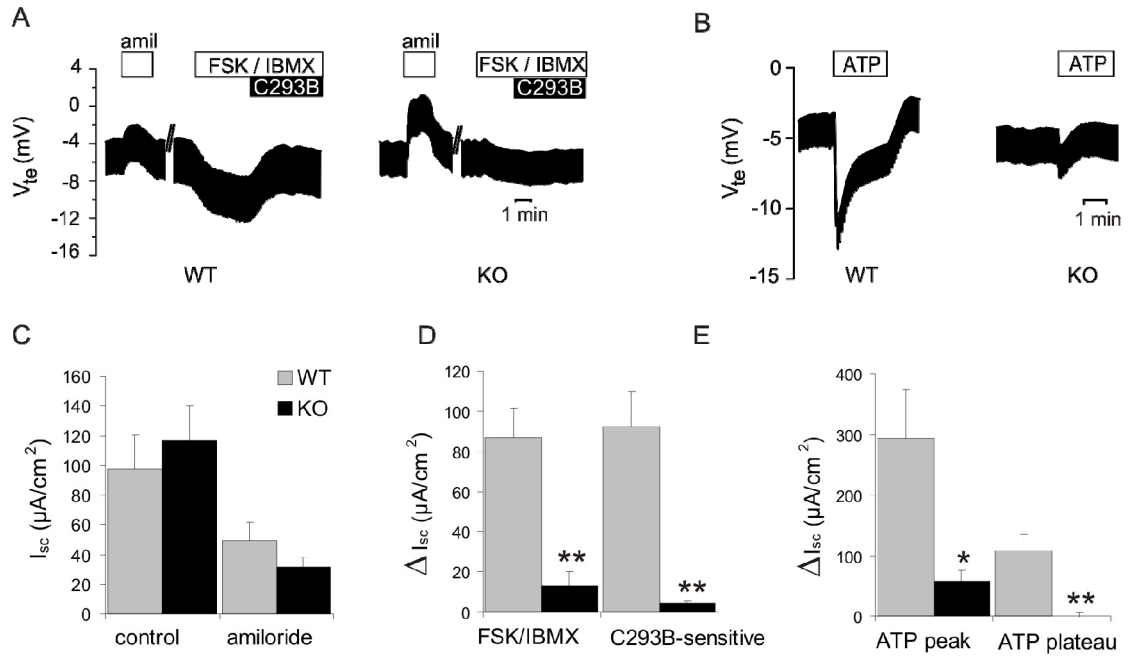


**Figure 5.19. Effect of secretagogues on ion transport by tracheal epithelia from wild type and *kcne3*$^{-/-}$ mice measured under current-clamp conditions. A** and **B,** original continuous Ussing-chamber recording of transepithelial voltage (Vte) for wild type (left) and *kcne3*$^{-/-}$ (right) tracheas. The upper line shows $V_{te}$, the length of the voltage pulses reflects the transepithelial resistance (Rte). Luminal amiloride (20 µM), serosal forskolin (FSK; 2 µM), serosal IBMX (100 µM), serosal chromanol 293B (C293B; 10µM) and luminal ATP (100µM) applications are shown above the traces. Luminal application of amiloride or FSK, and C293B in the presence of FSK are shown in A. Luminal application of ATP (B) caused a biphasic response in wild type tracheas (left): a rapid transient increase ("peak") of Vte was followed by a steady state lumen-negative Vte. Both deflections were drastically reduced in *kcne3*$^{-/-}$ tissues. **C,** bar graph summary of the mean calculated short circuit current (Isc) from wild type and *kcne3*$^{-/-}$ tracheas under control and luminal application of amiloride (10 µM) (WT, n = 12; KO, n=11). **D,** bar graphs summarizing differential currents (ΔIsc) by serosal application of forskolin (FSK; 2µM) plus IBMX (100 µM) (left bars), and calculated C293B-sensitive component of forskolin–stimulated current (right bars) of wild type and *kcne3*$^{-/-}$ tracheas. *Kcne3*$^{-/-}$ tissues showed a drastic reduction in current response to serosal application of FSK and IBMX as well as almost complete absence of C293B-sensitive currents (C293B 10µM). **E,** maximal (peak) and steady-state (plateau) differential currents ΔIsc induced by 100 µM ATP showing a significant lower ATP peak and plateau for the *kcne3*$^{-/-}$ trachea (WT, n = 12; KO, n = 10). Data are means ± SEM. * $p<0.05$ ** $p<0.005$. The resistance of the tracheal tissue samples was 42.2 ± 2.6 and 46.1 ± 2.6 Ω cm$^2$. The resistance of the fluid in the Ussing chamber was 3.4 ± 2.1 Ω cm$^2$.

In a first set of experiments, we analyzed cAMP-stimulated $Cl^-$ secretion in *kcne3*$^{-/-}$ tracheas by monitoring $I_{sc}$ after forskolin application. Compared to wild type controls, *kcne3*$^{-/-}$ tracheas exhibited lower levels of luminal $Cl^-$ secretion induced by application of forskolin plus IBMX (that prevents cAMP from being degraded) (Figure 5.19A and D; WT IBMX+FSK -86.73 ± 14.95 µA/cm$^2$ n=11 ; KO IBMX+FSK -13.5 ± 7.09 µA/cm$^2$ n=8).

The addition of the specific KCNQ1 inhibitor chromanol 293B ($IC_{50}$= 1-10 µM), abolished about 90% of the wild type current induced by forskolin and IBMX (Figure

5.19A and D; Figure 5.20). Chromanol 293B had no effect on *kcne3*$^{-/-}$ trachea (WT chromanol 293B 92.41 ± 15.16 μA/cm$^2$ n= 11; KO C293 4.11 ± 1.48 μA/cm$^2$ n=8).

In a second set of experiments, we used carbachol application to monitor $Ca^{++}$ dependent $Cl^-$ secretion from *kcne3*$^{-/-}$ and wild type tracheal tissues (Figure 5.20). In wild type trachea, carbachol application led to a massive increase in $I_{sc}$ that was reduced in *kcne3*$^{-/-}$ trachea (Figure 5.20).

In a subsequent set of experiments, $Cl^-$ secretion from *kcne3*$^{-/-}$ and wild type tracheas was induced by ATP application (100 μM) (Figure 5.19B and E; Figure 5.20). ATP binds to luminal P2Y receptors and raise both intracellular cAMP and $Ca^{++}$ levels (Kottgen et al. 2003; Mounkaila et al. 2005), thereby activating apical $Cl^-$ secretion via CFTR and CaCC.

Upon ATP application, wild type trachea $I_{sc}$ was increased approximately 4-fold at its peak and then declined to a plateau value that was about twice as large as control. This effect of ATP was drastically reduced in *kcne3*$^{-/-}$ trachea (Figure 5.19B and E; Figure 5.20; wild type ATP -293.62 ± 80.54 μA/cm$^2$ n= 12 ; KO ATP -58.10 ± 17.41 μA/cm$^2$ n=10). These results indicate that basolateral $K^+$ secretion through KCNQ1/KCNE3 is also needed under parallel activation of cAMP and $Ca^{++}$ intracellular pathways.

Note that compared to forskolin/IBMX (Figure 5.19A and D), the increase in wild type $I_{sc}$ was larger when we applied ATP (Figure 5.19B and E), which raised both intracellular cAMP and $Ca^{++}$ levels, leading to a synergistic potentiation of $Cl^-$ efflux.

In addition, a new set of experiments was done in the presence of the ENaC channel inhibitor amiloride (10 μM) (Figure 5.20) in order to better isolate $Cl^-$ currents, and to assess the contribution of $Na^+$ absorption to the recorded $I_{sc}$. Also in the presence of amiloride, ATP, forskolin/IBMX and carbachol stimulated currents were decreased in *kcne3*$^{-/-}$ tracheas compared to wild type controls (Figure 5.20).

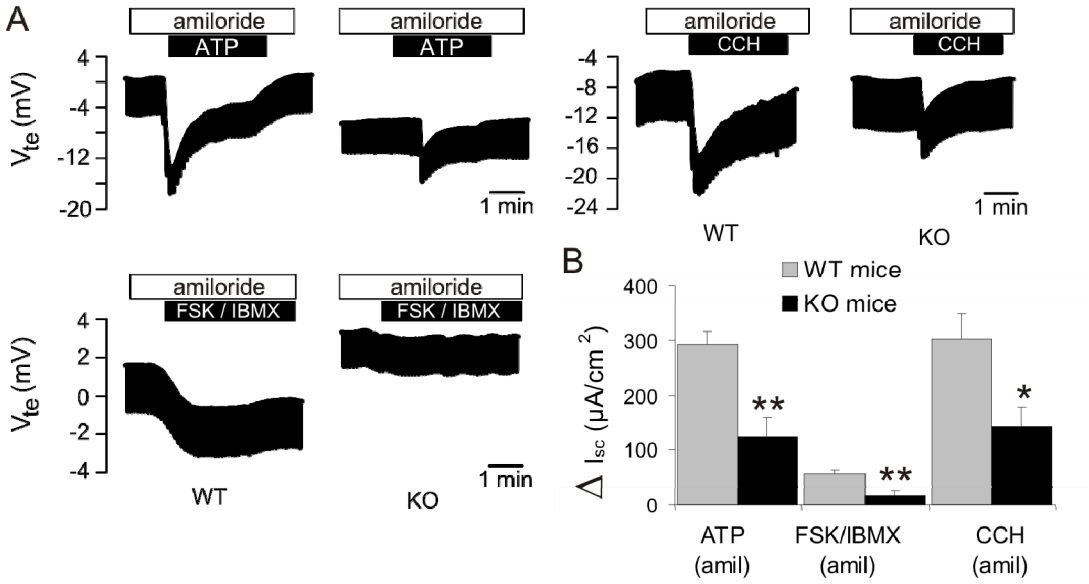


**Figure 5.20**. **Effect of secretagogues on ion transport by tracheal epithelia in the presence of 20 µM amiloride to abolish Na+- transport**. **A,** original recordings showing effects of luminal ATP (100 µM), FSK (2 µM) + IBMX (100 µM), and carbachol (100 µM) on wild type and *kcne3*$^{-/-}$ tracheas. **B,** mean differential currents (ΔIsc) induced by 100 µM ATP, 2 µM FSK + 100 µM IBMX, or 100 µM carbachol, always in the presence of 20 µM amiloride. Number of measurements (animals): WT, 7; KO, 7. *, $p<0.05$. **, $p<0.005$. The resistance of the tracheal tissue samples was 42.2 ± 2.6 and 46.1 ± 2.6 Ω cm$^2$. The resistance of the fluid in the Ussing chamber was 3.4 ± 2.1 Ω cm$^2$.

Altogether, our results indicate that KCNE3 containing $K^+$ channels, probably by increasing the driving force for apical $Cl^-$ exit, are involved in both cAMP- and $Ca^{++}$-activated apical $Cl^-$ secretion in tracheal tissues.

## 5.6.2 Analysis of Mucociliary Clearance

The mucociliary clearance is the mechanism to maintain the airways clear from any inhalated pollutants by transporting a viscous film of mucous upwards (Knowles and Boucher 2002). Mucociliary dysfunction is a common feature of chronic airway diseases in humans suffering from cystic fibrosis, asthma, and chronic bronchitis. However, the mechanisms that lead to deficient mucous clearance are still poorly understood. It is suggested that purines control the clearance by regulating the water transport and electrolyte secretion (Tarran et al. 2002; Hayashi et al. 2005).

In order to address the impact of KCNE3 deletion on mucociliary clearance, we measured *ex vivo* the ciliary transport of small (6 µm) polystyrene microspheres in isolated tracheas from *kcne3*$^{-/-}$ and wild type animals. Under control conditions, basal transport was similar in wild type and *kcne3*$^{-/-}$ tissues (Figure 5.21). Addition of ATP increased the particle transport rate in both genotypes (WT ATP 361.63 ± 78.01

µm/min, n=10; KO ATP 261.59 ± 51.58 µm/min, n=9). Interestingly, while in *kcne3*$^{-/-}$ tracheas MCC in the presence of ATP did not statistically differ from the control conditions, in wild type controls a significant increase was observed (Figure 5.21; WT control 191.48 ± 34.33 µm/min, n=10; KO control 206.43 ± 36.63 µm/min, n=9). ATP application had no effect in *kcne3*$^{-/-}$ tracheas, since the effect was not significantly different from the control solution. However, there was no significant difference between wild type and *kcne3*$^{-/-}$ particle movement after ATP stimulation. These results indicate that *kcne3*$^{-/-}$ tracheas do not display any impairment in mucociliary clearance, although they show a tendency to transport particles less efficiently that wild type control under ATP stimulation, which would indicate that they might secrete less fluid under these conditions.

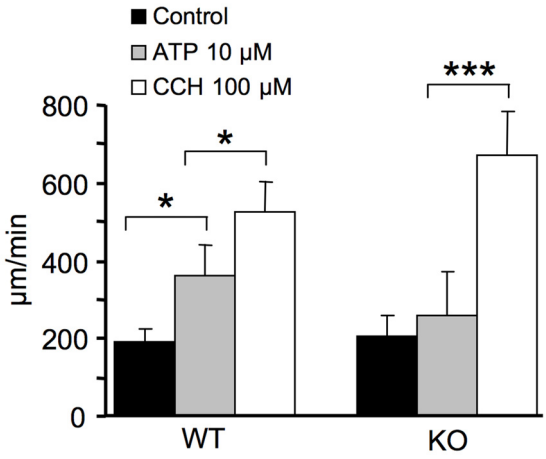


**Figure 5.21. Summarized effects of mucoci liary clearance**. MCC was determined by measurement of the transport of polystyrene microspheres (diameter 6 ± 0.58 µm) in isolated wild type and *kcne3*$^{-/-}$ tracheas after apical application of ATP (10 µM) or CCHO (100µM). *Kcne3*$^{-/-}$ *tra*cheas showed a decreased ATP induced MCC compared to wild type (WT, n = 10; KO, n = 9) Data are means ± SEM. * $p<0.05$ ** $p<0.005$ *** $p<0.0005$.

Compared to control conditions the lack of increased MCC upon ATP observed in the *kcne3*$^{-/-}$ epithelia correlates with the decreased ATP stimulated $Cl^-$ secretion observed Ussing chamber experiments of *kcne3*$^{-/-}$ tracheal rings.

Additionally, *kcne3*$^{-/-}$ and wild type tracheas displayed a very similar degree of particle movement under carbachol stimulation, that was significantly different form control and ATP stimulated MCC (Figure 5.21; WT CCOH 523 ± 82.02 µm/min, n=10; KO CCOH 674.52 ± 112.86 µm/min, n=10).

Altogether, these preliminary results suggest that, despite the fact that there is no statistically significant difference among particle movements in wild type and *kcne3*$^{-/-}$ tracheas under ATP stimulation, there is a tendency in *kcne3*$^{-/-}$ tracheas to transport particles more slowly, which might indicate that they secrete fluid at a lower rates.

## 5.7 Role of KCNE3 in Skeletal Muscle

In agreement with our experimental data, which failed to detect KCNE3 mRNA (Figure 5.3A) and protein (Figure 5.5B) in skeletal muscle, we never observed spontaneous paralysis nor myotonia or uncoordinated movements in *kcne3*$^{-/-}$ mice. *Kcne3*$^{-/-}$ mice behaved normally in rotarod assays, which examine motor coordination.

In addition, histological analysis of skeletal muscle did not reveal any morphological abnormalities (Figure 5.22A-D), contrasting with the vacuoles and tubular aggregates observed in muscle biopsies from some of the patients affected by periodic paralysis, carrying the R83H in the KCNE3 gene (Abbott et al. 2001; Abbott. et al 2006). In these patients, as described by Abbott *et al.* attacks often occur after exercise or when having low $K^+$ blood levels. In order to mimic these conditions and to test more stringently the effect of KCNE3 deletion under low $K^+$ blood levels, we also put *kcne3*$^{-/-}$ and their littermates on $K^+$-depleted diet for two weeks and tested them for motor performance on rotarod test.

Although this diet decreased serum $K^+$ level from 6.5 to 3.5 mM in both genotypes, no attacks of paralysis were observed. Rotarod tests did not reveal any differences between the genotypes, either. The time mice were able to stay on the turning and slowly accelerating rods were 4.02 ± 0.42 min (WT) versus 4.24 ± 0.8 min (KO) under normal diet, and 4.23 ± 029 min (WT) vs. 4.36 ± 0.45 min (KO) under $K^+$-depleted diet (n=6) (Figure 5.22E).

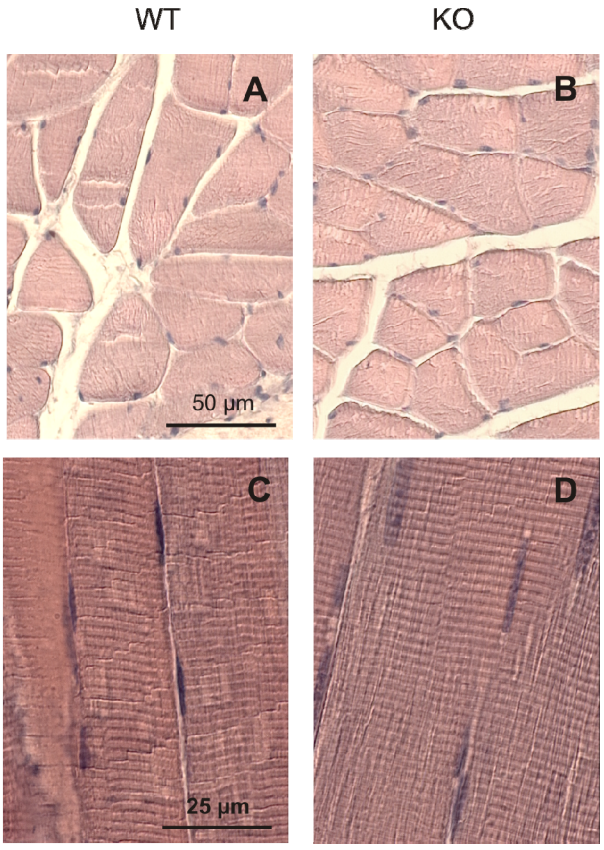


E

| | Control | Hypokalemic |
|---|---|---|
| WT | 4,02 ± 0,42 min | 4,23 ± 0,29 min |
| KO | 4,24 ± 0,18 min | 4,36 ± 0,45 min |

**Figure 5.22. Muscle morphology and motor performance. A-D**, Hematoxylin/eosin (H/E) stained muscle sections from 1 year-old wild type and *kcne3*$^{-/-}$ mice. Transversal (A-B) and longitudinal (C-D) sections of hind limb skeletal muscle from wild type (A and C) and *kcne3*$^{-/-}$ (B and D) mice. Scale bars denote same lengths for *kcne3*$^{-/-}$ and wild type. No obvious morphological differences were observed between tissues from the two genotypes. To note that no degeneration neither vacuoles nor aggregates were observed in *kcne3*$^{-/-}$ skeletal muscle. **E,** rotarod performance averaged times from wild type and *kcne3*$^{-/-}$ mice under control or hypokalemic diet. No significant differences were observed between genotypes. All performance times are within the normal range.

We can therefore conclude that KCNE3 does not play a crucial role in muscle physiology. These data on *kcne3*$^{-/-}$ animals strongly reinforce the doubts (Sternberg et al. 2003; Jurkat-Rott and Lehmann-Horn 2004) on the assertion that KCNE3 mutations can underlie periodic paralysis in humans (Abbott et al. 2001; Abbott et al. 2006).

## 5.8 Role of KCNE3 in Central Nervous System

Whereas KCNE3 levels in brain were below the detection limit in our studies (Figure 5.3A, 5B) others (McCrossan et al. 2003; Lewis et al. 2004) have reported that KCNE3 interacts with Kv2.1, Kv3.1 and Kv3.2 $K^+$-channels in brain.

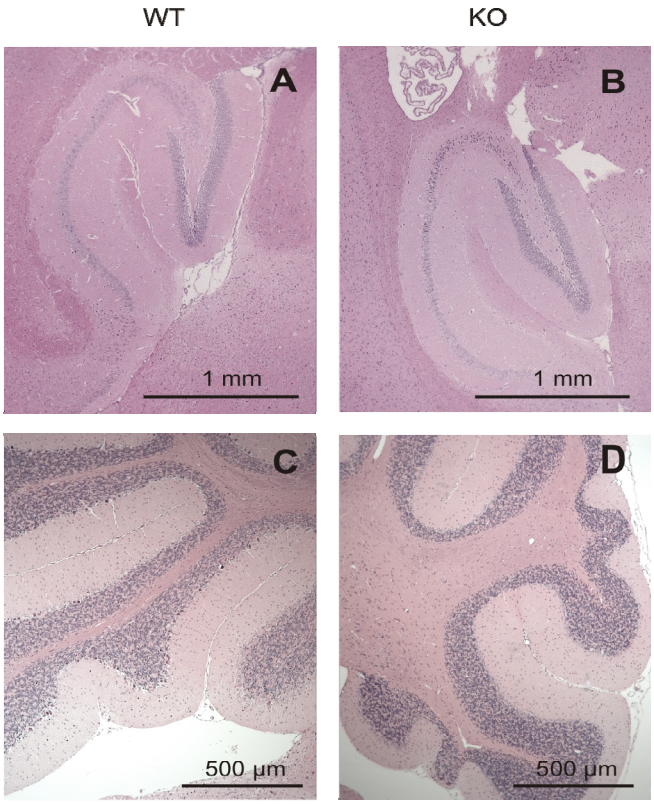


**Figure 5.23. brain morphology A-D** Hematoxylin/eosin (H/E) stained brain sections from 1 year-old wild type and *kcne3*$^{-/-}$ mice. H/E stained brain sections showing hippocampus of wild type (A) and *kcne3*$^{-/-}$ mice (B) and cerebellum of wild type (C) and *kcne3*$^{-/-}$ (D) mice. Scale bars denote same lengths for *kcne3*$^{-/-}$ and wild type. No obvious morphological differences were observed between tissues from the two genotypes. To note that no degeneration neither apoptotic regions were observed in the *kcne3*$^{-/-}$ brain.

Therefore, we further investigated the *kcne3*$^{-/-}$ brain morphology. We neither detected morphological brain abnormalities (Figure 5.23), nor in hippocampal neither in cerebellar region. Besides, no obvious neurological defects, balance problems or abnormal behavior were observed in *kcne3*$^{-/-}$ animals.

# 6 DISCUSSION

## 6.1 Expression Pattern of KCNE3

In recent years, the expression pattern of KCNE3 has been matter of debate (Abbott et al. 2001;Pannaccione et al. 2007; Sternberg et al. 2003; Jurkat-Rott and Lehmann-Horn 2004; Jurkat-Rott and Lehmann-Horn 2007; Lundquist et al. 2005 and 2006). Part of these controversies might have arisen from the current absence of reliable tools to investigate KCNE3 expression pattern, namely a specific and reliable anti-KCNE3 antibody and *kcne3*$^{-/-}$ mice. *Kcne3*$^{-/-}$ tissues from KO animals represent the optimal and most specific control to test and validate expression data. In the absence of KOs, controls by omission of primary antibodies, replacement with non-immune immunoglobulins, preadsorption with antigens, or staining with 2 different antibodies that recognized non-overlapping epitopes of the same protein, have been widely used to achieve some level of specificity in conventional biochemical and immunohistochemical techniques. These controls however do not provide definitive information about the specificity of the reactions (Fritschy 2008).

The generation of a new, specific antibody tested against wild type and *kcne3*$^{-/-}$ tissues was necessary. Our anti-KCNE3 antibody proved to be specific in Western blot (Figure 5.4 and 5.5) and immunohistochemistry (Figure 5.7, 5.9, 5.11 and 5.13), to perform a systematic analysis on KCNE3 expression in murine tissues by employing *kcne3*$^{-/-}$ samples as controls. By these means, KCNE3 expression has been restricted to gastrointestinal tissue and upper airways. Moreover, we addressed the subcellular localization of the KCNQ1/KCNE3 in these tissues.

### 6.1.1 KCNE3 Subunits can be Detected only in Secreting Epithelia

The *kcne3* gene contains 4 exons, of which only exon 4 codes for the entire KCNE3 protein. Exons 1 to 3 form part of the 5´UTR and undergo alternative splicing. This long UTR region might serve to tightly regulate KCNE3 gene expression at the translational level in different tissues.

Most of the published work on KCNE3 expression has been performed at the mRNA level and the data were not further confirmed at the protein level, probably due to the lack

of reliable anti-KCNE3 antibodies. Besides, given that KCNE3 exons 1-3 undergo extensive splicing, it is not possible to design appropriate intron-spanning primers (that produce only one PCR product) for real-time quantitative PCR (RT-PCR) reactions. Intron-spanning primers are generally used in RT-PCR analysis to avoid co-amplification of contaminating genomic DNA. The RT-PCR is a very sensitive method, where careful experimental design, application and validation are needed to avoid amplification of nonspecific PCR products that cause false-positive signals. We therefore believe that the majority of the KCNE3 expression studies reported by other groups, which were performed only at the mRNA level, should be further validated by using other complementary approaches to detect the KCNE3 protein as well. Therefore, our analysis on the expression pattern of KCNE3 was performed at both mRNA and protein level, by employing biochemical (e.g. Western and Northern Blotting) and immunohistochemical techniques (Preston et al. 2010).

At the mRNA level, KCNE3 expression was observed in the entire gastrointestinal tract (stomach, duodenum, jejunum, ileum, caecum and colon; Figure 5.3), while a number of other tissues (brain, kidney, heart and skeletal muscle) were not positive for *kcne3* expression. Similarly, also at the protein level KCNE3 was found to be highly expressed in gastrointestinal tissues. Outside of the gastrointestinal tract, we observed KCNE3 expression only in trachea, while kidney, skeletal muscle, heart, and brain were devoid of specific signals (Figure 5.5).

In order to get additional evidence for the absence of KCNE3 in the above mentioned tissues, we performed immunohistochemical experiments. These experiments also failed to report KCNE3-specific signals (data not shown). In particular, multiple tests were performed aiming at improving the immunoreaction by varying methods of tissue fixation, tissue processing and stringency of the binding reaction. In none of the conditions tested we were able to observe specific signals above background levels (data not shown).

Altogether, these data strongly support the absence of significant KCNE3 expression outside of the gastrointestinal tract, with the exception of tracheal tissue. These results are quite surprising, in view of recent works that reported KCNE3 expression and possible physiological role in murine and human brain (McCrossan et al. 2003; Pannaccione et al. 2005; Pannaccione et al. 2007); rat and human skeletal muscle (Abbott et al. 2001; Abbott et al. 2006); murine and human heart (Ohya et al. 2002;

Bendahhou et al. 2005; Lundquist et al. 2005; Lundquist et al. 2006); human kidney (Schroeder et al. 2000; Duranton et al. 2010).

The discrepancies between the expression pattern of KCNE3 observed in human tissues and their murine counterparts (e.g. in heart, kidney and skeletal muscle) might be a consequence on species-specific differences. We however believe that the studies mentioned above suffer from major limitations, given the lack of appropriate controls (*kcne3*$^{-/-}$ tissues) which are necessary to perform a reliable study of KCNE3 expression pattern. Our data on the other hand provide a more direct and clear evidence for the presence or absence of KCNE3 in the analyzed tissues (Figure 5.3 and 5.5).

Interestingly, although we (Figure 5.5D) and others (Grahammer et al. 2001b) have shown expression of KCNE3 in trachea, we did not observe expression in lung tissue neither by Northern blot (Figure 5.3) nor by immunohistochemical techniques (data not shown). Although upper airways and lungs are part of the same functional system and share many common properties, they seem to differ in respect to the rates of mucus secretion. In contrast to lungs, upper airways can in fact produce higher amounts of mucus (Van der Schans 2007), which aids in the protection of the lungs by trapping foreign particles (e.g. dust, particulate pollutants, allergens, infectious agents, bacteria) that enter in the respiratory system during breathing (Mall 2008). Given this major functional difference, it is therefore conceivable to believe that trachea and lungs express a different subset of ion channels, which in turn might account for their differential secretory properties. In this regard, by being expressed only in trachea and not in lungs (Figure 5.3, 5.5 and 5.13), KCNE3 would be part of this molecular and functional heterogeneity.

Nonetheless, it should be mention that very low KCNE3 mRNA or protein levels might have gone undetected in this study because they were below the detection limit of the techniques we employed. Low amounts of KCNE3 protein in a specific cell population might be indeed sufficient to achieve a specific function (e.g. in cardiac tissue). There might also be that in some organs KCNE3 is expressed only under very specific physiological or pathological circumstances (e.g. bacterial renal infections (Duranton et al. 2010)).

Altogether, our analysis on the expression pattern of KCNE3, which has been validated by the use of *kcne3*$^{-/-}$ animals as controls, allowed us to draw a reliable picture of KCNE3 expression in murine tissues. By being highly enriched in the gastrointestinal

tract and in trachea, our data point to a general function of KCNE3 in supporting epithelial secretory functions together with its cognate subunit KCNQ1 (Figure 5.14). In all other tissues, we failed to detect KCNE3 expression (Figure 5.3 and 5.5). This is a valuable piece of evidence that contradicts previous reports and provides to date the most extensive and well validated analysis on the expression pattern of KCNE3 in mouse tissues.

### 6.1.2 KCNE3 Expression in Gastric Epithelia

Our data clearly demonstrate KCNE3 expression in stomach (Figure 5.3, 5.5 and 5.7), where it localizes to the basolateral membranes of epithelial cells found in basal gastric gland (Figure 5.7). These are the first data showing KCNE3 expression in gastric epithelia, which would suggest an involvement of this subunit in the secretory function of this organ.

It is known that KCNQ1 is expressed together with KCNE2 in tubulovesicular and apical membranes of acid secreting parietal cells in the stomach (Grahammer et al. 2001a; Heitzmann et al. 2004). The complex formed by KCNQ1/KCNE2 is constitutively open, and it is found in mid-apical parts of gastric glands. KCNQ1/KCNE2 currents are increased upon cAMP, $PIP_2$ or acidic pH (Tinel et al. 2000; Heitzmann et al. 2007). The channel complex has a major role in acid secretion, as it recycles the $K^+$ ions necessary for the $H^+/K^+$ ATPase to secrete protons. Indeed animal models lacking one or other of the above mentioned components develop achlorhydria, gastric hyperplasia, and vitamin B12 deficit, and as a consequence macrocytic anemia (Lee et al. 2000, Roepke et al. 2006).

It had never been shown before that KCNQ1 is also located in basolateral membranes of the epithelial cells at the bottom of gastric glands (Figure 5.7G-I). This localization pattern is consistent with a possible interaction of KCNQ1 with KCNE3 in basal glands, since we have shown that KCNE3 is also present in these membranes (Figure 5.7A, C and D). Interestingly, the staining in the parietal cells was found to be more cytoplasmatic, probably due to their high plasma membrane invaginations and abundant number of intracellular vesicular/tubular structures which were positive for KCNQ1/KCNE2 complex (Heitzmann and Warth 2008). On the other hand, cells located at the basal part of the gland displayed a KCNQ1 staining lining the plasma membrane, similar to the one observed for KCNE3.

*Kcne3*$^{-/-}$ mice did not show any aberrant gastric morphology (Figure 5.6), that differs from *kcne2*$^{-/-}$ and *kcnq1*$^{-/-}$ mouse models, where striking morphological alterations were evident (Lee et al. 2000, Roepke et al. 2006). Most probably the impaired acid secretion from parietal cells, where KCNQ1 (Figure 5.7H-I) and KCNE2 (Roepke et al. 2006) are co-expressed is the cause of these morphological alterations. The discrepancy between the phenotypes of the *kcnq1*$^{-/-}$ and *kcne2*$^{-/-}$ mice on one hand, and the *kcne3*$^{-/-}$ on the other seems also to correlate with the expression pattern of the respective proteins. The absence of morphological alterations in *kcne3*$^{-/-}$ stomach, together with the preserved gastric gland morphology and acid-secreting parietal cells morphology, indirectly suggest that acid production was not altered.

We speculate that in analogy to its intestinal function, gastric KCNQ1/KCNE3 localization at the bottom of the gastric glands is involved in salt- and fluid secretion. Such fluid secretion would flush and dilute the contents of the gastric gland up to the gastric pit and lumen.

There is a possibility that the presence of electroneutral $K^+$-$Cl^-$ cotransporter (known as KCCs) type 3 in the basolateral membranes of gastric gland cells (Fujii et al. 2008), together with the residual activity of KCNQ1 homooligomers, might suffice to carry out $K^+$ efflux and possibly compensate for the lack of the KCNE3 subunit in *kcne3* $^{-/-}$ mice.

## 6.2 KCNQ1 in the Absence of KCNE3

KCNQ1 expression and localization was not altered in the absence of its beta subunit KCNE3 (Figure 5.9, 5.11 and 5.14). This finding shows that the beta subunit KCNE3 is not required for correct targeting of its alpha subunit KCNQ1 to the plasma membrane.

Our results show that KCNQ1 protein stability is not depending on KCNE3 interaction. However in some cases the beta subunit is required for the proper function of the channel. That is the case of ClC7, which interaction with Ostm1 is important for protein stability and essential for bone resorption and lysosomal function. In fact, loss of function of the *ClC7* or *Ostm1* gene cause osteopetrosis.

On the same way, Barttin is an essential beta subunit for CLC-Ka and CLC-Kb which are coexpressed in $K^+$ secreting epithelia of the inner ear and renal tubules (Estevez et al. 2001). Mutations on CLC-Kb or Barttin gene cause Bartter syndrome type III or IV respectively, the latter characterized not only by renal failure but also by sensorineural deafness. Barttin functions as an activator of CLC-K channels, changing CLC-K

biophysical properties and enhancing its membrane insertion (Waldegger et al. 2002). Unlike KCNQ1, CLC-Kb is retained in the Golgi apparatus in the absence of its beta subunit. Instead, CLC-Ka is able to travel to the plasma membrane but shows a reduced unitary conductance and altered voltage dependence of activation without Barttin (Scholl et al. 2006).

In conclusion, KCNQ1 alone can reach the plasma membrane, probably via the default secretory pathway without requiring pre-assembly with a beta subunit. This is supported by the fact that KCNQ1 homomers are functionally expressed in the plasma membrane in hetereologous systems (Barhanin et al. 1996; Sanguinetti et al. 1996).

The KCNE localization in the absence of KCNQ1 is source of controversy. Schroeder et al. (2000) reported that in the absence of its alpha subunit KCNQ1, KCNE3 was not targeted to the plasma membrane but accumulated in the ER compartment. A recent publication however showed that KCNE3 targeted to membrane lipid rafts when expressed alone in mammalian cells (Roura-Ferrer et al. 2010). Both are *in vitro* studies that use similar overexpression systems but show contradictory data. To resolve this issue, it would be interesting to analyze KCNE3 protein localization in *kcnq1*$^{-/-}$ epithelial cells.

*In vivo*, the heteromers formed by KCNQ1/KCNE1 (Chouabe et al. 1997) and KCNQ1/KCNE2 (Heitzmann et al. 2004) reside in apical surfaces of marginal cells in the stria vascularis and in intracellular canalicular membranes of parietal cells in the gastric epithelia respectively. However, the abilility of KCNE subunits to target KCNQ1 channels to specific subcellular compartments is still a matter of debate. It had been reported that in MDCK (Madin-Darby Canine Kidney) cells, KCNQ1 was able to travel alone to basolateral membranes and that KCNQ1 targeting was not affected by KCNE co-expression (Jespersen et al. 2004). However, other groups showed by colocalization studies in hetereologous systems (Roura-Ferrer et al. 2010) and by analysis of KCNE1 mutants that impair KCNQ1 surface expression (Krumerman et al. 2004) that KCNE subunits provide additional signals for intracellular targeting of the KCNE/KCNQ1 complex. More invetigations are however needed to elucidate the dependence of KCNQ1/KCNE complex targeting on the KCNE subunit and its cell type specificity.

## 6.3 KCNQ1/KCNE3 Channels in Transepithelial Ionic Transport

### 6.3.1 KCNE3 in Colonic Epithelial Ionic Transport

Pharmacological experiments using chromanol 293B suggested KCNQ1 as an important player in epithelial transport (Lohrmann et al. 1995). Because KCNE3 had not yet been identified as a β-subunit for KCNQ1, it was first hypothesized that KCNQ1/KCNE1 complexes were involved in transepithelial ion transport (Suessbrich et al. 1996; Busch et al. 1997). However, in contrast to KCNE3, KCNE1 could be detected neither in colonic nor in tracheal tissues (Grahammer et al. 2001b), and the *kcne1*$^{-/-}$ mice did not show any impairment in forskolin-stimulated intestinal $Cl^-$ secretion (Arrighi et al. 2001; Warth et al. 2002). Moreover, KCNQ1/KCNE1 channels activate at membrane potential of -20 mV, and the negative membrane potential of intestinal epithelial cells would prevent the channel complex from being open.

Assembly of KCNQ1 with KCNE1 renders the complex voltage dependent (Barhanin et al. 1996; Sanguinetti et al. 1996). KCNE1 slows KCNQ1 activation kinetics, and dramatically increase KCNQ1 current amplitude without altering the deactivation tail currents. KCNE1 shifts the activation threshold potential -40 mV (for KCNQ1) to -20 mV (for KCNQ1+KCNE1) allowing the channel to be fully open in apical membranes of the marginal cells of the stria vascularis where the membrane voltage reaches +5 mV (Vetter et al. 1996). This voltage dependency however predicts that the channel will be closed at the membrane potential of epithelial cells in colon (-60 mV) (Greger et al. 1997) or in upper airways (-35 mV) (Rickheit et al. 2008), thereby rendering a functional involvement of KCNQ1/KCNE1 complexes in these tissues unlikely.

On the other hand, KCNQ1/KCNE3 heteromers are constitutively open (Schroeder et al. 2000): their voltage independence is compatible with the expression in non-excitable tissues, like gut or airway epithelia. In addition, several studies have speculated a possible role of KCNQ1/KCNE3 complexes in basolateral $K^+$ recycling. Our work represents the first genetic study that addresses the function of the KCNE3 subunit, and provides strong evidence supporting the involvement of basolateral KCNQ1/KCNE3 heteromers in colonic $Cl^-$ secretion. Our Ussing chamber experiments showed that current response to forskolin stimulation was almost completely abolished in *kcne3*$^{-/-}$ colonic tissues, with ~80% reduction in the elicited averaged currents compared to control values (Figure 5.15). This residual current might result from secretion of another anion (like $HCO_3^-$).

Additional lines of evidence come from the colocalization of KCNQ1 and KCNE3 in basolateral membranes of colonic epithelia (Figure 5.11), and the nearly complete loss of chromanol 293B-inhibitable currents in *kcne3*$^{-/-}$ mice (Figure 5.15).

The fact that *kcne3*$^{-/-}$ mice exhibit strongly reduced transepithelial transport in colonic tissue, although neither KCNQ1 expression nor localization were altered indicates that KCNQ1 homomers are not able to support $K^+$ recycling in the absence of KCNE3. As predicted by their outward-rectification properties, KCNQ1 homomers are in fact incompatible with a role in transepithelial transport in both colonic and tracheal epithelia, since in these tissues they are predicted to be largely closed at resting membrane potential (Greger et al. 1997; Barhanin et al. 1996; Sanguinetti et al. 1996). Moreover, KCNQ1/KCNE3 channels mediate currents that are 3 times larger than homomeric KCNQ1 channels in overexpressing COS (Bendahhou et al. 2005) or CHO (Ohno et al. 2009) cells.

Altogether, our functional analysis of transepithelial transport in *kcne3*$^{-/-}$colonic tissue enabled us to clearly assign a functional role to KCNQ1/KCNE3 complexes in basolateral $K^+$ extrusion, a recycling pathway that is necessary to provide electrochemical driving force for $Cl^-$ secretion.

### 6.3.2 Calcium Stimulated Chloride Secretion in Colonic Mucosa

Our Ussing chamber experiments on *ex vivo* tissue preparations show that carbachol application induced a similar increase in $Cl^-$ efflux in both wild type (after C293B addition) and *kcne3*$^{-/-}$ epithelia (Figure 5.15). These results indicate that, while cAMP-stimulated $Cl^-$ secretion is strongly impaired in *kcne3*$^{-/-}$ colon, $Ca^{++}$ stimulated secretion is largely unaffected. It seems therefore plausible that $Ca^{++}$ is able to activate basolateral $K^+$ conductances, which can compensate for the loss of functional KCNQ1/KCNE3 complexes in KO tissues. Recent reports suggest that intermediate conductance, $Ca^{++}$-sensitive KCNN4 $K^+$ channels are activated in intestinal cells by stimulation of muscarinic receptors (Warth et al. 1999; Flores et al. 2007). Therefore, activation of KCNN4 by carbachol would facilitate an alternative $K^+$ recycling pathway and allow $Cl^-$ secretion in cAMP stimulated *kcne3*$^{-/-}$ epithelia. Note that $Ca^{++}$ stimulated $Cl^-$ secretion requires coactivation of CFTR by cAMP.

In conclusion, our *ex vivo* (Figure 5.15) and *in vivo* data (Figure 5.18) provide a strong evidence for a cooperativity of the two $Ca^{++}$ and cAMP mediated responses. Effects of

the second messenger cAMP and $Ca^{++}$ in intestinal epithelia promote a massive $Cl^-$ secretion that is reduced by 50% in *kcne3*$^{-/-}$ animals. In particular, given that KCNE3 deletion mutant mice did not show any obvious deficit in intestinal physiology *in vivo*, and that cholera toxin stimulated fluid loss occurred normally in KO animals (Figure 5.18), we believe that this remaining $Ca^{++}$ stimulated $Cl^-$ secretion is able to compensate for impaired cAMP cascade under basal and pathophysiological conditions.

Along this line *kcnn4*$^{-/-}$ mice, though suffering from impaired $Ca^{++}$-stimulated intestinal Cl- secretion, do not display any major intestinal complication *in vivo* (Flores et al. 2007). The lack of major *in vivo* effects of the KCNE3 and KCNN4 deletions indicates that in the gastrointestinal tract $Ca^{++}$ and cAMP work synergistically, thereby masking individual signaling cascade defects in the single mutants.

### 6.3.3 KCNE3 and Cholera Toxin-Stimulated $Cl^-$ Secretion

Cholera toxin (CT) directly stimulates cAMP-stimulated $Cl^-$ secretion in enterocytes, which ultimately results in water loss and diarrhea, by activating adenylate cyclase (Cassel and Pfeuffer 1978; Gill and Meren 1978). Intracellular cAMP levels increase CFTR open probability by PKA induced phosphorylation (Clarke et al. 1992). cAMP also stimulates NKCC1, the basolateral $Na^+/2Cl^-/K^+$ cotransporter (Lytle and Forbush 1992), by enhancing its insertion into the membrane from intracellular storage sites (Reynolds et al. 2007). Increased cAMP, via PKA-induced phosphorylation, activates KCNQ1/KCNE3 complex (Schroeder et al. 2000) that will repolarize the cell membrane counteracting the depolarizing effect of opening an apical $Cl^-$ channel.

Selective and specific molecular therapies have been designed to block CFTR activation, thus effects of cholera toxin (Ma et al. 2002; Li and Naren 2005; Li et al. 2007). An alternative approach could target instead basolateral $K^+$ channels, whose activity is necessary to provide the electrochemical driving force for $Cl^-$ extrusion. Our experiments indicate that one potential target might be the KCNQ1/KCNE3 complex (Figure 5.15 and 4.17). To directly test if the functional lack of this complex has an impact on the cholera toxin-induced water-loss phenotype, we performed *in vivo* experiments in *kcne3*$^{-/-}$ intestine. Our experiments however showed that *kcne3*$^{-/-}$ and wild type colon responded very similarly to cholera toxin injections (Figure 5.18), indicating that *in vivo* KCNE3/KCNQ1 activity does not play a major role on cholera toxin stimulated fluid loss.

Plausibly, *in vivo* cholera toxin effects are complex and do not simply rely on stimulation of adenylate cyclase in epithelial cells. Cholera toxin might act on multiple signaling pathways (Pothoulakis et al. 1998; Farthing et al. 2004) and its effect could be possibly mediated by multiple cell types. Cholera toxin might not only act on adenylate cyclase in epithelial cells, but also in enterochromaffin cells. These cells would consequently secrete serotonin, which leads to enteric nervous system stimulation and local acetylcholine and vasoactive intestinal peptide (VIP) secretion that cause smooth muscle contractions and promote intracellular cAMP and $Ca^{++}$ cascades also in epithelial cells. Besides, activation of mast cells that secrete histamine would lead to general epithelium inflammation and prostaglandins release, also increasing cAMP and $Ca^{++}$ intracellular levels. Under these circumstances, $Na^{+}$ and $Cl^{-}$ absorption will be prevented in the surface epithelia, whilst the crypts will be flushed with $Cl^{-}$ and water secretion. In addition, it had been suggested that cholera toxin might directly promote $Ca^{++}$ stimulated $Cl^{-}$ secretion cascade, thereby producing a synergistic cascade and massive fluid loss (Nocerino et al. 1995; Field 2003).

In agreement with our conclusions other ligated-loop experiments, where fluid secretion could be blocked only by coinjection of cholera toxin with either CFTR inhibitors (Ma et al. 2002) or clotrimazole, an inhibitor for both KCNQ1/KCNE3 and KCNN4 channels (Rufo et al. 1997). This evidence further supports the cooperativity of cAMP and $Ca^{++}$ signaling to produce a synergistic action *in vivo*, since blocking both recycling pathways was shown to be necessary to prevent the effects of cholera toxin injection in intestinal fluid secretion**.**

### 6.3.4 KCNE3 Function at the Single Cell Level: Whole Cell Recordings of Colonic Crypts

Whole-cell recording from intact colonic crypt cells is a challenging technique used to study ion channel activity at the single cell level (Schroeder et al. 2000; O'Mahony et al. 2007). The recorded current is the resultant of many different ionic conductances across the plasma membrane. In this configuration, it is therefore complex to resolve the contribution of individual ionic conductances to the total measured current. Selective removal of specific ions from bath and/or internal solution has been a useful way to circumvent this problem. Unfortunately, in our preparation of mouse colonic crypts, we were not able to cancel out $Cl^{-}$ conductances as other groups did with rat or rabbit

colonic by substituting $Cl^-$ for gluconate from the bath solution (Schroeder et al. 2000), since this had deleterious effects on the quality of the preparation and on the stability of the recordings. Murine colonic crypts seem therefore to be more sensitive than their equivalent preparations in rabbit or rat, to $Cl^-$ removal. Our experiments were therefore performed in the presence of physiological $Cl^-$ concentrations, both intracellular and extracellular (see material and methods for further details).

Forskolin application promoted a general membrane depolarization in both genotypes compatible with prominent $Cl^-$ secretion through CFTR activation (Figure 5.17C). Surprisingly, total whole-cell current was not increased by forskolin, though cAMP should increase currents through both CFTR and KCNQ1/KCNE3. Another group obtained similar results described previously in comparable preparations (Diener et al. 1996).

This paradoxical whole cell effects of forskolin can be explained by assuming that in addition to promote $Cl^-$ secretion, raising intracellular cAMP concentration might as well lead to inactivation of other conductances in the cell, which are active before forskolin addition (e.g. KCNN4 and ENaC). On one hand, inactivation of $Ca^{++}$ activated $K^+$ channels KCNN4, which opened because of increases in intracellular $Ca^{++}$ (because of cell swelling, or through stretch-activated channels (Hoyer et al. 1994), possibly due to mechanical pressure exerted by the patch pipette onto the plasma membrane), could lead to decreased total currents. On the other hand, inhibition of $Na^+$ conductances through ENaC, as an indirect effect of cAMP-stimulated $Cl^-$ efflux, could also negatively affect whole cell conductances. Although, the epithelial sodium channel ENAC is reported to be expressed mostly in surface epithelial cells (Amasheh et al. 2009).

As expected, while in wild type the C293B-sensitive $K^+$ current displayed a reversal potential of about -75 mV, which is close to the $K^+$ reversal potential (-86 mV), in *kcne3*$^{-/-}$ cells this current was completely abolished (Figure 5.17E).

Altogether, our data from whole-cell recording of intestinal crypt cells clearly showed the lack of chromanol 293B sensitive $K^+$ channel activity in the *kcne3*$^{-/-}$ mouse. This is consistent with loss of functional KCNQ1/KCNE3 complexes in colonic tissue.

### 6.3.5 KCNE3 and Small Intestine Function

Small intestine and colon are specialized segments of the intestinal tract, which have distinct biophysical properties and serve different functions. While the first is mainly responsible for nutrient absorption, the last is involved in fluid and electrolyte absorption (Heitzmann et al 2004).

For these reasons, the contribution of specific basolateral $K^+$ channels to the secretory response may differ between colon and small intestine. Whereas the cAMP-stimulated current component is almost totally dependent on KCNQ1/KCNE3 channels in colon, we believe that in small intestine the contribution of KCNQ1/KCNE3 is much lower. Recent work on bioelectrical properties of small intestine have shown that forskolin stimulated currents were reduced by only about ~50% in *kcnq1*$^{-/-}$ animals (Grubb et al. 2000; Vallon et al. 2005) instead of being completely abolished as it would be expected if KCNQ1-containing channels were the only conductance supporting basolateral $K^+$ recycling. In addition, also *nkcc1*$^{-/-}$ small intestine displayed a similar phenotype, with only a partial impairment in cAMP stimulated $Cl^-$ secretion (Grubb et al. 2000) though in this case *nkcc1*$^{-/-}$ suffer of mild intestinal obstruction (Flagella et al. 1999).

These experiments clearly indicate that in small intestine alternative basolateral $K^+$ and $Cl^-$ conductances are activated under cAMP stimulation, as was also suggested by electrophysiological and pharmacological experiments in isolated crypt cells (McNicholas et al. 1994; Heitzmann et al. 2004).

In particular, cAMP stimulated $Cl^-$ secretion is not fully dependent on KCNQ1/KCNE3 channels, but there seems to be extensive functional redundancy between alternative cotransporters in this epithelium. Although we did not directly test this hypothesis, we believe that, the overall impact of the KCNE3 deletion in cAMP-stimulated $Cl^-$ secretion in the small intestine would be minor than in colon.

Given absorptive function of the small intestine, a functional impairment is expected to have major consequences on growth and ionic homeostasis. However, *kcne3*$^{-/-}$ animals did not suffer from any malnutrition, growth retardation, abnormal intestinal morphology and all the analyzed parameters in serum, feces and urine samples were within the normal range. In comparison, *kcnq1*$^{-/-}$ mice suffered from fecal loss of $Na^+$ and $K^+$ (Vallon et al. 2005) and *kcnn4*$^{-/-}$ present decreased $Na^+$ and water contents in the feces (Flores et al. 2007). Although these altered parameters, neither *kcnq1*$^{-/}$ nor *kcnn4*$^{-/-}$

show any intestinal impairment (besides the reduced $Cl^-$ secretion), and its overall intestinal morphology was preserved.

In small intestine there should exist some yet unknown alternative pathways for basolateral $K^+$ transport that partially compensate for the loss of KCNQ1 and KCNE3 in the respective KO mouse models. Although this hypothesis has not yet been tested, this compensatory role might be played by other cAMP stimulated basolateral $K^+$ conductances and/or for instance by the electroneutral KCC cotransporter.

### 6.3.6 Genetic Evidences for the Biophysical Cell Model of Epithelial Chloride Secretion

In a simplified biophysical model of transepithelial transport, only KCNQ1/KCNE3 would provide the basolateral $K^+$ conductance and CFTR would be the sole apical $Cl^-$ channel (Figure 6.1). This basic model can be extended by taking into account the contribution of KCNN4, a $Ca^{++}$ activated basolateral $K^+$ channel, which sustains $Ca^{++}$ stimulated $Cl^-$ secretion. This model for $K^+$ recycling has been supported by several genetic evidences.

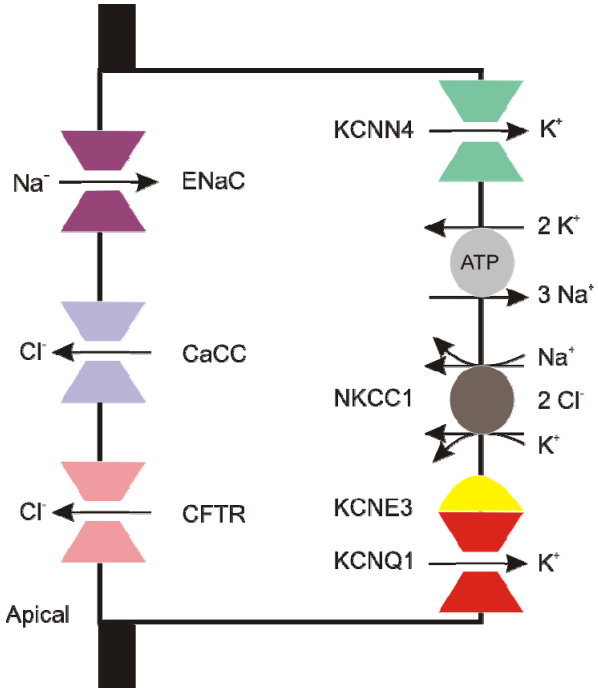


**Figure 6.1. Cell model for Cl- secretion by a colonic/tracheal epithelial cell**. Driven by the Na+ gradient established by the basolateral Na+/K+-ATPase, Na+ powers the basolateral NKCC1 cotransporter, raising intracellular Cl- above its electrochemical equilibrium. Hence, Cl- can exit the cell passively through apical, cAMP-stimulated CFTR Cl- channels (and/or Ca++-activated Cl- channels in airway), resulting in Cl- secretion. Basolateral K+ channels are needed to recycle K+. These channels additionally render the cell interior more negative, increasing the driving force for apical Cl- exit. Epithelial cells express both cAMP activated KCNQ1/KCNE3 K+ channels and Ca++-activated KCNN4 (SK4, KCa3.1) K+ channels. The epithelial sodium channel Note that, ENaC, is expressed at low level in colonic crypt cells.

In kidney, KCNQ1 is expressed in mid and late proximal tubules, together with KCNE1 (Arrighi et al. 2001; Demolombe et al. 2001). However interesting to notice that the

animal models for each protein showed dissimilar kidney phenotypes. While *kcnq1*$^{-/-}$ mice suffered from impaired kidney function only under pathological substrate overload conditions (Vallon et al. 2005), *kcne1*$^{-/-}$ mice not only displayed high aldosterone levels under basal conditions, but also hypokalemia, $Na^+$ and glucose renal excretion, and fecal loss of $Na^+$ and $K^+$ loss (Arrighi et al. 2001). The reasons for these discrepancies are currently unknown.

On the other hand, the fact that we could not detect KCNE3 in murine kidney (Figure 5.3 and 5.5) is consistent with the balanced ionic homeostasis and body fluids composition observed in *kcne3*$^{-/-}$ mice (table 5.1). In particular, unlike the KCNQ1 deletion, $K^+$ and $Na^+$ excretion and homeostasis were unaffected by the KCNE3 deletion. The fact that in colon ENaC is expressed in surface epithelial cells (Greig et al. 2004) and not in colonic crypts, the predominant site of KCNQ1/KCNE3 expression, would already argue against a major impact of the KCNE3 deletion on aldosterone-induced colonic $Na^+$ absorption.

In addition, the analysis of *kcnn4*$^{-/-}$ mice has provided insights into the molecular mechanisms of $Cl^-$ secretion, revealing that under KCNQ1/KCNE3 inhibition, $Ca^{++}$ stimulated $Cl^-$ secretion was completely abolished in absence functional KCNN4 channels (Flores et al. 2007). However, the fact that KCNQ1/KCNE3 conductances were inhibited by C293B throughout the experiment makes the contribution of individual channel difficult to assess.

CFTR is believed to be the major player in both cAMP and $Ca^{++}$ stimulated $Cl^-$ secretion in the intestine. As expected, CFTR deletion leads to major defects in transepithelial transport, and to massive degeneration of the tissue (Clarke et al. 1992). These degenerative effects of the mutation have not been described neither for KCNE3 (Figure 5.8 and 5.10) nor for KCNN4 deletions. In particular, in *kcne3*$^{-/-}$ we did not observe any atypical immune cell infiltration or mucus accumulation (Figure 5.10), as it would be expected in intestinal obstructive or irritative pathologies, as seen in the *cftr1*$^{-/-}$ or *nkcc1*$^{-/-}$mice.

Altogether, our data corroborate the biophysical model for $Cl^-$ secretion from intestinal epithelial cells, and provide additional evidence concerning the molecular nature of the ion channels involved in basolateral $K^+$ recycling. This is an important contribution that extends our understanding towards an emerging global picture of intestinal transepithelial transport.

## 6.4 KCNE3 and Airways Physiology

The present study shows that in mouse trachea KCNQ1/KCNE3 channels contribute significantly to the driving force for apical $Cl^-$ exit through either CFTR or $Ca^{++}$-activated $Cl^-$ channels.

For the first time KCNQ1/KCNE3 complex was immunolocalized to the basolateral membrane of the lining epithelia of the trachea. Other groups detected KCNE3 expression in trachea by PCR some years ago (Grahammer et al. 2001b; Cowley and Linsdell 2002). In addition, KCNQ1/KCNE3 mediated hyperpolarization should increase $Na^+$ absorption, but in our Ussing chambers experiment (Figure 5.19C) differences between the amiloride sensitive currents of WT and KO tracheas were not statistically significant. However, there is a borderline effect on *kcne3*$^{-/-}$ amiloride-sensitive currents, indicating that KCNQ1/KCNE3 complex might contribute in $Na^+$ absorption.

In trachea there is not only cAMP stimulated $Cl^-$ secretion via CFTR, but also there is an important contribution from $Ca^{++}$-activated $Cl^-$ channels ( probably TMEM16A (Rock et al. 2009)). This secretion is supported by $K^+$ extrusion by either cAMP stimulated KCNQ1/KCNE3 complex or $Ca^{++}$ activated $K^+$ channel, probably KCNN4 (Thompson-Vest et al. 2006). Therefore, in trachea, unlike in colonic epithelia, cAMP and $Ca^{++}$ signaling can independently stimulate $Cl^-$ secretion through different $Cl^-$ channels. In this tissue, in fact carbachol is able to induce $Cl^-$ secretion also in absence of forskolin.

Stimulation of $Cl^-$ secretion by either forskolin or carbachol application was drastically reduced in *kcne3*$^{-/-}$ tracheal tissues compared to controls (Figure 5.20 and 5.21), indicating that, in contrast to what we observed in colon (Figure 5.15), in tracheal tissue KCNQ1/KCNE3 complexes are also needed to sustain $Ca^{++}$ stimulated $Cl^-$ secretion.

This functional difference between these two epithelia might be explain in part by the presence in trachea of the $Ca^{++}$ stimulated $Cl^-$ channel which operates in parallel to CFTR. Moreover, KCNN4 would not fully compensate the loss of functional KCNQ1/KCNE3 as seen in *kcne3*$^{-/-}$ colonic epithelia. Therefore, in trachea it seems that the basal activity of KCNQ1/KCNE3 (without cAMP-stimulation) would contribute to the driving force for $Cl^-$ secretion through $Ca^{++}$ stimulated $Cl^-$ secretion.

To closely mimic the *in vivo* situation, we also monitored $Cl^-$ secretion under ATP stimulation. Application of ATP, which leads to increase of intracellular $Ca^{++}$ and

cAMP (Kottgen et al. 2003; Mounkaila et al. 2005) promoted a massive $Cl^-$ secretion through both CFTR and CaCC that was reduced by 50% in *kcne3*$^{-/-}$ tissues compared to controls (Figure 5.20B and D). The response to ATP does not only involve apical $Cl^-$ secretion via CFTR or CaCC, but also basolateral $K^+$ recycling, activating both $K^+$ channels.

Interestingly, ATP and carbachol induced currents three times larger than currents obtained under forskolin stimulation, indicating that first, $Ca^{++}$ mediated response promotes larger $Cl^-$ secretion than cAMP; second, $Ca^{++}$ and cAMP have a synergistic effect on $Cl^-$ secretion. In agreement with these conclusions, ATP and carbachol stimulated secretion were decreased to a lesser (50%) extent by the KCNE3 deletion compared to forskolin stimulated currents (80%).

In summary, seeing that current responses to forskolin, carbachol and ATP applications in our Ussing chamber experiments were strongly reduced in *kcne3*$^{-/-}$ animals, we conclude that KCNE3 deletion has a strong impact on tracheal $Cl^-$ secretion.

## 6.5 Mucociliary Clearance Experiments

In order to functionally characterize the impaired $Cl^-$ secretion we observed in *ex vivo* tracheal tissue preparations from *kcne3*$^{-/-}$ animals, we performed mucociliary clearance (MCC) experiments. These experiments consist in quantifying the transport of small microspheres on the tracheal epithelial surface, to assess defects in the self-clearing mechanism of airways tissues.

These experiments did not reveal any functional impairment in *kcne3*$^{-/-}$ tissues compared to controls (Figure 5.22). Both carbachol and ATP applications, which in Ussing chambers promoted massive $Cl^-$ secretion that was reduced to 50% in the *kcne3*$^{-/-}$ trachea, stimulated MCC with similar efficiencies in both genotypes (Figure 5.22). It is interesting to mention however that the MCC observed in *kcne3*$^{-/-}$ tissues by ATP appeared to be much less pronounced than the effect observed in control tissues, although this difference did not reach statistical significance. This trend in our data set might indicate that minor effects of the mutation could have gone undetected, possibly due to the scarse sensitivity of the MCC assay.

The discrepancy between Ussing chamber and MCC experiments might however be due to different tissue preparations. In the Ussing chamber experiments the net ion transport across the membrane were analyzed in an epithelium devoid of muscular layer and

innervations. Instead, MCC experiments were performed on intact tissue, where ATP not only promotes epithelial $Cl^-$ secretion but also stimulates neuromuscular activity, which might in turn boost mucociliary transport and render it quite insensitive to minor ion transport impairments in epithelial cells.

In addition, the lack of a functional impairment in *kcne3*$^{-/-}$ tracheas, assessed by MCC experiments, might be due to the remaining activity of $Ca^{++}$ stimulated $Cl^-$ secretion in this tissue (Figure 5.21). We speculate that in murine trachea *in vivo,* $Ca^{++}$ activated $Cl^-$ channel would take over loss of CFTR function (Clarke et al. 1994; Grubb et al. 1994), hereby avoiding the dramatic phenotype seen in the human CF patients.

In addition to the absence of an obvious impairment in respiratory phenotype, *kcne3*$^{-/-}$ mice also did not show any sign of diseased upper airway morphology, nor mucus accumulation or immune cells infiltration in this tissue (Figure 5.12).

Altogether, these evidences suggest that the remaining $Cl^-$ secretion that we observe in *ex vivo* tissue preparations from *kcne3*$^{-/-}$ animals seems to be sufficient to support normal trachea physiology *in vivo*. We cannot exclude however that this impairment in $Cl^-$ secretion becomes crucial under altered physiopathological conditions, or in combination with other genetic manipulations (e.g. KCCN4 deletion).

## 6.6 KCNE3 and Skeletal Muscle

The present study contradicts the hypothesis of Kv3.4/KCNE3 $K^+$ channel complex being involved in setting the resting membrane potential of skeletal muscle and being a cause of a genetically heterogeneous human disease called periodic paralysis (Abbott et al 2001 and 2006).

First of all, neither KCNE3 mRNA nor protein was detected in murine skeletal muscle (Figure 5.3 and 5.5). Second, *kcne3*$^{-/-}$ animals did not show any uncoordinated movement, myotonia or periodic paralysis before, during or after exercise as seen in rotarod experiments performed also under hypokalemic diet conditions (Figure 5.23). Third, histological analysis of skeletal muscle from *kcne3*$^{-/-}$ mice did not reveal any morphological abnormalities. In particular, we did not observe any vacuoles or tubular aggregates similar to the ones reported in muscle biopsies from human patients affected by periodic paralysis (Abbott et al. 2001).

In addition to our study, other groups have provided evidence against a functional involvement of KCNE3 in muscle physiology and periodic paralysis in humans. The

R83H substitution in the KCNE3 gene was shown to be a benign polymorphism, rather than a mutation linked to periodic paralysis, since it had been found in healthy individuals (Sternberg et al. 2003; Jurkat-Rott and Lehmann-Horn 2004). Indeed, it had been reported at frequency of 1% in healthy controls. Also the expression of KCNE3 in human skeletal muscle has been recently questioned by the work of Lundquist and collaborators, which failed to detect KCNE3 expression in this tissue (Lundquist et al. 2006).

## 6.7 KCNE3 and the Central Nervous System

Several groups had reported KCNE3 to be highly expressed in the mammalian brain, and proposed its functional interaction with Kv2.1 and Kv3.1 (McCrossan et al. 2003), Kv3.1 and Kv3.2 (Lewis et al. 2004) or Kv3.4 $K^+$ channels (Pannaccione et al. 2007). The latter complex had been also implicated in Alzheimer disease, since it had been shown to be upregulated by direct action of the beta amyloid peptide (Pannaccione et al. 2007). Furthermore, single nucleotide polymorphisms (SNPs) in KCNE3 gene had been related to Ménière's disease (MD) (Doi et al. 2005), a disorder of the inner ear characterized by tinnitus, vertigo, and sensorineural hearing loss. However, it has been recently reported that SNPs in KCNE3 are not associated with MD (Campbell et al. 2010).

These studies however suffer from major technical limitations. Most of the conclusions were in fact based on *in vitro* experimental evidences from heterologous expression systems and electrophysiological analysis from transfected cells. Systems that rely on overexpression of the protein(s) of interest are often prone to artifacts and, although very valuable for collection of preliminary data, these approaches should be routinely supported by evidences from *in vivo* or intact tissues.

Our study on the other hand provides well validated *in vivo* evidences for the absence of KCNE3 expression and function in the mouse brain. Not only KCNE3 mRNA and protein were not detected in murine brain (Figure 5.3 and 5.5), but also we did not detected any obvious neurological defects in rotarod performances, which requires good sensorimotor coordination and is sensitive to cerebellar and basal ganglia dysfunction (Crawley 1999). We observed neither impaired neurological reflexes nor morphological abnormalities in brains from young and aged *kcne3*$^{-/-}$ animals (Figure 5.24). Altogether,

these evidences suggest that KCNE3 protein does not play a major role in murine CNS physiology.

## 6.8 KCNE3 and Cardiac Function

Unlike the present study, experimental evidences on KCNE3 expression in heart are weakened by the lack of optimal controls (e.g. *kcne3*$^{-/-}$ tissues) or by the use of questionable approaches for mRNA detection (e.g. RT-PCR to amplify internal exonic sequences) (Franco et al. 2001; Bendahhou et al. 2005; Lundquist et al. 2005; de Castro et al. 2006; Radicke et al. 2006). In addition, some conclusions have been solely based on experimental evidences from heterologous expression systems, and non conclusive genetic studies of single patients or families carrying putative mutations in the KCNE3 gene missing statistical linkage analysis (Delpon et al. 2008; Lundby et al. 2008; Ohno et al. 2009).

In conclusion, we believe that further investigations are necessary to clearly elucidate the putative functional involvement of KCNE3 in cardiac physiology.

We did not observe KCNE3 expression in murine heart, neither at mRNA nor at the protein level, and *kcne3*$^{-/-}$ mice reached about 2 years of age without any major pathological consequences, and did not display any obvious phenotype. Our findings therefore arise some doubts concerning the implication of KCNE3 in cardiac muscle repolarization and its link to cardiac pathologies.

# 7 CONCLUSIONS

The present analysis of *kcne3*$^{-/-}$ mice strongly supports a crucial role of KCNQ1/KCNE3 channels in salt- and fluid secretion across intestinal and airway epithelia. In particular, we found that KCNQ1/KCNE3 heteromers are present in basolateral membranes of intestinal and tracheal epithelial cells where they facilitate transepithelial $Cl^-$ secretion through basolateral recycling of $K^+$ ions and by increasing the electrochemical driving force for apical $Cl^-$ exit. Because the abundance and subcellular localization of KCNQ1 was unchanged in *kcne3*$^{-/-}$ mice, the modification of biophysical properties of KCNQ1 by KCNE3 is essential for its role in intestinal and tracheal transport. Whereas inhibition of KCNQ1/KCNE3 channels is unlikely to be useful in treating cholera or other severe forms of diarrhea, specific activators of these channels in combination with other therapies, might hold promise in alleviating the pulmonary symptoms of cystic fibrosis.

In addition, our work does not support the postulated role of KCNE3 heteromers in skeletal muscle, heart and CNS physiology, and raises considerable doubts concerning its implication in human pathologies which affect these tissues (Abbott et al. 2001; Ohno et al. 2009; Delpon et al. 2008; Lundby et al. 2008; Pannaccione et al. 2007).

# 8 BIBLIOGRAPHY


Abbott, G.W., Butler, M.H., Bendahhou, S., Dalakas, M.C., Ptacek, L.J., & Goldstein, S.A. (2001). MiRP2 forms potassium channels in skeletal muscle with Kv3.4 and is associated with periodic paralysis. *Cell, 104*, 217-231.

Abbott, G.W., Butler, M.H., & Goldstein, S.A. (2006). Phosphorylation and protonation of neighboring MiRP2 sites: function and pathophysiology of MiRP2-Kv3.4 potassium channels in periodic paralysis. *Faseb J, 20*, 293-301.

Amasheh, S., Milatz, S., Krug, S.M., Bergs, M., Amasheh, M., Schulzke, J.D., & Fromm, M. (2009). Na+ absorption defends from paracellular back-leakage by claudin-8 upregulation. *Biochem Biophys Res Commun, 378*, 45-50.

Arrighi, I., Bloch-Faure, M., Grahammer, F., Bleich, M., Warth, R., Mengual, R., Drici, M.D., Barhanin, J., & Meneton, P. (2001). Altered potassium balance and aldosterone secretion in a mouse model of human congenital long QT syndrome. *Proc Natl Acad Sci U S A, 98*, 8792-8797.

Barhanin, J., Lesage, F., Guillemare, E., Fink, M., Lazdunski, M., & Romey, G. (1996). K(V)LQT1 and lsK (minK) proteins associate to form the I(Ks) cardiac potassium current. *Nature, 384*, 78-80.

Bas, A., Forsberg, G., Hammarstrom, S., & Hammarstrom, M.L. (2004). Utility of the housekeeping genes 18S rRNA, beta-actin and glyceraldehyde-3-phosphate-dehydrogenase for normalization in real-time quantitative reverse transcriptase-polymerase chain reaction analysis of gene expression in human T lymphocytes. *Scand J Immunol, 59*, 566-573.

Bendahhou, S., Marionneau, C., Haurogne, K., Larroque, M.M., Derand, R., Szuts, V., Escande, D., Demolombe, S., & Barhanin, J. (2005). In vitro molecular interactions and distribution of KCNE family with KCNQ1 in the human heart. *Cardiovasc Res, 67*, 529-538.

Busch, A.E., Busch, G.L., Ford, E., Suessbrich, H., Lang, H.J., Greger, R., Kunzelmann, K., Attali, B., & Stühmer, W. (1997). The role of the IsK protein in the specific pharmacological properties of the $I_{Ks}$ channel complex. *Br J Pharmacol, 122*, 187-189.

Campbell, C.A., Della Santina, C.C., Meyer, N.C., Smith, N.B., Myrie, O.A., Stone, E.M., Fukushima, K., Califano, J., Carey, J.P., Hansen, M.R., Gantz, B.J., Minor, L.B., & Smith, R.J. (2010). Polymorphisms in KCNE1 or KCNE3 are not associated with Meniere disease in the Caucasian population. *Am J Med Genet A, 152A*, 67-74.

Chandrasekhar, K.D., Bas, T., & Kobertz, W.R. (2006). KCNE1 subunits require co-assembly with K+ channels for efficient trafficking and cell surface expression. *J Biol Chem, 281*, 40015-40023.

Chouabe, C., Neyroud, N., Guicheney, P., Lazdunski, M., Romey, G., & Barhanin, J. (1997). Properties of KvLQT1 K+ channel mutations in Romano-Ward and Jervell and Lange-Nielsen inherited cardiac arrhythmias. *Embo J, 16*, 5472-5479.

Clarke, L.L., Grubb, B.R., Gabriel, S.E., Smithies, O., Koller, B.H., & Boucher, R.C. (1992). Defective epithelial chloride transport in a gene-targeted mouse model of cystic fibrosis. *Science, 257*, 1125-1128.

Crawley, J.N. (1999). Behavioral phenotyping of transgenic and knockout mice: experimental design and evaluation of general health, sensory functions, motor abilities, and specific behavioral tests. *Brain Res, 835*, 18-26.

Dedek, K., & Waldegger, S. (2001). Colocalization of KCNQ1/KCNE channel subunits in the mouse gastrointestinal tract. *Pflugers Arch, 442*, 896-902.

Delpon, E., Cordeiro, J.M., Nunez, L., Thomsen, P.E., Guerchicoff, A., Pollevick, G.D., Wu, Y., Kanters, J.K., Larsen, C.T., Burashnikov, E., Christiansen, M., & Antzelevitch, C. (2008). Functional Effects of KCNE3 Mutation and its Role in the Development of Brugada Syndrome. *Circ Arrhythm Electrophysiol, 1*, 209-218.

Diener, M., Hug, F., Strabel, D., & Scharrer, E. (1996). Cyclic AMP-dependent regulation of K+ transport in the rat distal colon. *Br J Pharmacol, 118*, 1477-1487.

Doi, K., Sato, T., Kuramasu, T., Hibino, H., Kitahara, T., Horii, A., Matsushiro, N., Fuse, Y., & Kubo, T. (2005). Meniere's disease is associated with single nucleotide polymorphisms in the human potassium channel genes, KCNE1 and KCNE3. *ORL J Otorhinolaryngol Relat Spec, 67*, 289-293.

Duranton, C., Rubera, I., L'Hoste, S., Cougnon, M., Poujeol, P., Barhanin, J., & Tauc, M. (2010). KCNQ1 K+ channels are involved in lipopolysaccharide-induced apoptosis of distal kidney cells. *Cell Physiol Biochem, 25*, 367-378.

Estevez, R., Boettger, T., Stein, V., Birkenhager, R., Otto, E., Hildebrandt, F., & Jentsch, T.J. (2001). Barttin is a Cl- channel beta-subunit crucial for renal Cl-reabsorption and inner ear K+ secretion. *Nature, 414*, 558-561.

Farthing, M.J., Casburn-Jones, A., & Banks, M.R. (2004). Enterotoxins, enteric nerves, and intestinal secretion. *Curr Gastroenterol Rep, 6*, 177-180.

Field, M. (2003). Intestinal ion transport and the pathophysiology of diarrhea. *J Clin Invest, 111*, 931-943.

Flagella, M., Clarke, L.L., Miller, M.L., Erway, L.C., Giannella, R.A., Andringa, A., Gawenis, L.R., Kramer, J., Duffy, J.J., Doetschman, T., Lorenz, J.N., Yamoah, E.N., Cardell, E.L., & Shull, G.E. (1999). Mice lacking the basolateral Na-K-2Cl cotransporter have impaired epithelial chloride secretion and are profoundly deaf. *J Biol Chem, 274*, 26946-26955.

Flores, C.A., Melvin, J.E., Figueroa, C.D., & Sepulveda, F.V. (2007). Abolition of Ca2+-mediated intestinal anion secretion and increased stool dehydration in mice lacking the intermediate conductance Ca2+-dependent K+ channel Kcnn4. *J Physiol, 583*, 705-717.

Fritschy, J.M. (2008). Is my antibody-staining specific? How to deal with pitfalls of immunohistochemistry. *Eur J Neurosci, 28*, 2365-2370.

Fujii, T., Takahashi, Y., Itomi, Y., Fujita, K., Morii, M., Tabuchi, Y., Asano, S., Tsukada, K., Takeguchi, N., & Sakai, H. (2008). K+-Cl- Cotransporter-3a Up-regulates Na+,K+-ATPase in Lipid Rafts of Gastric Luminal Parietal Cells. *J Biol Chem, 283*, 6869-6877.

Gage, S.D., & Kobertz, W.R. (2004). KCNE3 truncation mutants reveal a bipartite modulation of KCNQ1 K+ channels. *J Gen Physiol, 124*, 759-771.

Gamper, N., Li, Y., & Shapiro, M.S. (2005). Structural requirements for differential sensitivity of KCNQ K+ channels to modulation by Ca2+/calmodulin. *Mol Biol Cell, 16*, 3538-3551.

Goldman, A.M., Glasscock, E., Yoo, J., Chen, T.T., Klassen, T.L., & Noebels, J.L. (2009). Arrhythmia in heart and brain: KCNQ1 mutations link epilepsy and sudden unexplained death. *Sci Transl Med, 1*, 2ra6.

Grahammer, F., Herling, A.W., Lang, H.J., Schmitt-Graff, A., Wittekindt, O.H., Nitschke, R., Bleich, M., Barhanin, J., & Warth, R. (2001a). The cardiac K+ channel KCNQ1 is essential for gastric acid secretion. *Gastroenterology, 120*, 1363-1371.

Grahammer, F., Warth, R., Barhanin, J., Bleich, M., & Hug, M.J. (2001b). The small conductance $K^+$ channel, KCNQ1: expression, function, and subunit composition in murine trachea. *J Biol Chem, 276*, 42268-42275.

Greger, R., Bleich, M., Riedemann, N., van Driessche, W., Ecke, D., & Warth, R. (1997). The role of K+ channels in colonic Cl- secretion. *Comp Biochem Physiol A Physiol, 118*, 271-275.

Greig, E.R., Boot-Handford, R.P., Mani, V., & Sandle, G.I. (2004). Decreased expression of apical Na+ channels and basolateral $Na^+$, $K^+$-ATPase in ulcerative colitis. *J Pathol, 204*, 84-92.

Grubb, B.R., Lee, E., Pace, A.J., Koller, B.H., & Boucher, R.C. (2000). Intestinal ion transport in NKCC1-deficient mice. *Am J Physiol Gastrointest Liver Physiol, 279*, G707-718.

Grunnet, M., Jespersen, T., MacAulay, N., Jorgensen, N.K., Schmitt, N., Pongs, O., Olesen, S.P., & Klaerke, D.A. (2003). KCNQ1 channels sense small changes in cell volume. *J Physiol, 549*, 419-427.

Gutman, G.A., Chandy, K.G., Adelman, J.P., Aiyar, J., Bayliss, D.A., Clapham, D.E., Covarriubias, M., Desir, G.V., Furuichi, K., Ganetzky, B., Garcia, M.L., Grissmer, S., Jan, L.Y., Karschin, A., Kim, D., Kuperschmidt, S., Kurachi, Y., Lazdunski, M., Lesage, F., Lester, H.A., McKinnon, D., Nichols, C.G., O'Kelly, I., Robbins, J., Robertson, G.A., Rudy, B., Sanguinetti, M., Seino, S., Stuehmer, W., Tamkun, M.M., Vandenberg, C.A., Wei, A., Wulff, H., & Wymore, R.S. (2003). International Union of Pharmacology. XLI. Compendium of voltage-gated ion channels: potassium channels. *Pharmacol Rev, 55*, 583-586.

Heinemann, S.H., Rettig, J., Graack, H.R., & Pongs, O. (1996). Functional characterization of Kv channel beta-subunits from rat brain. *J Physiol, 493 ( Pt 3)*, 625-633.

Heitzmann, D., Grahammer, F., von Hahn, T., Schmitt-Graff, A., Romeo, E., Nitschke, R., Gerlach, U., Lang, H.J., Verrey, F., Barhanin, J., & Warth, R. (2004). Heteromeric KCNE2/KCNQ1 potassium channels in the luminal membrane of gastric parietal cells. *J Physiol, 561*, 547-557.

Heitzmann, D., Koren, V., Wagner, M., Sterner, C., Reichold, M., Tegtmeier, I., Volk, T., & Warth, R. (2007). KCNE beta subunits determine pH sensitivity of KCNQ1 potassium channels. *Cell Physiol Biochem, 19*, 21-32.

Heitzmann, D., & Warth, R. (2008). Physiology and pathophysiology of potassium channels in gastrointestinal epithelia. *Physiol Rev, 88*, 1119-1182.

Howard, R.J., Clark, K.A., Holton, J.M., & Minor, D.L., Jr. (2007). Structural insight into KCNQ (Kv7) channel assembly and channelopathy. *Neuron, 53*, 663-675.

Hoyer, J., Distler, A., Haase, W., & Gogelein, H. (1994). Ca2+ influx through stretch-activated cation channels activates maxi K+ channels in porcine endocardial endothelium. *Proc Natl Acad Sci U S A, 91*, 2367-2371.

Jentsch, T.J. (2000). Neuronal KCNQ potassium channels: physiology and role in disease. *Nat Rev Neurosci, 1*, 21-30.

Jespersen, T., Rasmussen, H.B., Grunnet, M., Jensen, H.S., Angelo, K., Dupuis, D.S., Vogel, L.K., Jorgensen, N.K., Klaerke, D.A., & Olesen, S.P. (2004). Basolateral localisation of KCNQ1 potassium channels in MDCK cells: molecular identification of an N-terminal targeting motif. *J Cell Sci, 117*, 4517-4526.

Jiang, M., Tseng-Crank, J., & Tseng, G.N. (1997). Suppression of slow delayed rectifier current by a truncated isoform of KvLQT1 cloned from normal human heart. *J Biol Chem, 272*, 24109-24112.

Knowles, M.R., & Boucher, R.C. (2002). Mucus clearance as a primary innate defense mechanism for mammalian airways. *J Clin Invest, 109*, 571-577.

Krumerman, A., Gao, X., Bian, J.S., Melman, Y.F., Kagan, A., & McDonald, T.V. (2004). An LQT mutant minK alters KvLQT1 trafficking. *Am J Physiol Cell Physiol, 286*, C1453-1463.

Kubisch, C., Schroeder, B.C., Friedrich, T., Lutjohann, B., El-Amraoui, A., Marlin, S., Petit, C., & Jentsch, T.J. (1999). KCNQ4, a novel potassium channel expressed in sensory outer hair cells, is mutated in dominant deafness. *Cell, 96*, 437-446.

Lee, M.P., Ravenel, J.D., Hu, R.J., Lustig, L.R., Tomaselli, G., Berger, R.D., Brandenburg, S.A., Litzi, T.J., Bunton, T.E., Limb, C., Francis, H., Gorelikow, M., Gu, H., Washington, K., Argani, P., Goldenring, J.R., Coffey, R.J., & Feinberg, A.P. (2000). Targeted disruption of the Kvlqt1 gene causes deafness and gastric hyperplasia in mice. *J Clin Invest, 106*, 1447-1455.

Lerche, C., Scherer, C.R., Seebohm, G., Derst, C., Wei, A.D., Busch, A.E., & Steinmeyer, K. (2000). Molecular cloning and functional expression of KCNQ5, a potassium channel subunit that may contribute to neuronal M-current diversity. *J Biol Chem, 275*, 22395-22400.

Lewis, A., McCrossan, Z.A., & Abbott, G.W. (2004). MinK, MiRP1, and MiRP2 diversify Kv3.1 and Kv3.2 potassium channel gating. *J Biol Chem, 279*, 7884-7892.

Li, C., Krishnamurthy, P.C., Penmatsa, H., Marrs, K.L., Wang, X.Q., Zaccolo, M., Jalink, K., Li, M., Nelson, D.J., Schuetz, J.D., & Naren, A.P. (2007). Spatiotemporal coupling of cAMP transporter to CFTR chloride channel function in the gut epithelia. *Cell, 131*, 940-951.

Li, C., & Naren, A.P. (2005). Macromolecular complexes of cystic fibrosis transmembrane conductance regulator and its interacting partners. *Pharmacol Ther, 108*, 208-223.

Lohrmann, E., Burhoff, I., Nitschke, R.B., Lang, H.J., Mania, D., Englert, H.C., Hropot, M., Warth, R., Rohm, W., Bleich, M., & et al. (1995). A new class of inhibitors of cAMP-mediated $Cl^-$ secretion in rabbit colon, acting by the reduction of cAMP-activated $K^+$ conductance. *Pflugers Arch, 429*, 517-530.

Lundby, A., Ravn, L.S., Svendsen, J.H., Hauns, S., Olesen, S.P., & Schmitt, N. (2008). KCNE3 mutation V17M identified in a patient with lone atrial fibrillation. *Cell Physiol Biochem, 21*, 47-54.

Lundquist, A.L., Manderfield, L.J., Vanoye, C.G., Rogers, C.S., Donahue, B.S., Chang, P.A., Drinkwater, D.C., Murray, K.T., & George, A.L., Jr. (2005). Expression of multiple KCNE genes in human heart may enable variable modulation of I(Ks). *J Mol Cell Cardiol, 38*, 277-287.

Lundquist, A.L., Turner, C.L., Ballester, L.Y., & George, A.L., Jr. (2006). Expression and transcriptional control of human KCNE genes. *Genomics, 87*, 119-128.

Ma, T., Thiagarajah, J.R., Yang, H., Sonawane, N.D., Folli, C., Galietta, L.J., & Verkman, A.S. (2002). Thiazolidinone CFTR inhibitor identified by high-throughput screening blocks cholera toxin-induced intestinal fluid secretion. *J Clin Invest, 110*, 1651-1658.

MacKinnon, R. (1991). Determination of the subunit stoichiometry of a voltage-activated potassium channel. *Nature, 350*, 232-235.

Mall, M.A. (2008). Role of cilia, mucus, and airway surface liquid in mucociliary dysfunction: lessons from mouse models. *J Aerosol Med Pulm Drug Deliv, 21*, 13-24.

McCrossan, Z.A., & Abbott, G.W. (2004). The MinK-related peptides. *Neuropharmacology, 47*, 787-821.

McCrossan, Z.A., Lewis, A., Panaghie, G., Jordan, P.N., Christini, D.J., Lerner, D.J., & Abbott, G.W. (2003). MinK-related peptide 2 modulates Kv2.1 and Kv3.1 potassium channels in mammalian brain. *J Neurosci, 23*, 8077-8091.

McNicholas, C.M., Fraser, G., & Sandle, G.I. (1994). Properties and regulation of basolateral K+ channels in rat duodenal crypts. *J Physiol, 477 ( Pt 3)*, 381-392.

Nicolas, M., Dememes, D., Martin, A., Kupershmidt, S., & Barhanin, J. (2001). KCNQ1/KCNE1 potassium channels in mammalian vestibular dark cells. *Hear Res, 153*, 132-145.

Nocerino, A., Iafusco, M., & Guandalini, S. (1995). Cholera toxin-induced small intestinal secretion has a secretory effect on the colon of the rat. *Gastroenterology, 108*, 34-39.

O'Mahony, F., Alzamora, R., Betts, V., LaPaix, F., Carter, D., Irnaten, M., & Harvey, B.J. (2007). Female gender-specific inhibition of KCNQ1 channels and chloride secretion by 17beta-estradiol in rat distal colonic crypts. *J Biol Chem, 282*, 24563-24573.

Ohno, S., Toyoda, F., Zankov, D.P., Yoshida, H., Makiyama, T., Tsuji, K., Honda, T., Obayashi, K., Ueyama, H., Shimizu, W., Miyamoto, Y., Kamakura, S., Matsuura, H., Kita, T., & Horie, M. (2009). Novel KCNE3 mutation reduces repolarizing potassium current and associated with long QT syndrome. *Hum Mutat, 30*, 557-563.

Ohya, S., Horowitz, B., & Greenwood, I.A. (2002). Functional and molecular identification of ERG channels in murine portal vein myocytes. *Am J Physiol Cell Physiol, 283*, C866-877.

Panaghie, G., & Abbott, G.W. (2007). The role of S4 charges in voltage-dependent and voltage-independent KCNQ1 potassium channel complexes. *J Gen Physiol, 129*, 121-133.

Pannaccione, A., Boscia, F., Scorziello, A., Adornetto, A., Castaldo, P., Sirabella, R., Taglialatela, M., Di Renzo, G.F., & Annunziato, L. (2007). Up-regulation and increased activity of KV3.4 channels and their accessory subunit MinK-related peptide 2 induced by amyloid peptide are involved in apoptotic neuronal death. *Mol Pharmacol, 72*, 665-673.

Pothoulakis, C., Castagliuolo, I., & LaMont, J.T. (1998). Nerves and Intestinal Mast Cells Modulate Responses to Enterotoxins. *News Physiol Sci, 13*, 58-63.

Preston, P., Wartosch, L., Gunzel, D., Fromm, M., Kongsuphol, P., Ousingsawat, J., Kunzelmann, K., Barhanin, J., Warth, R., & Jentsch, T.J. (2010). Disruption of the K+ channel beta-subunit KCNE3 reveals an important role in intestinal and tracheal Cl- transport. *J Biol Chem, 285*, 7165-7175.

Pusch, M., Magrassi, R., Wollnik, B., & Conti, F. (1998). Activation and inactivation of homomeric KvLQT1 potassium channels. *Biophys J, 75*, 785-792.

Richardson, S.H., Giles, J.C., & Kruger, K.S. (1984). Sealed adult mice: new model for enterotoxin evaluation. *Infect Immun, 43*, 482-486.

Rickheit, G., Maier, H., Strenzke, N., Andreescu, C.E., De Zeeuw, C.I., Muenscher, A., Zdebik, A.A., & Jentsch, T.J. (2008). Endocochlear potential depends on Cl- channels: mechanism underlying deafness in Bartter syndrome IV. *Embo J, 27*, 2907-2917.

Rocheleau, J.M., Gage, S.D., & Kobertz, W.R. (2006). Secondary structure of a KCNE cytoplasmic domain. *J Gen Physiol, 128*, 721-729.

Rock, J.R., O'Neal, W.K., Gabriel, S.E., Randell, S.H., Harfe, B.D., Boucher, R.C., & Grubb, B.R. (2009). Transmembrane protein 16A (TMEM16A) is a Ca2+-regulated Cl- secretory channel in mouse airways. *J Biol Chem, 284*, 14875-14880.

Roura-Ferrer, M., Sole, L., Oliveras, A., Dahan, R., Bielanska, J., Villarroel, A., Comes, N., & Felipe, A. (2010). Impact of KCNE subunits on KCNQ1 (Kv7.1) channel membrane surface targeting. *J Cell Physiol*.

Routtenberg, A. (1995). Knockout mouse fault lines. *Nature, 374*, 314-315.

Rudy, B., Chow, A., Lau, D., Amarillo, Y., Ozaita, A., Saganich, M., Moreno, H., Nadal, M.S., Hernandez-Pineda, R., Hernandez-Cruz, A., Erisir, A., Leonard, C., & Vega-Saenz de Miera, E. (1999). Contributions of Kv3 channels to neuronal excitability. *Ann N Y Acad Sci, 868*, 304-343.

Rufo, P.A., Merlin, D., Riegler, M., Ferguson-Maltzman, M.H., Dickinson, B.L., Brugnara, C., Alper, S.L., & Lencer, W.I. (1997). The antifungal antibiotic, clotrimazole, inhibits chloride secretion by human intestinal T84 cells via blockade of distinct basolateral K+ conductances. Demonstration of efficacy in intact rabbit colon and in an in vivo mouse model of cholera. *J Clin Invest, 100*, 3111-3120.

Sagne, C., Isambert, M.F., Henry, J.P., & Gasnier, B. (1996). SDS-resistant aggregation of membrane proteins: application to the purification of the vesicular monoamine transporter. *Biochem J, 316 ( Pt 3)*, 825-831.

Sanger, F., & Brownlee, G.G. (1970). Methods for determining sequences in RNA. *Biochem Soc Symp, 30*, 183-197.

Sanguinetti, M.C., Curran, M.E., Zou, A., Shen, J., Spector, P.S., Atkinson, D.L., & Keating, M.T. (1996). Coassembly of K(V)LQT1 and minK (IsK) proteins to form cardiac I(Ks) potassium channel. *Nature, 384*, 80-83.

Scholl, U., Hebeisen, S., Janssen, A.G., Muller-Newen, G., Alekov, A., & Fahlke, C. (2006). Barttin modulates trafficking and function of ClC-K channels. *Proc Natl Acad Sci U S A, 103*, 11411-11416.

Schroeder, B.C., Waldegger, S., Fehr, S., Bleich, M., Warth, R., Greger, R., & Jentsch, T.J. (2000). A constitutively open potassium channel formed by KCNQ1 and KCNE3. *Nature, 403*, 196-199.

Schwake, M., Jentsch, T.J., & Friedrich, T. (2003). A carboxy-terminal domain determines the subunit specificity of KCNQ K+ channel assembly. *EMBO Rep, 4*, 76-81.

Schwenk, F., Baron, U., & Rajewsky, K. (1995). A cre-transgenic mouse strain for the ubiquitous deletion of loxP-flanked gene segments including deletion in germ cells. *Nucleic Acids Res, 23*, 5080-5081.

Shebani, E., Shahana, S., Janson, C., & Roomans, G.M. (2005). Attachment of columnar airway epithelial cells in asthma. *Tissue Cell, 37*, 145-152.

Suessbrich, H., Bleich, M., Ecke, D., Rizzo, M., Waldegger, S., Lang, F., Szabo, I., Lang, H.J., Kunzelmann, K., Greger, R., & Busch, A.E. (1996). Specific blockade of slowly activating $I_{sK}$ channels by chromanols -- impact on the role of $I_{sK}$ channels in epithelia. *FEBS Lett, 396*, 271-275.

Takumi, T., Ohkubo, H., & Nakanishi, S. (1988). Cloning of a membrane protein that induces a slow voltage-gated potassium current. *Science, 242*, 1042-1045.

Tu, L., & Deutsch, C. (1999). Evidence for dimerization of dimers in K+ channel assembly. *Biophys J, 76*, 2004-2017.

Ullrich, S., Su, J., Ranta, F., Wittekindt, O.H., Ris, F., Rosler, M., Gerlach, U., Heitzmann, D., Warth, R., & Lang, F. (2005). Effects of I(Ks) channel inhibitors in insulin-secreting INS-1 cells. *Pflugers Arch, 451*, 428-436.

Vaarala, M.H., Porvari, K.S., Kellokumpu, S., Kyllonen, A.P., & Vihko, P.T. (2001). Expression of transmembrane serine protease TMPRSS2 in mouse and human tissues. *J Pathol, 193*, 134-140.

Vallon, V., Grahammer, F., Volkl, H., Sandu, C.D., Richter, K., Rexhepaj, R., Gerlach, U., Rong, Q., Pfeifer, K., & Lang, F. (2005). KCNQ1-dependent transport in renal and gastrointestinal epithelia. *Proc Natl Acad Sci U S A, 102*, 17864-17869.

Van der Schans, C.P. (2007). Bronchial mucus transport. *Respir Care, 52*, 1150-1156; discussion 1156-1158.

Vetter, D.E., Mann, J.R., Wangemann, P., Liu, J., McLaughlin, K.J., Lesage, F., Marcus, D.C., Lazdunski, M., Heinemann, S.F., & Barhanin, J. (1996). Inner ear defects induced by null mutation of the isk gene. *Neuron, 17*, 1251-1264.

Waldegger, S., Jeck, N., Barth, P., Peters, M., Vitzthum, H., Wolf, K., Kurtz, A., Konrad, M., & Seyberth, H.W. (2002). Barttin increases surface expression and changes current properties of ClC-K channels. *Pflugers Arch, 444*, 411-418.

Wang, H.S., Pan, Z., Shi, W., Brown, B.S., Wymore, R.S., Cohen, I.S., Dixon, J.E., & McKinnon, D. (1998). KCNQ2 and KCNQ3 potassium channel subunits: molecular correlates of the M-channel. *Science, 282*, 1890-1893.

Warth, R., Garcia Alzamora, M., Kim, J.K., Zdebik, A., Nitschke, R., Bleich, M., Gerlach, U., Barhanin, J., & Kim, S.J. (2002). The role of KCNQ1/KCNE1 $K^+$ channels in intestine and pancreas: lessons from the KCNE1 knockout mouse. *Pflügers Arch, 443*, 822-828.

Warth, R., Hamm, K., Bleich, M., Kunzelmann, K., von Hahn, T., Schreiber, R., Ullrich, E., Mengel, M., Trautmann, N., Kindle, P., Schwab, A., & Greger, R. (1999). Molecular and functional characterization of the small $Ca^{2+}$-regulated $K^+$ channel (rSK4) of colonic crypts. *Pflügers Arch, 438*, 437-444.

Welsh, M.J. (1987). Electrolyte transport by airway epithelia. *Physiol Rev, 67*, 1143-1184.

Wiener, R., Haitin, Y., Shamgar, L., Fernandez-Alonso, M.C., Martos, A., Chomsky-Hecht, O., Rivas, G., Attali, B., & Hirsch, J.A. (2008). The KCNQ1 (Kv7.1) COOH terminus, a multitiered scaffold for subunit assembly and protein interaction. *J Biol Chem, 283*, 5815-5830.

Yang, W.P., Levesque, P.C., Little, W.A., Conder, M.L., Shalaby, F.Y., & Blanar, M.A. (1997). KvLQT1, a voltage-gated potassium channel responsible for human cardiac arrhythmias. *Proc Natl Acad Sci U S A, 94*, 4017-4021.

Yus-Najera, E., Santana-Castro, I., & Villarroel, A. (2002). The identification and characterization of a noncontinuous calmodulin-binding site in noninactivating voltage-dependent KCNQ potassium channels. *J Biol Chem, 277*, 28545-28553.

# Abbreviations

### Amino acid code

| | | | |
|---|---|---|---|
| A | Alanine | M | Methionine |
| C | Cysteine | N | Asparagine |
| D | Aspartic acid | P | Proline |
| E | Glutamic acid | Q | Glutamine |
| F | Phenyl alanine | R | Arginine |
| G | Glycine | S | Serine |
| H | Histidine | T | Threonine |
| I | Isoleucine | V | Valine |
| K | Lysine | W | Tryptophan |
| L | Leucine | Y | Tyrosine |

### Units

| | | | |
|---|---|---|---|
| A | Ampere (current) | kDa | Kilodalton |
| bp | Base pair | L | Liter |
| °C | Grad Celsius (temperature) | M | Meter |
| Ci | Curie | M | mol/l (molarity) |
| cpm | Counts per min | Min | Minute |
| F | Farad (capacitance) | Ω | Ohm (resistance) |
| G | Gram | Rpm | Revolutions per min |
| H | Hour | S | Seconds |
| Hz | Hertz (frequency) | U | Enzymatic activity |
| kb | Kilobase | V | Volt (voltage) |

### Other

| | |
|---|---|
| Amp | Ampicilline |
| ATP | Adenosine triphosphate |
| BCA | Bicinchoninic acid |
| BSA | Bovine serum albumin |
| cAMP | Cyclic adenosine triphosphate |
| CCHO | Carbachol (2-carbamoyloxyethyl- trimethyl- azanium) |
| cDNA | Deoxyribonucleic acid |
| CFTR | Cystic Fibrosis Transmembrane Conductance Regulator |
| CTx | Cholera toxin |
| Chromanol 293B | Trans-6-cyano-4-(N-ethylsulfonyl-N-methylamino)-3-hydroxy-2,2-dimethyl-chromane |

| | |
|---|---|
| C-Terminus | Carboxy terminus |
| dCTP | Deoxycytidine triphosphate |
| DEPC | Diethylpyrocarbonat |
| DMEM | Dulbecco's modified Eagle Medium |
| DMSO | Dimethylsulfoxid |
| DNA | Deoxyribonucleic acid |
| dNTP | Deoxynucleotide triphosphate |
| DTT | Dithiothreitol |
| EDTA | Ethylenediaminetetraacetic |
| ENac | Epithelial sodium channel |
| ES | Embryonic stem cells |
| EST | Expressed sequence tag |
| FSK | Forskolin |
| HA | Influenza hemagglutinin-epitope |
| HE | Hematoxilyn-Eosin |
| HEPES | N-(2-Hydroxyethyl)piperazin-N'-2-ethansulfonic acid |
| HRP | Horse radish peroxidase |
| IBMX | 3-isobutyl-1-methylxanthine |
| $I_{sc}$ | Short-circuit current |
| KO | Knock-Out |
| LB | Luria Broth |
| Lox | Locus of crossover in P1 |
| µ | Micro |
| MCC | Mucociliary clearance |
| MEF | Murine embryonic fibroblast |
| mRNA | Messenger RNA |
| N | Nano |
| Neo | Neomycin-resistance gene |
| NGS | Normal goat serum |
| NP-40 | Nonidet P40 |
| N-Terminus | Aminoterminus |
| P | Pico |
| PBS | Phosphate buffer saline |
| PCR | Polymerase chain reaction |
| PFA | Paraformaldehyde |
| pH | Negative decimal logarithm of the hydrogen ion activity in a solution |
| PNGase | peptide N-glycosidase F |
| qRT-PCR | Quantitative real-time polymerase chain reaction |
| RNA | Ribonucleic acid |
| RNase | Ribonuclease |
| RT | Room temperature |
| RT-PCR | Reverse transcriptase polymerase chain reaction |
| SDS | Sodiumdodecylsulfate |
| SDS-PAGE | Sodiumdodecylsulfate-polyacrylamide gel electrophoresis |

| | |
|---|---|
| SEM | Standard error of mean |
| TAE | Tris-Acetat-EDTA-buffer |
| Taq | Thermus aquaticus |
| TE | Tris-EDTA-buffer |
| TEVC | Two electrode voltage clamp |
| UV | Ultraviolet |
| v/v | Volume per volume |
| WB | Western Blot |
| WT | Wild type |
| w/v | Weight per volume |

# Affidavit

Hereby I declare that my thesis entitled “Functional Analysis of the Potassium Channel Beta Subunit KCNE3” has been written independently and with no other sources and aids than quoted.

Patricia Preston Ferrer

Berlin, June 17th 2010

## Acknowledgements

I would like to thank Prof. Thomas Jentsch for giving me the opportunity to work in his lab on this project, which enabled me to learn many valuable techniques and to develop critical thinking, writing and presentation skills.

I want to acknowledge all scientists who contribute to publish this work, especially Prof. Richard Warth and PD Dr. Dorothee Günzel for their helpful discussions, ideas and advices.

I am grateful to my lab mates for their assistance, in particular to Ina Lauterbach and Irm Hermans-Borgmeyer for their technical help, to Dr. Rubén Vicente García for fruitful discussions and to Silke, Ruth, Vanessa and Eun-yeong for the friendly environment.
I also thank Dr. Guillermo Spitzmaul (for his patience teaching me electrophysiology and for giving me good advices), Dr. Gaia Novarino (for her unconditional support in and outside the lab) and to almost- Dr. Lilia Leisle (for the fun, laughs and the beers we drank in the S-bahn going back home).
I sincerely thank my lovely friends from Girona, for reminding me during these years who I am and where I belong.

Finally, my deep thankfulness to Andrea Burgalossi, for being always there as an awesome friend, a great husband and wonderful father, you know that without you this thesis wouldn't be possible. I also thank his little assistant, our son Dídac, and his magic smiles, which are able to erase all doubts and frustrations, leaving instead pure happiness.

I dedicate this thesis to my beloved family who pushed me forward where I would be seen, my aunts, my mother, my father, and specially to my grandparents who believed in me blindly.

# List of Publications

Preston P., Wartosch L., Günzel D., Fromm M., Kongsuphol P., Ousingsawat J., Kunzelmann K., Barhanin J., Warth R. & Jentsch T.J. **"Disruption of the $K^+$ channel β-subunit KCNE3 reveals an important role in intestinal and tracheal $Cl^-$ transport"**

*J Biol Chem. 2010 Jan 5 (Epub ahead of print).*

Patricia Preston Ferrer

Berlin, June 17th 2010